HYDROTHERMAL SYNTHESIS AND CHARACTERIZATION OF NOVEL

THORIUM, URANIUM, AND NEPTUNIUM SOLIDS

Except where reference is made to the work of others, the work described in this dissertation is my own or was done in collaboration with my advisory committee. This dissertation does not include proprietary or classified information.

_____

Tyler Andrew Sullens

Certificate of Approval:

_____	_____
Thomas E. Albrecht-Schmitt, Chair Associate Professor Chemistry	Thomas R. Webb Associate Professor Chemistry
_____	_____
Holly R. Ellis Assistant Professor Chemistry	Curtis G. Shannon Associate Professor Chemistry

_____

Stephen L. McFarland
Acting Dean
Graduate School

HYDROTHERMAL SYNTHESIS AND CHARACTERIZATION OF NOVEL THORIUM, URANIUM, AND NEPTUNIUM SOLIDS

Tyler Andrew Sullens

A Dissertation

Submitted to

The Graduate Faculty of

Auburn University

In Partial Fulfillment of the

Requirements for the

Degree of

Doctor of Philosophy

Auburn, Alabama

August 8, 2005

HYDROTHERMAL SYNTHESIS AND CHARACTERIZATION OF NOVEL

THORIUM, URANIUM, AND NEPTUNIUM SOLIDS

Tyler Andrew Sullens

_____
Signature of Author

_____
Date of Graduation

VITA

Tyler Andrew Sullens, son of Terry H. Sullens and Gloria J. (Spikes) Sullens, was born on November 23, 1978, in Birmingham, Alabama. He graduated from John Carroll High School in Birmingham, Alabama, in 1997. He then attended the University of Alabama at Birmingham for two years before transferring to the University of Montevallo, where he graduated in May of 2001 with a Bachelor of Science degree in Chemistry under the direction of Dr. Houston Byrd and Dr. Prakash Bharara. He then entered Auburn University in the fall of 2001 to pursue a Doctoral degree in Inorganic Chemistry under the tutelage of Dr. Thomas E. Albrecht-Schmitt.

DISSERTATION ABSTRACT

HYDROTHERMAL SYNTHESIS AND CHARACTERIZATION OF NOVEL THORIUM, URANIUM, AND NEPTUNIUM SOLIDS

Tyler A. Sullens

Doctor of Philosophy, August 8, 2005
(B. S., University of Montevallo, 2001)

203 Typed Pages

Directed by Thomas E. Albrecht-Schmitt

Hydrothermal synthesis has been utilized to synthesize several compounds involving thorium, uranium, and neptunium. These compounds have one-, two-, and three-dimensional structural typologies. A majority of the compounds reported are strictly inorganic in composition; however, some examples of solids with the incorporation of organic molecules are reported. The compounds reported consist of thorium(IV) selenites, selenates, chromates, tellurates, and iodates, uranium(VI) periodates, transition metal uranium(IV) fluorides, and neptunium(IV) fluorides. The structural characteristics of these molecules augment the knowledge base of the chemical complexity of these early actinide elements. All structures were delineated through the use of single crystal X-ray diffraction with the aid of EDAX and IR analysis. Structure

properties of the synthetic phases were examined as necessary. These structural aspects include second-harmonic generation of light and ion exchange. Examples of open-framework and channel structures are also reported.

ACKNOWLEDGEMENT

Although there are many people that I feel that I need to thank for their help during this work, I wish to first thank the Department of Energy, Heavy Elements Program, for providing the funding for this research. I could not have imagined working for a better, more understanding, or friendlier person than Thomas Albrecht-Schmitt. This entire process could have been excruciating without him. I wish to thank my parents for their love and support throughout all of this. The friends that I have made here, especially Phil, Akin, Henry, Robert, and Rodney, have made my years at Auburn bearable, with a few nights in there that were way too much fun, mostly at the Buffalo's and the Sup(p)er Club.

But, I think above all, the person I need to thank the most is Lane Simmons. He has stuck beside me through all of this and more. We grew up together. He's the best friend anyone can have. He has a fine, steady hand. Although everyone else that we've known has fallen to the way side, we have always managed to stay together, whether we've deserved it or not. We've managed to survive The Dark Days, Wyoming, New Orleans, Ivan, Bushmills, ex's, bears, boulders, cliffs, and the occasional catapult. I think that getting this far without his support would have been nearly impossible. I can't thank him enough. I would hope to think that he would tell me "Way to go, Donny!" Skulnick.

Style manual or journal used:

American Chemical Society style

Computer software used:

Microsoft Word 2000, Microsoft Excel, Atoms v.5.0, CorelDRAW 10

TABLE OF CONTENTS

LIST OF FIGURES

LIST OF TABLES

Chapter 1

INTRODUCTION

RESEARCH GOALS

The study of the actinides in various reaction environments has roots that extend back over 50 years. The separation and purification of actinides through the precipitation of complexes of these elements with anions such as iodate and fluoride is a well-known process. Thorium alone has been shown to form complexes with a plethora of oxoanions including, but not limited to, iodate, bromate, nitrate, chlorate, sulfate, phosphate, and molybdate, as well as fluoride.[1] Uranium is known to complex with similar anions. The separation of uranium isotopes includes methods such as laser separation, gaseous diffusion, and gas centrifuge separation; all utilize UF_6. Yet with the importance of obtaining pure samples of actinide compounds, with special emphasis on isotope purification for weapons or energy needs, little is known about the complexes that form in these processes.[2,3]

It is essential to understand the interactions between the actinides and other chemical moieties that develop under particular conditions in order not only to purify the actinides, but to do so under the most ideal and efficient ways possible, primarily due to the radioactive nature of the elements under scrutiny. Since the discovery of nuclear fission by Hahn and Strassmann in 1938, the greatest purity ^{235}U and ^{238}U are required to obtain specific percentages of these isotopes of for weapons and energy production.

Extraction of uranium from a pitch of natural sources can be cumbersome owing to the presence of nearly 40 elements in the mixture, not to mention the wide range of isotopes that must be separated to achieve the specific percentages necessary.[4]

Removal, storage, and clean-up of the waste from nuclear fission more clearly accentuate the need for structural understanding of actinides. A large number of experiments remain to be conducted for the chemical nature of uranium to be understood. The lack of characterization of uranium-containing compounds demands further exploration of the structural aspects of this element. Any correlations that could be developed between uranium, thorium, and neptunium, along with the remaining actinides, would augment the knowledge base for this relatively poorly understood section of the periodic table.

The purpose of this research is to increase the information available for the fundamental knowledge of the chemistry of the early actinides, as well as advance the possibility of practical application of compounds containing these elements.

HYDROTHERMAL SYNTHESIS

Defined as a chemical process that involves the use of water as a solvent and reaction conditions at a temperature in excess of 100 ºC and pressure above 1 bar,[5] the mild hydrothermal synthetic method is preferred for several reasons. The ability to mimic natural geological processes is ideal for recreating the conditions under which minerals are formed.[6] This technique can thus be used to synthesize the minerals in the laboratory.[7,8] When attempting to understand the types of compounds that are formed by the actinides in the environment, whether the actinides are deposited through natural

sources or because of fission reactor waste, the hydrothermal method can bring insight into the interactions of these elements and other components in the mixture through the manufacture of crystalline solids. The structures of these compounds may be identical to or resemble the coordination environments of the actinides in environmental conditions. For example the mineral uraninite is a natural analogue of reactor waste. This, as well as other mineral structures, can be synthesized using this method, which therefore mimics natural geological processes. The study of such naturally occurring actinide compounds may lead to the eventual discovery of cleaning processes or storage mechanisms for the radioactive elements.

Each of the mild hydrothermal reactions in this report was carried out in a PARR 4749 autoclave which consists of a 23-mL PTFE liner encapsulated by a stainless steel reaction bomb (Figure 1.1). The reactants were loaded into the liner with the water added drop-wise to the solid reactants. Any acid or base solutions were then added drop-wise to the reaction mixture. The autoclave was then sealed and placed in a box oven preheated to 100 to 230 ºC. Temperatures above that range risk the break-down of the PTFE liner. Autogenetic pressure created within the liner is proportional to the amount of water in and temperature of the autoclave. The reaction mixture was heated for a number of days, usually between one and six days, and then cooled to room temperature. The rate of cooling can have a high impact on not only the size of the crystals,[9] but the product itself.[10]

The compounds synthesized can be extremely sensitive to temperature, volume of water, pH, stoichiometry of reactants, and rate of cooling. Solvation of reactants that are rather insoluble in aqueous media can be achieved under these conditions. The

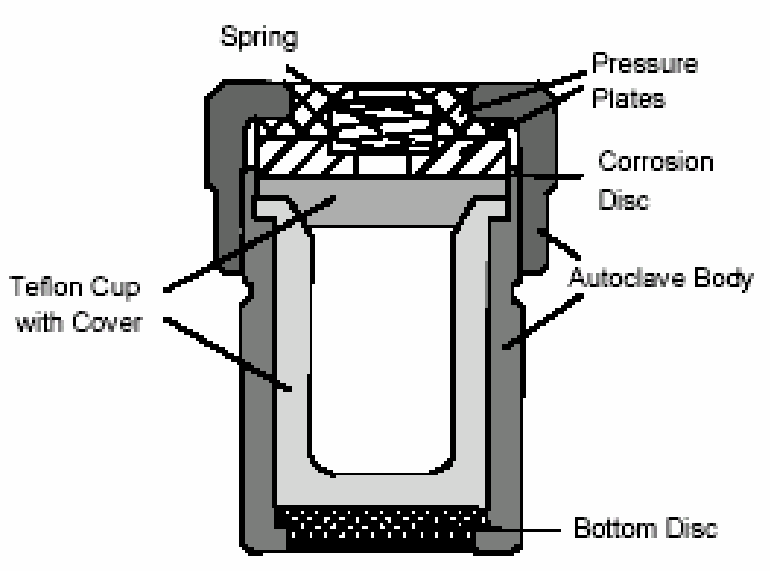

Figure 1.1. A diagram of a PARR 4749 autoclave. The reactant mixture is held inside the Teflon cup with the body, spring disc, and plates containing the autogenetic pressure.

addition of mineralizing agents, such as F^-,[11] Cl^-,[12] OH^-,[13] and NO_3^-,[14] into the reaction mixture can also aid in the dissolution of the reactants, whereas without these agents, no reaction would occur. Due to the sensitivity of the reactions conditions, the use of a modified compositional diagram is necessary to vary these conditions in order to synthesize crystalline phases (Figure 1.2).[11]

THE ACTINIDES

The vast interest in the chemistry of the actinides can be attributed to several factors. Oxidation states of the early actinides that are rare in other elements are accessible and extremely stable in the solid state (Table 1.1).[15,16] This stability along with the ability to form numerous coordination modes[17] can yield large numbers of extremely varied compounds. Although the lanthanides contain the same types of valence orbitals as the actinides (Table 1.2), namely the lanthanide 4*f* and the actinide 5*f*, the actinides can participate in more covalent bonding than the lanthanides. The 4*f* electrons are buried deep within the core of the atom and are therefore heavily shielded, thus restricting the covalency of the bonding of the atom. The 5*f* orbitals are much more accessible to ligating atoms leading to varied and strong bonding motifs.

Higher oxidation states of early actinide elements require a counter to the strain of the high charge. This is achieved in the case of the actinides, namely uranium, neptunium, and plutonium, with a valency of V or higher, with a *trans* dioxo actinyl unit forming as an AnO_2^{n+} (n = 1 or 2) cation (Figure 1.3). This dioxo cation is nearly linear in nature and is highly symmetrical with little deviation in bond length between the metal center and the two different oxo atoms. Other examples of this phenomenon include

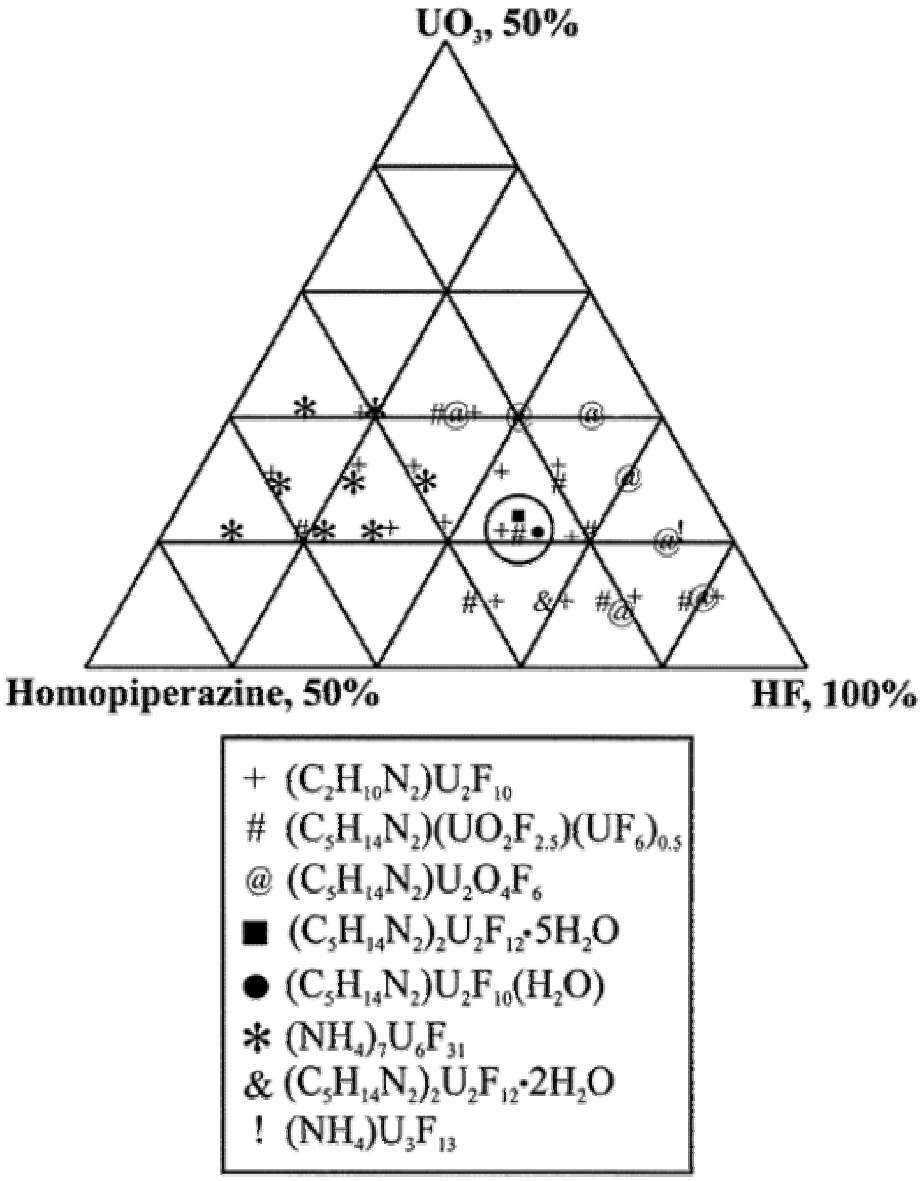

Figure 1.2. A compositional diagram of UO_3, HF, and homopiperazine showing the variation of reaction stoichiometries and compounds produced. The reactants were in 1mL of water at 180 ºC for 72 h.

Table 1.1. The oxidation states of the early actinide series. The environmentally important actinides are in bold.

Th	**Pa**	**U**	**Np**	**Pu**	**Am**	**Cm**
III	III	III	III	III	**III**	**III**
IV	IV	**IV**	IV	**IV**	IV	IV
	V	V	**V**	**V**	V	
		VI	VI	**VI**	VI	
			VII	VII		

Table 1.2. The ground-state electron configuration of the lanthanides and the actinides.

Lanthanide		Configuration			Actinide		Configuration		
La	lanthanum		$5d^1$	$6s^2$	Ac	actinium		$6d^1$	$7s^2$
Ce	cerium	$4f^1$	$5d^1$	$6s^2$	Th	thorium	$5f^1$	$6d^1$	$7s^2$
Pr	praseodymium	$4f^3$		$6s^2$	Pa	protactinium	$5f^2$	$6d^1$	$7s^2$
Nd	neodymium	$4f^4$		$6s^2$	U	uranium	$5f^3$	$6d^1$	$7s^2$
Pm	promethium	$4f^5$		$6s^2$	Np	neptunium	$5f^4$	$6d^1$	$7s^2$
Sm	samarium	$4f^6$		$6s^2$	Pu	plutonium	$5f^6$		$7s^2$
Eu	europium	$4f^7$		$6s^2$	Am	americium	$5f^7$		$7s^2$
Gd	gadolinium	$4f^7$	$5d^1$	$6s^2$	Cm	curium	$5f^7$	$6d^1$	$7s^2$
Tb	terbium	$4f^9$		$6s^2$	Bk	berkelium	$5f^9$		$7s^2$
Dy	dysprosium	$4f^{10}$		$6s^2$	Cf	californium	$5f^{10}$		$7s^2$
Ho	holmium	$4f^{11}$		$6s^2$	Es	einsteinium	$5f^{11}$		$7s^2$
Er	erbium	$4f^{12}$		$6s^2$	Fm	fermium	$5f^{12}$		$7s^2$
Tm	thulium	$4f^{13}$		$6s^2$	Md	mendelevium	$5f^{13}$		$7s^2$
Yb	ytterbium	$4f^{14}$		$6s^2$	No	nobelium	$5f^{14}$		$7s^2$
Lu	lutetium	$4f^{14}$	$5d^1$	$6s^2$	Lr	lawrencium	$5f^{14}$	$6d^1$	$7s^2$

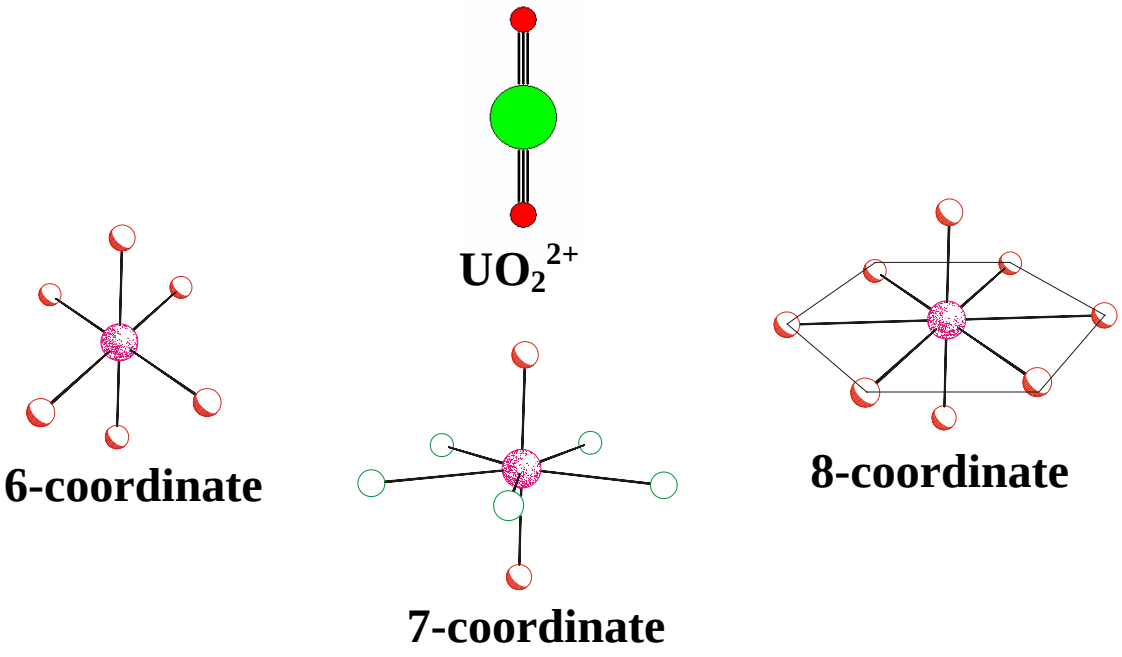

Figure 1.3. The UO_2^{2+} uranyl unit exists as a nearly linear trans dioxo unit. It generally forms in the solid state as a 6-coordinate tetragonal bipyramid, 7-coordinate pentagonal bipyramid, or an 8-coordinate hexagonal bipyramid.

VO_2^+, MoO_2^{2+}, and WO_2^{2+}, though these cations exist as a highly bent *cis* dioxo unit. These AnO_2^{n+} oxygen atoms maintain a relatively short bond distance to the central heavy metal and do not usually participate in bonding to adjacent atoms when the central atom has a valency of VI or more, since the electron density of the oxygen atom is being siphoned to the electron deficient atom. Metal–oxygen bond distances in the actinyl cation average approximately 1.83 Å for An(V), and are somewhat shortened for An(VI) to approximately 1.79Å.

Though these cations rarely bind in the axial direction, coordination is exuberant equatorially. These moieties commonly form three types of polyhedra: the six-coordinate tetragonal bipyramid, the seven-coordinate pentagonal bipyramid, and the eight-coordinate hexagonal bipyramid.[18,19] In the case of UO_2^{2+}, the pentagonal bipyramidal polyhedron is dominant and is contained in approximately 85% of known uranium(VI) structures.[18]

Due to the terminal nature of this dioxo unit in the axial direction, a majority of the structures that are formed in the solid state containing these cations are of low dimensionality, rarely exceeding the two-dimensional sheet topology.[18] Extended structures are formed through edge-sharing or corner-sharing interactions with adjacent actinyl units, or by being coordinated by ligands that act as bridging molecules to other actinyl cations[19](Figure 1.4). Depending on the variety of coordination modes available to a ligand, high dimensionality can be achieved through a combination of bridging and chelation, thus making the selection of ligand an important consideration.

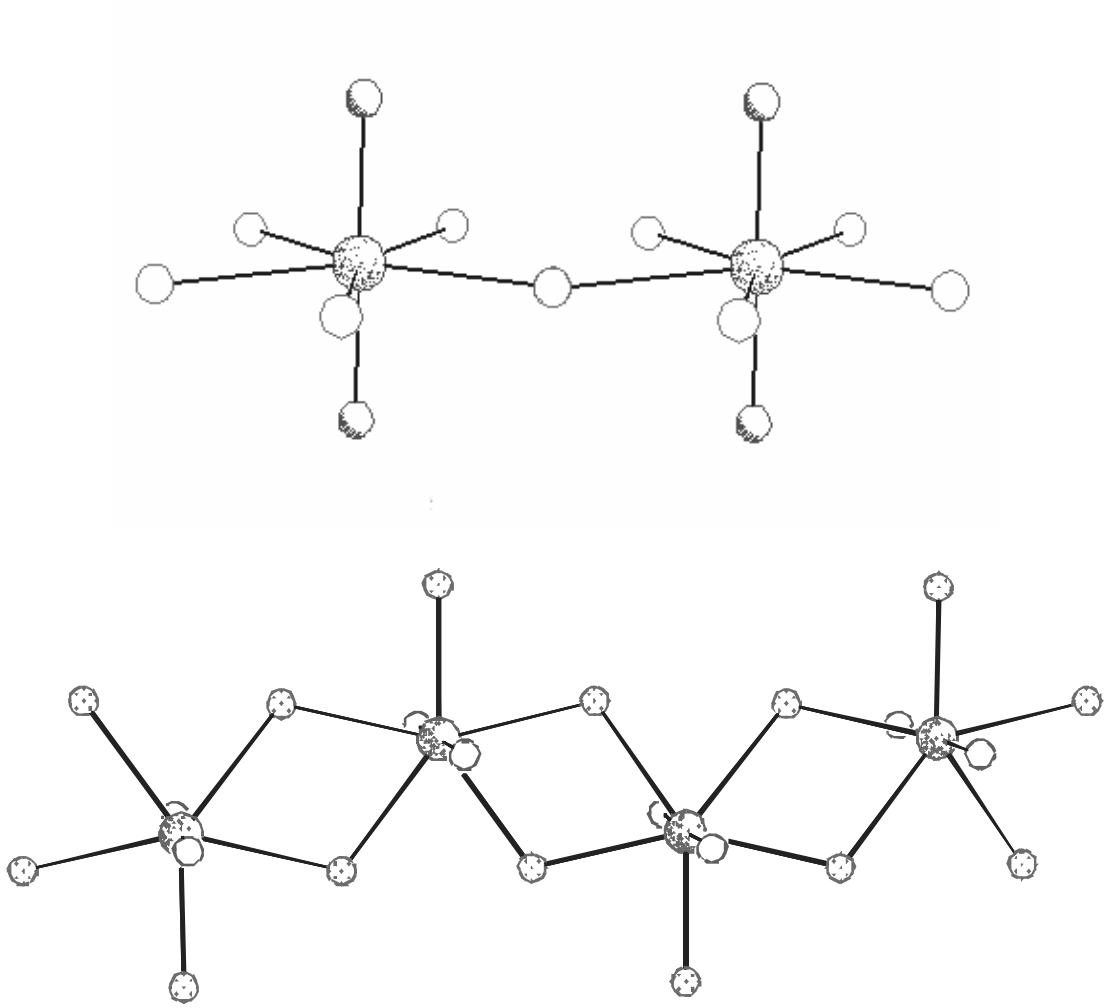

Figure 1.4. A depiction of the types of bonding in which the $AnO_2[X_5]$ pentagonal bipyramid participates. The top illustration is of corner-sharing; the bottom is of edge-sharing. No face-sharing of this unit has yet been discovered.

There are few examples of these actinyl cations forming what is known as a cation-cation interaction (CCI). This interaction occurs as the normally terminal axial oxo atom of AnO_2^{n+} coordinates to an equatorial site of an adjacent metal cation. With the actinide ion in the +V oxidation state, the terminal oxo atom does have a partial negative charge, which can and does allow for this actinyl cation to form bonds via the oxo atom (Figure 1.5). However, with the central ion in +VI or higher, the charge on the oxo atom then becomes partially positive, leading to this atom being particularly terminal. These interactions quite often occur between two actinyl units.[20] CCI's were first indicated by Sullivan *et al.* in 1961 as the oxo atoms of NpO_2^+ coordinated to UO_2^{2+} in solution.[21] Another 23 years would pass before the first solid-state example of CCI would be discovered in $Na_4(NpO_2)_2(C_{12}O_{12})\cdot 8H_2O$ through single crystal X-ray crystallography.[22] To date few examples of CCI have been observed containing the UO_2^{2+} cation exclusively.[10,23-26]

Those actinides in lower oxidation states also exhibit a variety of coordination environments. Th(IV) for example has been observed to inhabit an eight-coordinate dodecahedron[27] or square anti-prism,[28] a nine-coordinate tricapped trigonal prism,[27] and a ten-coordinate bicapped cube or bicapped square anti-prism.[29] This diversity in complexation, as well as the ability to coordinate to a larger number of molecules than actinides in higher oxidation states, causes interest in the chemistry of thorium that overcomes the lack of accessible oxidation states. The lack of terminal oxo actinyl atoms with atoms such as Th(IV) and U(IV) also increases the likelihood of obtaining extended structures with high dimensionality.[30-34]

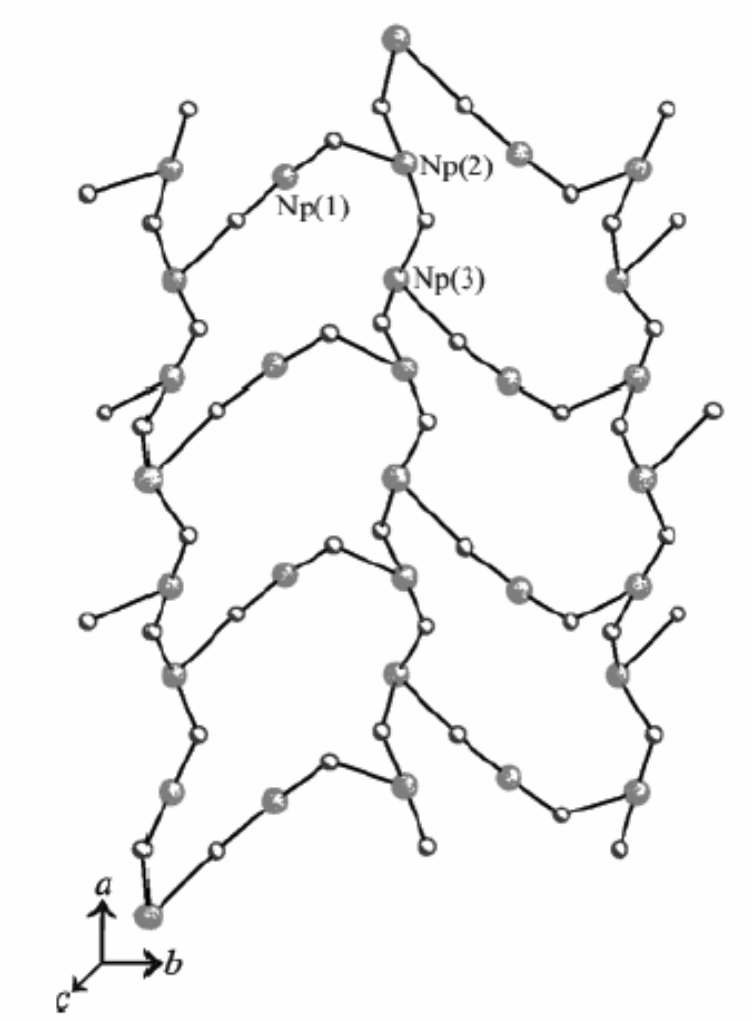

Figure 1.5. An example of a cation-cation interaction (CCI) in a sheet typology made exclusively of neptunyl units.

Developing the knowledge of the fundamental chemistry and complexation of the actinides has particular use in the field of nuclear fission waste containment. All elements above atomic number 92 (uranium) are man-made, and therefore can not be examined in natural settings. This presents a problem in that no known minerals can be discovered and evaluated to determine the types of compounds that can be created due to environmental conditions in which these synthesized elements will one day exist. Any correlation that can be developed between these natural and synthesized crystalline compounds would serve to enhance storage and containment at and clean-up of sites such as Yucca Mountain, NV, and Hanford, WA.

ORGANIC TEMPLATING

The incorporation of structure-directing molecules in an extended structure is of interest due to the structural properties that can result, such as ion-exchange, absorption, magnetic ordering, and catalytic properties.[35-38] These structure-directing molecules are typically organic in nature and often result in a desired low-dimensional extended structure (Figure 1.6). Lower dimensionality enables a higher level of interaction between the compound and the environment, which can result in an increase in efficiency of structural properties such as ion exchange.

The main use for these molecules in this body of work is to act as a bulky group in order to direct the structure to form around the molecule. Assorted interactions, such as hydrogen bonding, between the structure-directing agent and the superstructure can affect the specific topology that forms in the structure. Porous networks are quite often formed by the production of the superstructure around such entities as the ethylene

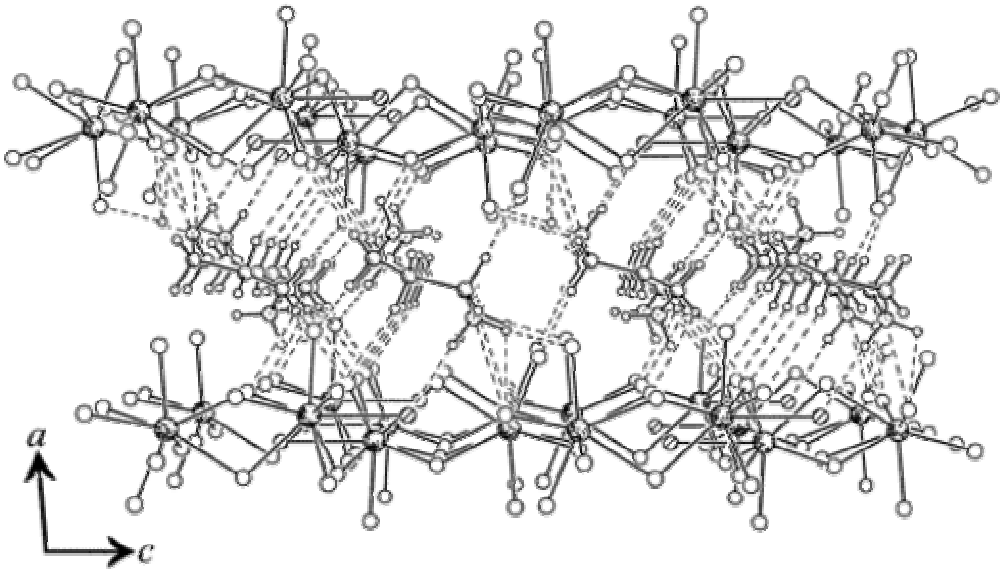

Figure 1.6. A view down the *b* axis of the two-dimensional $[C_5H_{14}N_2][U_2F_{10}(H_2O)]$. The uranium fluoride layers remain separated by homopiperazinium dications.

diammonium and piperazinium cations, followed by elimination of the organic by decomposition, yielding the intact superstructure with an organic fragment or a simple proton remaining within the structure.

STRUCTURE-PROPERTY RELATIONSHIPS

The second-harmonic generation (SHG) of light requires that the structure be in a noncentrosymmetric space group. These types of compounds are known as NLO, or nonlinear optical, materials. One method to prepare such structures, beyond serendipity, is to attempt to incorporate asymmetric moieties into the structure. The acquisition of SHG data is made by the use of 1064 nm (infrared) light source, in which the frequency of the light is doubled thus halving the wavelength of the incident light producing 532 nm (green) light.[50] In order to most accurately describe the actual response of a compound, the sample must be sieved and then generally compared to the intensity of the response of alpha quartz. Due to the weak response of this standard, the results are usually reported as being n × α-quartz with no specific units.

The creation of an ion-exchange material is another difficult task. The incorporation of cations or anions that have weak interactions with the superstructure into a structure of a compound can possibly have what is known as ion-exchange ability. This structure property is the ability to uptake ions from the surrounding environment by replacing those ions with internal ions from the structure. The rate at which the replacement occurs can vary according to the size of the gap which the ion occupies, conditions of the environment (i.e. the temperature of a surrounding solution, concentration of ions in the solution), and with the size of the ion. The charge of the ion

is not always a controlling factor in the ions that are exchangeable with the original cation. $Cs[UO_2Ga(PO_4)_2]$ (Figure 1.7) is a three-dimensional structure that shows no exchange with H^+, Na^+, or K^+, but conversely exhibits a large uptake of both Ca^{2+} and Ba^{2+}.[39]

Although low-dimensional structures contain large gaps in which the ions can occupy, three-dimensional structures also have the ability to engage in ion exchange. An additional benefit to high dimensionality is structure stability with ions that have been exchanged with ions that are smaller than those that were synthesized within the structure. Three-dimensional structures with this ability are usually either classified as channel structures or open-framework structures. These two structure types differ in that open frameworks generally have three intersecting channels perpendicular to the faces of the unit cell of a crystalline solid. Both of these structure types can also be described as porous materials. Robust actinide-containing ion-exchange materials have been largely focused upon due to the need for ion selective materials for ^{90}Sr and ^{137}Cs. The extraction of these cations is essential for the storage and disposal of fission waste and the clean-up of nuclear waste contamination sites.[40-43]

DESIRED ANIONS

One of the particular aspects of the compounds reported in this work concerns the anions used in this research. The creation of compounds with particular structural properties can be a factor in considering a choice of ion to incorporate into the structure. Anions such as iodate (IO_3^-)[44,45] (Figure 1.8) and selenite (SeO_3^{2-})[46,47] (Figure 1.9) are both C_{3v} anions which have a stereochemically active lone electron pair that cause the atomic geometry to be trigonal prismatic. IO_4^{3-} [48,49] (Figure 1.10) is an approximate C_{2v}

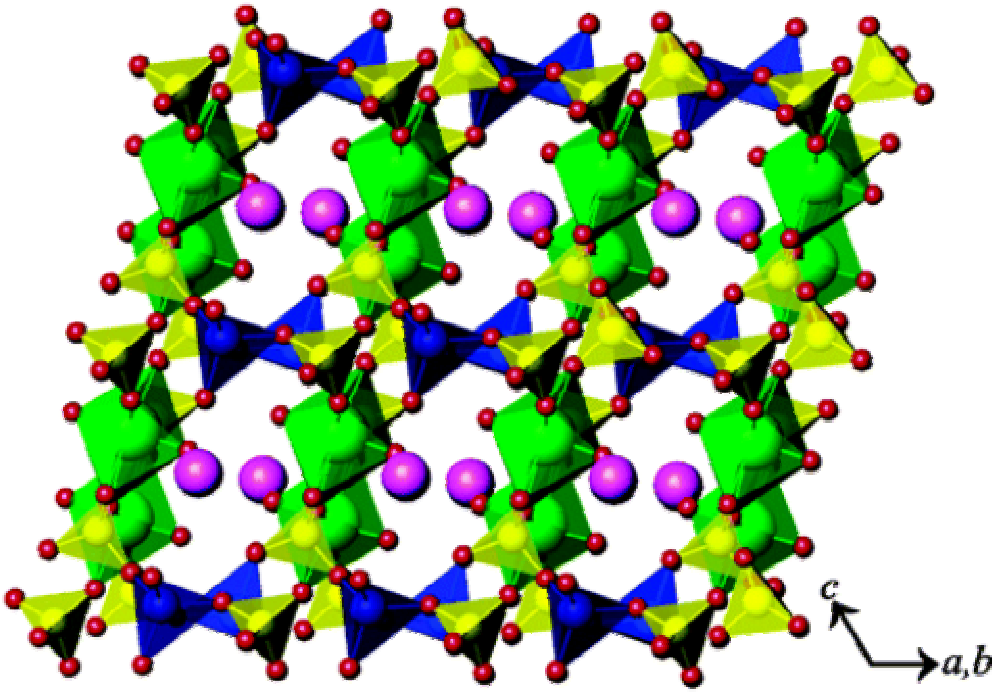

Figure 1.7. A depiction of one of the two intersecting channels that project down the *a* and *b* axes in the three-dimensional $^{3}_{\infty}$ $[UO_2Ga(PO_4)_2]^{1-}$ framework of $Cs[UO_2Ga(PO_4)_2]$.

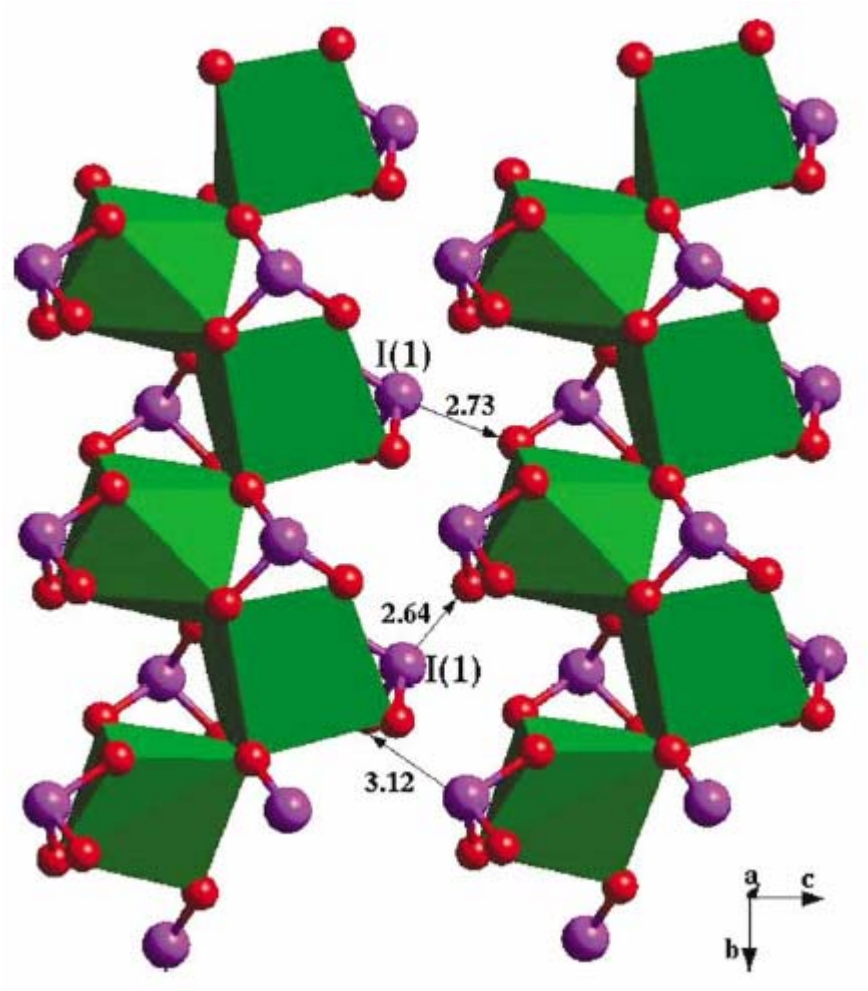

Figure 1.8. A projection of the structure of $Hg(IO_3)_2$ viewed along the *a*-axis (Hg = green, I = violet, O = red).

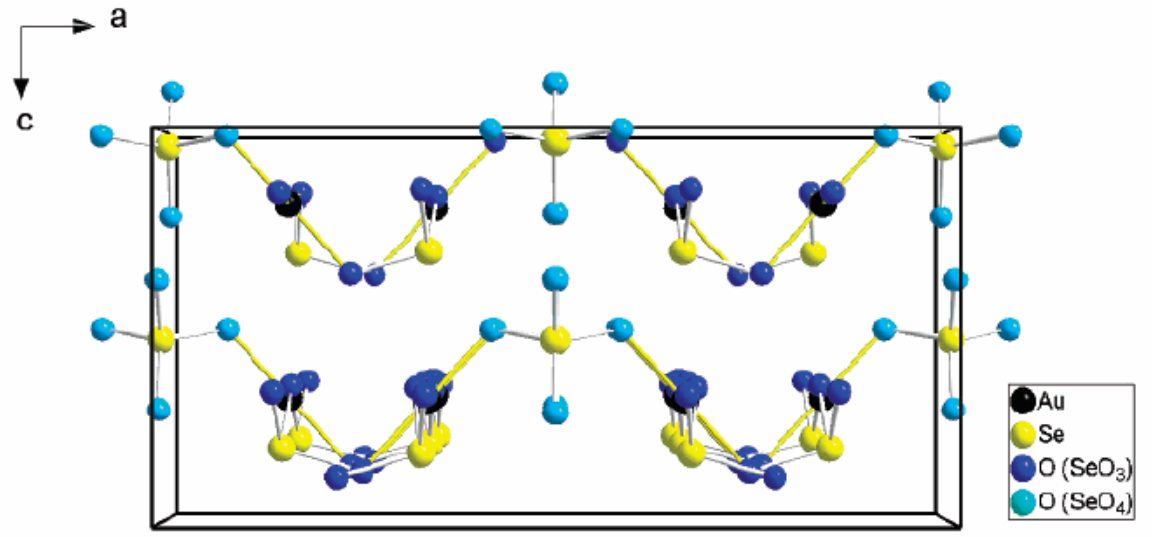

Figure 1.9. A depiction of the crystal structure of $Au_2(SeO_3)_2(SeO_4)$ viewed along the *b* axis.

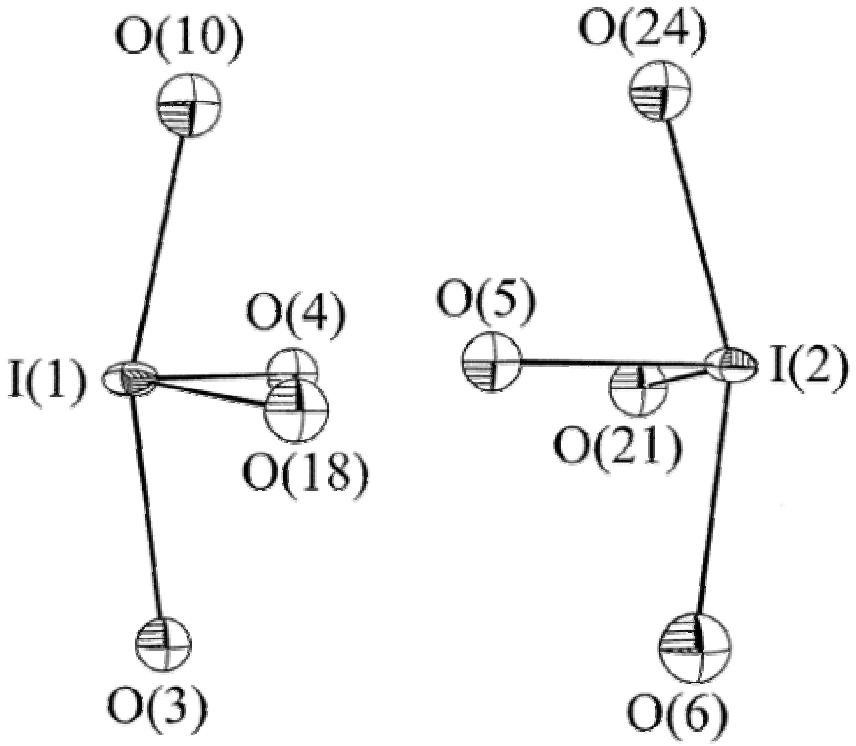

Figure 1.10. A depiction of the IO_4^{3-} anion with lone electron pairs in polar opposite directions.

anion with the same stereochemically active lone pair. Alignment of these electron pairs would cause the structure to adopt a polar space group, thus yielding a compound which is likely to have an SHG response.

Incorporation of polar anions is no guarantee of success in creating such NLO materials. Quite often these electron pairs align in one section of the compound and, due to a mirror plane or inversion center, have an electron pair opposing it. This occurrence will cancel any SHG response that would be there otherwise. In the examples of $Ag_2(UO_2)(SeO_3)_2$, $M[(UO_2)(HSeO_3)(SeO_3)]$ (M = K, Rb, Cs, Tl), and $Pb(UO_2)(SeO_3)_2$, only $Pb(UO_2)(SeO_3)_2$ has an SHG response to the infrared light, because this compound crystallizes in the space group $Pmc2_1$ which is polar about the *c*-axis. The polarity in its structure can be attributed to the alignment of PbO_5 polyhedra rather than alignment of the selenite anions (Figure 1.11). Two metal centers with stereochemically active lone electron pairs were utilized in this structure in order to increase the probability of producing a compound with a polar structure.[51-54]

Other types of anions can assist in the creation of NLO materials. Tetrahedral and more often octahedral anions can undergo a second-order Jahn-Teller distortion,[48,55-57] making these initially symmetric anions polar. IO_6^{5-} [10,48,58-60] and TeO_6^{6-} [61-63] (Figures 1.12-13) can then act as the clearly polar anions do, thereby resulting in a possible noncentrosymmetric structure. Quite often the structures containing these slightly polar anions owing to the large number of coordination possibilities of the oxoanions can result in an SHG response, or the occurrence of channeled or open framework structures, or both. The large numbers of coordination modes that exist with such anions promote the formation of high dimensionality in the crystallized product.

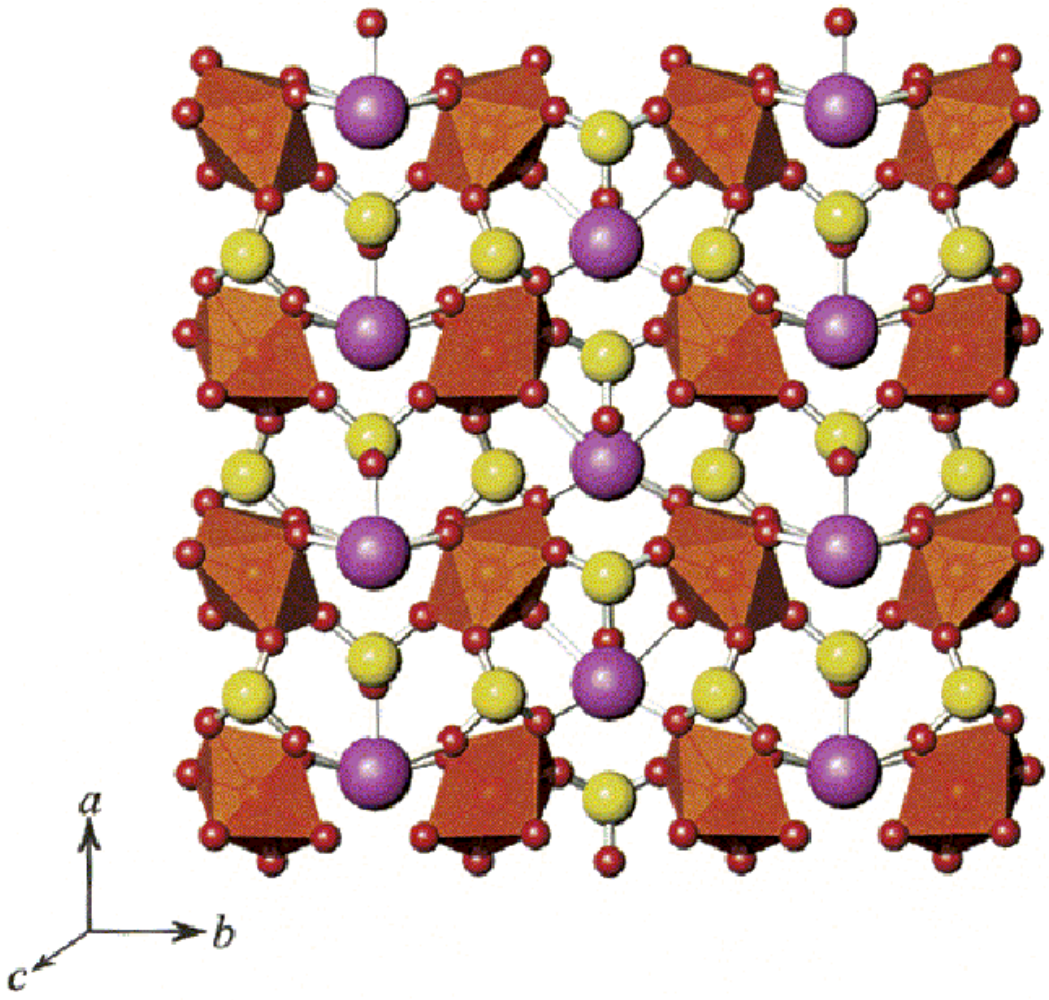

Figure 1.11. This depiction of $Pb(UO_2)(SeO_3)_2$ reveals the alignment of the PbO5 unit causing a positive SHG response.

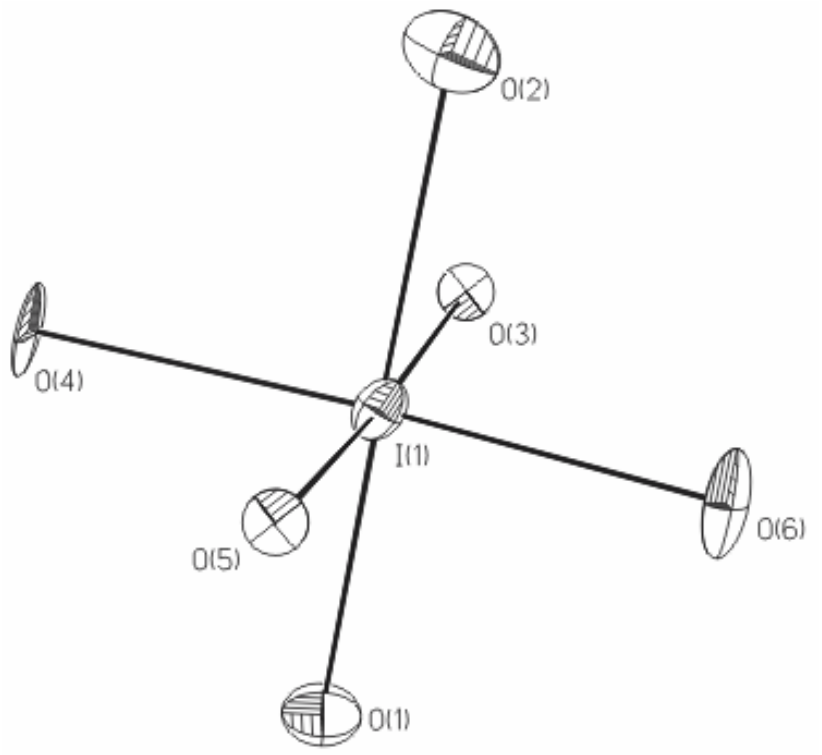

Figure 1.12. A depiction of a symmetric periodate (IO_6^{5-}) anion.

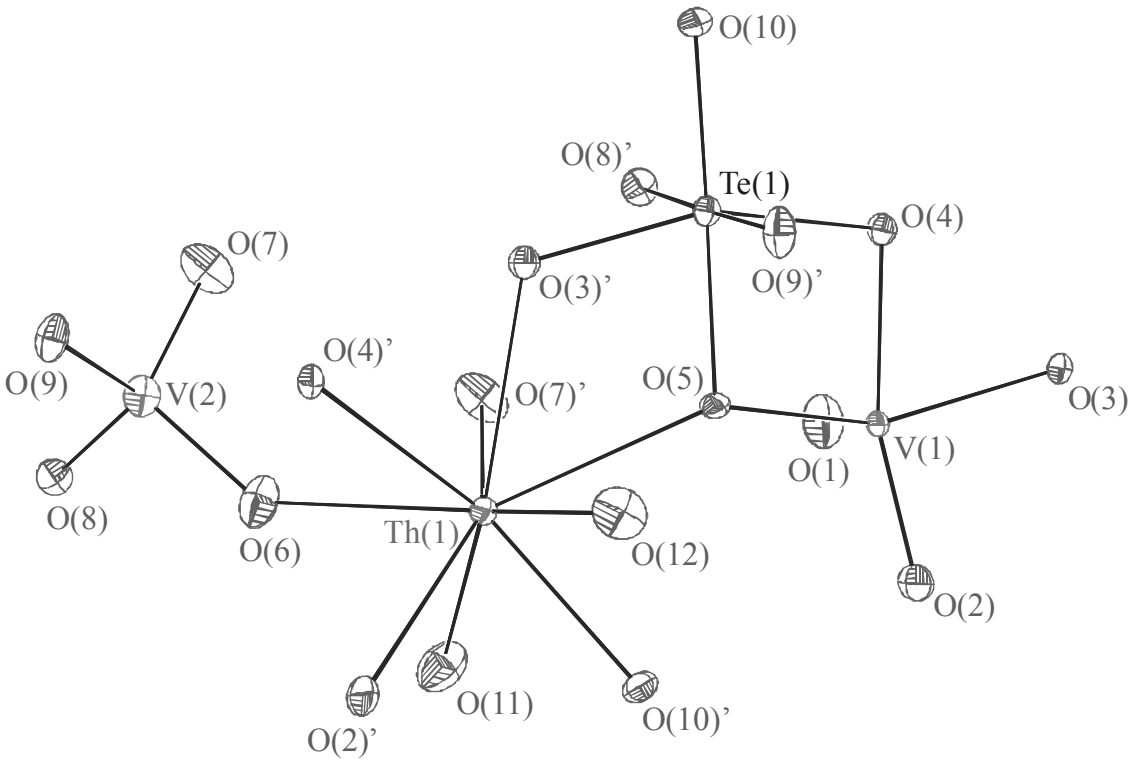

Figure 1.13. The thermal ellipsoid of $Th(VO_2)_2(TeO_6)(H_2O)_2$. This clearly shows the extent of distortion that can be attributed to a second-order Jahn-Teller distortion.

In the instance of $K_2[(UO_2)_2(VO)_2(IO_6)_2O]\cdot H_2O$, the distorted octahedra throughout the structure crystallize to form a polar structure with an SHG response of 300 × α-quartz (Figure 1.14). These octahedra also form a channel structure that contains the hydrating water molecule and K^+ cations (Figure 1.15). Though ion exchange experiments were not conducted on this particular compound, the large gaps that exist in this structure are ideal for the replacement of K^+ with other cations.

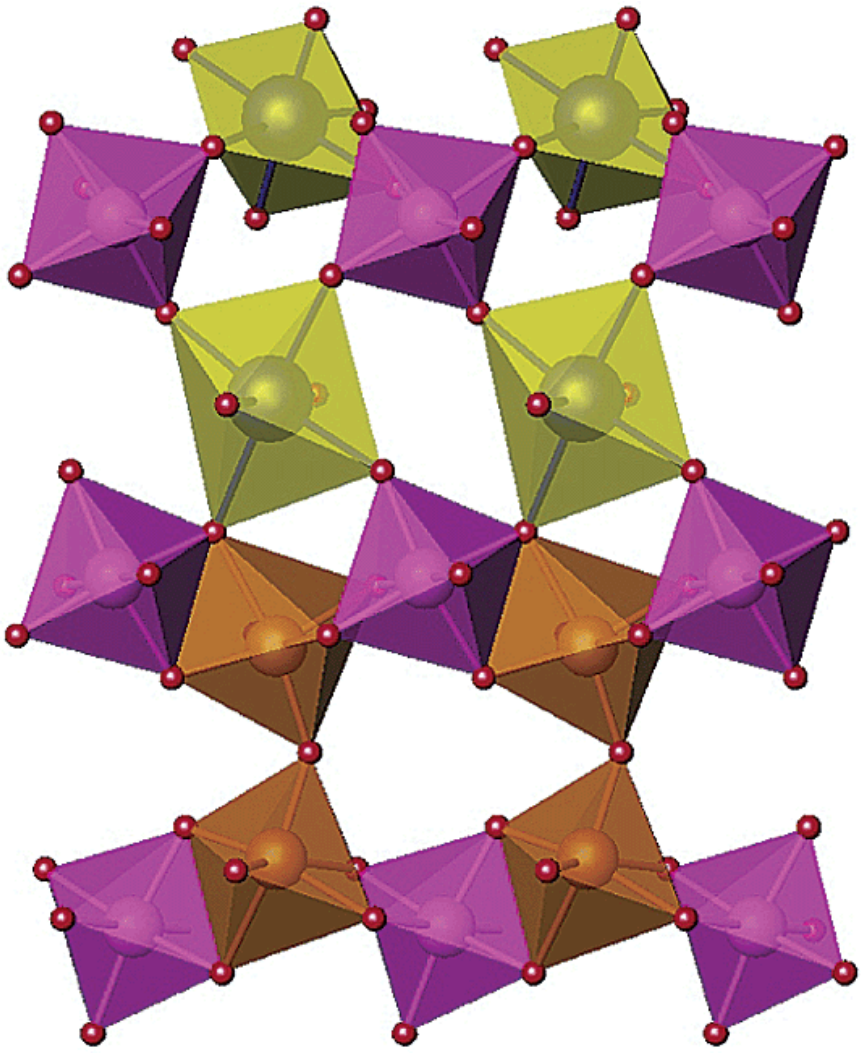

Figure 1.14. A depiction of $K_2[(UO_2)_2(VO)_2(IO_6)_2O]\cdot H_2O$ showing the alignment of the distortions of the VO_6 and IO_6 units forming the overall polar structure.

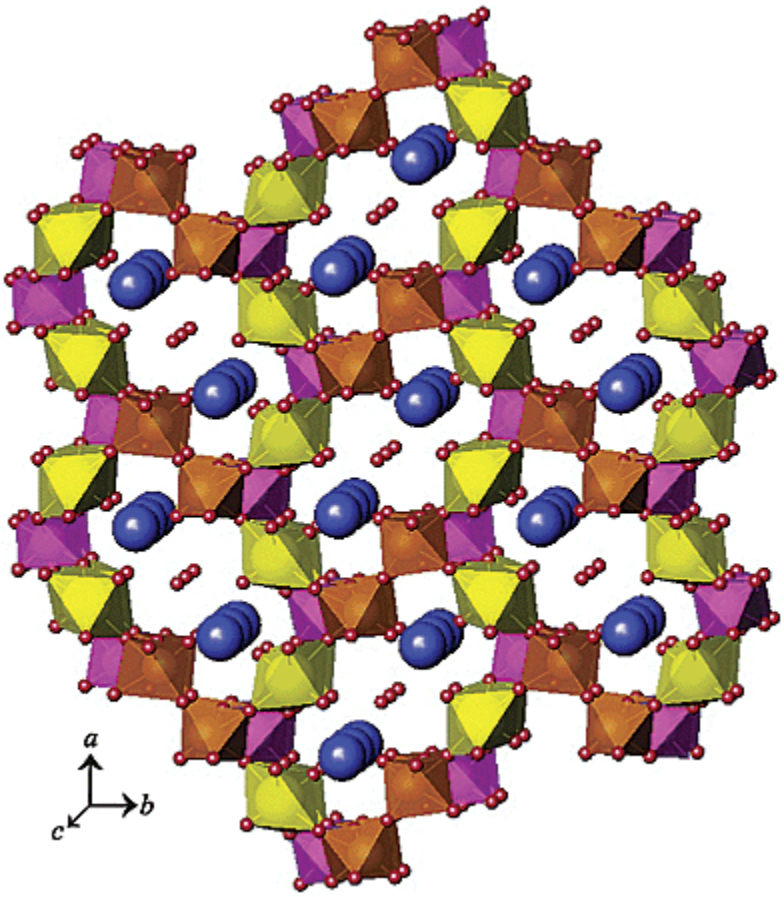

Figure 1.15. A second view of $K_2[(UO_2)_2(VO)_2(IO_6)_2O]\cdot H_2O$ showing the elliptical channels that are filled with K^+ cations and hydrating water molecules.

REFERENCES

1. Katzin, L. I.; Sonnenberger, D. C. Thorium. In *The Chemistry of the Actinide Elements*, 2nd ed.; Katz, J. J., Seaborg, G. T., Morss, L. R., Eds.; Chapman and Hall: London, 1986; Chapter 3, pp 41-101.
2. a) Tsivadze, A. Y.; Krot, N. N.; Muchnik, B. I. *Proc. Moscow Symp. Chem. Transuranium Elem.* 1976, 89-94. b) Tsivadze, A. Y.; Muchnik, B. I. Krot, N. N. *Zh. Neorg. Khim.* **1972**, *17*, 3324.
3. Weigel, F.; Engelhardt, L. W. H. *J. Less-Common Met.* **1983**, *91*, 339.
4. Weigel, F. Uranium. In *The Chemistry of the Actinide Elements*, 2nd ed.; Katz, J. J., Seaborg, G. T., Morss, L. R., Eds.; Chapman and Hall: London, 1986; Chapter 5, pp 169-442.
5. Suchanek, W. L.; Lencka, M. M.; Riman, R. E. *Aq. Sys. at Elev. Temp. and Press.* **2004**, 717.
6. Li, Y.; Burns, P. C. *J. Nuclear Mater.* **2001**, *299*, 219.
7. Akasaka, M.; Suzuki, Y.; Watanabe, H. *Mineralogy and Petrology* **2003**, *77*, 25.
8. Huertas, F. J.; Cuadros, J.; Huertas, F.; Linares, J. *Am. J. Sci.* **2000**, *300*, 504.
9. Shiraki, T.; Wakihara, T.; Sadakata, M.; Yoshimura, M.; Okubo, T. *Microporous and Mesoporous Mater*. **2001**, *42*, 229.
10. Sullens, T. A.; Jensen, R. A.; Shvareva, T. Y.; Albrecht-Schmitt, T. E. *J. Am. Chem. Soc.* **2004**, *126*, 2676.
11. a) Shevchenko, A. V.; Dudnik, E. V.; Ruban, A. K.; Danilenko, N. V.; Red'ko, V. P. *Powder Metallurgy and Metal Ceramics* **2002**, *40*, 544. b) Almond, P. M.; Deakin, L.; Mar, A.; Albrecht-Schmitt, T. E. *Inorg. Chem.* **2001,** *40,* 886.

12. Almond, P. M.; Sykora, R. E.; Skanthakumar, S.; Soderholm, L.; Albrecht-Schmitt, T. E. *Inorg. Chem.* **2004**, *43*, 958.

13. Guillot, M.; Richard-Plouet, M.; Vilminot, S. *J. Mater. Chem.* **2002**, *12*, 851.

14. Tani, Eiji; Yoshimura, Masahiro; Somiya, Shigeyuki. *Koen Yoshishu - Jinko Kobutsu Toronkai*, **1979**, *24*, 55.

15. Clark, D. L. *Los Alamos Sci.* **2000**, *26*, 364.

16. Fahey, Ja. A. Neptunium. In *The Chemistry of the Actinide Elements*, 2nd ed.; Katz, J. J., Seaborg, G. T., Morss, L. R., Eds.; Chapman and Hall: London, 1986; Chapter 6, pp 443-498.

17. Shevchenko, A. P.; Serezhkin, V. N.; *Radiochem.*, **2002**, *44*, 5.

18. Burns, P. C.; Miller, M. L.; Ewing, R. C. Canadian Mineral. **1996**, *34*, 845.

19. Burns, P. C.; Ewing, R. C.; Hawthorne, F. C. *Canadian Mineral.* **1997**, *35*, 1551.

20. Albrecht-Schmitt, T. E. Almond, P. M.; Sykora, R. E.; Inorg. Chem. **2003**, *42*, 3788.

21. Sullivan, J. C.; Hindman, J. C.; Zielen, A. J. *J. Am. Chem. Soc.* **1961**, *83*, 3373.

22. Cousson, A.; Dabos, S.; Abazli, H. Nectoux, F.; Pagès, M.; Choppin, G. R. *J. Less-Common Met.* **1984**, *99*, 233.

23. Rose, D.; Chang, Y.-D.; Chen, Q.; Zubieta, J. *Inorg. Chem.* **1994**, *33*, 5167.

24. Thuéry, P.; Nierlich, M.; Souley, B.; Asfari, Z.; Vicens, J. *J. Chem. Soc., Dalton Trans.* **1999**, *15*, 2589.

25. Taylor, J. C.; Ekstrom, A.; Randall, C. H. *Inorg. Chem.* **1978**, *17*, 3285.

26. Brandenburg, N. P.; Loopstra, B. *Acta Cryst.* **1978**, *B34*, 3734.

27. Launay, S.; Mahe, P.; Quarton, M.; Robert, F. *J. Solid State Chem.* **1992**, *97*, 305.

28. Cremers, T. L.; Eller, P. G.; Penneman, R. A. *Acta Cryst*. **1983**, *C39*, 1165.

29. Abram, U.; Gatto, C. C.; Bonfada, E.; Lang, E. S. *Inorg. Chem.* **2002**, *5*, 461.

30. Kim, J.; Norquist, A. J.; O'Hare, D. *J. Am. Chem. Soc.* **2003**, *125*, 12688.

31. Piccoli, P. M. Briggs; Abney, K. D.; Schoonover, J. D.; Dorhout, P. K. *Inorg. Chem.* **2001**, *40*, 4871.

32. Bean, A. C.; Sullens, T. A.; Runde, W.; Albrecht-Schmitt, T. E. *Inorg. Chem.* **2003**, *42*, 2628.

33. Sutorik, A. C.; Patschke, R.; Schindler, J.; Kannewurf, C. R.; Kanatzidis, M. G. *Chemistry--A European Journal* **2000**, *6*, 1601.

34. Tanner, P. A.; Sze, To H.; Mak, T. C.; Yip, W. H. *J. Crystallo. and Spectro. Res.* **1992**, *22*, 25.

35. Sykora, R. E. & Albrecht-Schmitt, T. E. *Chem. Mater.*, **2001**, *13*, 4399.

36. Walker, S. M., Halasyamani, P. S., Allen, A., & O'Hare, D. *J. Am. Chem. Soc.*, **1999,** *121*, 10513.

37. Gier, T. E.; Stucky, G. D. *Nature* **1991**, *349*, 508.

38. Sullens, T. A.; Almond, P. M.; Albrecht-Schmitt, T. E. A*cta Cryst.* **2004**, *E60*, 973.

39. Shvareva, T. Y.; Sullens, T. A.; Shehee, T. C.; Albrecht-Schmitt, T. E. *Inorg. Chem.* **2005**, *44*, 300.

40. Ladd-Lively, J. L.; Spencer, B. B.; Counce, R. M. *Separation Sci. and Tech.* **2005**, *40*, 17.

41. Yamamoto, M.; Hoshi, M.; Takada, J.; Sakaguchi, A.; Apsalikov, K. N.; Gusev, B. I. *J. Radioanal. and Nuclear Chem.* **2004**, *262*, 607.

42. Du, Y.; Chen, W. J.; Qin, S. Y. *Chinese Chem. Let.* **2004**, *15*, 1219.

43. Tripathi, A.; Medvedev, D. G.; Clearfield, A. *J. Solid State Chem.* **2005**, *178*, 253.

44. Bentria, B.; Benbertal, D.; Bagieu-Beucher, M.; Mosset, A.; Zaccaro, *J. Solid State Sci.* **2003**, *5*, 359.

45. Shehee, T. C.; Sykora, R. E.; Ok, K. M.; Halasyamani, P. S.; Albrecht-Schmitt, T. E. *Inorg. Chem.* **2003**, *42*, 457.

46. Wickleder, M. S.; Buechner, O.; Wickleder, C.; el Sheik, S.; Brunklaus, G.; Eckert, H. *Inorg. Chem.* **2004**, *43*, 5860.

47. Almond, P. M.; Albrecht-Schmitt, T. E. *Inorg. Chem.* **2002**, *41*, 1177.

48. Sykora, R. E.; Wells, D. M.; Albrecht-Schmitt, T. E. *Inorg. Chem.* **2002**, *41*, 2697.

49. Bean, A. C.; Campana, C. F.; Kwon, O.; Albrecht-Schmitt, T. E. *J. Am. Chem. Soc.* **2001**, *123*, 8806.

50. Kurtz, S. K.; Perry, T. T. *J. Appl. Phys.* **1968**, *39*, 3798.

51. Halasyamani, P. S.; O'Hare, D. *Chem. Mater.* **1998**, *10*, 646.

52. Halasyamani, P. S.; O'Hare, D. *Inorg. Chem.* **1997**, *36*, 6409.

53. Porter, Y.; Bhuvanesh, N. S. P.; Halasyamani, P. S. *Inorg. Chem.* **2001**, *40*, 1172.

54. Porter, Y.; Ok, K. M.; Bhuvanesh, N. S. P.; Halasyamani, P. S. *Chem. Mater.* **2001**, *13*, 1910.

55. Halasyamani, P. S.; Poeppelmeier, K. R. *Chem. Mater.* **1998**, *10*, 2753.

56. Kunz, M.; Brown, I. D. *J. Solid State Chem.* **1995**, *115*, 395.

57. Goodenough, J. B.; Longo, J. M. Crystallographic and Magnetic Properties of Perovskite and Perovskite-related Compounds. In *Landolt-Bornstein*; Hellwege, K. H., Hellwege, A. M., Eds.; Springer-Verlag: Berlin, 1970; Vol. 4, pp 126-314.

58. Sykora, R. E.; Albrecht-Schmitt, T. E. *Inorg. Chem.* **2003**, *42*, 2179.

59. Alexandrova, M.; Haeuseler, H. *J. Molecular Struct.* **2004**, *706*, 7.

60. Hector, A. L.; Levason, W.; Webster, M. *Inorg. Chimica Acta* **2003**, *343*, 90.

61. Sullens, T. A.; Albrecht-Schmitt, T. E. *Inorg. Chem.* **2005**, *44*, 2282.

62. Becker, R.; Johnsson, M. *Solid State Sci.* **2004**, *6*, 519.

63. Meier, S. F.; Schleid, T. *J. Solid State Chem.* **2003**, *171*, 408.

Chapter 2

HYDROTHERMAL SYNTHESIS OF THE FIRST ORGANICALLY TEMPLATED NEPTUNIUM FLUORIDES

ABSTRACT

Organically templated neptunium fluoride compounds, $(C_2H_{10}N_2)Np_2F_{10}$ (**1**) and $(C_4H_{12}N_2)_2Np_2F_{12}\cdot H_2O$ (**2**), have been synthesized under mild hydrothermal conditions. The structure of **1** consists of NpF_9 tricapped trigonal prisms connected through edge- and corner-sharing interactions forming infinite two-dimensional $[Np_2F_{10}]^{2-}$ sheets, which are separated by the ethylenediammonium dications. The structure of **2** consists of NpF_8 dodecahedra connected through edge sharing to form $[Np_2F_{12}]^{2-}$ dimers which in turn form infinite one-dimensional chains. These chains are separated by the piperazinium dication and occluded water molecules. The $C_4H_{12}N_2^{2+}$ cations form hydrogen-bonding interactions with the $[Np_2F_{12}]^{2-}$ chains. Crystallographic data: $(C_2H_{10}N_2)Np_2F_{10}$, monoclinic, space group *C2/c*, a = 16.0190(11), b = 7.0570(5), c = 8.7203(6) Å, β = 91.536(1)º, Z = 4 (T = 193 K). Crystallographic data: $(C_4H_{12}N_2)_2Np_2F_{12}\cdot H_2O$, monoclinic, space group *C2/m*, a =12.8670(10), b = 12.4790(10), c = 6.5671(5) Å, β = 107.0950(10)º, Z = 2 (T = 193 K).

INTRODUCTION

Due to the various number of products that are accessible through the use of hydrothermal synthesis and in an effort to explore the structural properties of these various products, novel, low-dimensional, open-framework structures continue to be produced. These structure types have the ability to exhibit a range of structure specific properties such as ion-exchange, absorption, magnetic ordering, and catalytic properties, and can therefore have potential use on a technical basis.[1-9] An added benefit is the derivation of the fundamental aspects of the chemical nature of the components.

The large number of coordination modes and different accessible oxidation states[10] that are exhibited by neptunium products synthesized under hydrothermal conditions make the use of this and other actinide elements excellent candidates for starting materials for these applications.[11-15] With large numbers of binding possibilities[15] comes the ability to develop large numbers of products with desired structural properties. Fluoride demonstrates evidence of success as a ligand in synthesizing solid-state phases due to fluoride being a remarkable donor ligand and mineralizing agent and the large number of possible geometries with the actinides.[13,15-19] Actinide fluoride products[13-14] also show variation through the formation of oxofluoride,[14,20-24] yielding even further structural variation to this series.

The final component in this venture is the use of an organic molecule as a structure-directing agent.[25-27] Previous compounds have made great use of these or similar organic molecules as templating agents to influence the type of structure that is produced. These structure-directing molecules can be tailored in terms of charge, bulk, and shape to yield a desired result in many instances. The method of organic templating

systems to obtain results is further evidenced in this work.

As a continuation of previous work by Sykora, Almond, Walker, and co-workers, with the synthesis of $(C_2H_{10}N_2)M_2F_{10}$[1,2] and $(C_4H_{12}N_2)_2U_2F_{12}\cdot H_2O$[3] (M = Ce(IV) and U(IV)), this work is an example of the next logical step in understanding not only this area of structural synthesis, but can lead to new discoveries in the differences of chemical properties between electronically similar elements. Should isostructural compounds be synthesized under identical conditions, then the evidence for using readily available ^{238}U in place of limited ^{237}Np for some exploratory research would be emboldened. However, any differences between the two products would lead to the need for even further investigation into the factors that guide the formation of such products; either of these results is beneficial. In this instance both products, $(C_2H_{10}N_2)Np_2F_{10}$ and $(C_4H_{12}N_2)_2Np_2F_{12}\cdot H_2O$, prove to be isostructural with their respective analogues.

EXPERIMENTAL

Synthesis. $^{237}NpO_2$ (99.9%, Oak Ridge), HF (48% wt, Aldrich), homopiperazine ($C_5N_2H_{12}$, 98%, Aldrich), and anhydrous piperazine ($C_4N_2H_{12}$, 99%, Aldrich) were used as received. Distilled and Millipore-filtered water with a resistance of 18.2 MΩ·cm was used in all reactions. Reactions were run in Parr 4749 autoclaves with 10 mL PTFE liners.

Caution! ^{237}Np ($t_{1/2}$ = 2.14 x 10^6 y) represents a serious health risk owing to α and γ emission especially because of its decay to the short- lived isotope ^{233}Pa ($t_{1/2}$ = 27.0 d), which is a potent β and γ emitter. All studies were conducted in a lab dedicated to studies on transuranium elements. This lab is located in a nuclear science facility and is equipped

with a HEPA-filtered hood and glovebox that is ported directly into the hood. A series of counters continually monitor radiation levels in the lab. The lab is licensed by the state of Alabama (a NRC-compliant state) and Auburn University's Radiation Safety Office. All experiments were carried out with approved safety operating procedures. All free-flowing solids were handled in the glovebox, and products were only examined when coated with either water or Krytox oil and water.

$(C_2H_{10}N_2)Np_2F_{10}$ (1). NpO_2 (0.0100 g, $3.7x10^{-5}$ mol) and $C_5N_2H_{12}$ (0.0074 g, $7.4x10^{-5}$ mol) were loaded into a 10 mL PTFE-lined autoclave with 0.33 mL H_2O. 0.0094 mL 48% wt HF ($4.7x10^{-4}$ mol) was then added drop-wise to the reaction mixture. The autoclave was sealed and placed in a box oven preheated at 180 °C. The autoclave was heated for 72 h and then cooled at a rate of 9 °C per hour to room temperature. The final reaction mixture consisted of a brown mother liquor and prismatic emerald green crystals bounded by ten planes of **1**.

$(C_4H_{12}N_2)_2Np_2F_{12}\cdot H_2O$ (2). NpO_2 (0.100g, $3.7x10^{-5}$ mol) and $C_4N_2H_{10}$ (0.0074g, $7.4x10^{-5}$ mol) were loaded into a 10 mL PTFE-lined autoclave with 0.33 mL H_2O. 0.0094 mL 48% wt HF ($4.7x10^{-4}$ mol) was then added drop-wise to the reaction mixture. The autoclave was sealed and placed in a box oven preheated at 130 °C. The autoclave was heated for 72 hours and then cooled at a rate of 9 °C per hour to room temperature. The final reaction mixture consisted of a brown mother liquor and prismatic emerald green crystals and green prisms of **2**.

Crystallographic Studies. Single crystals of **1** and **2** were mounted on a glass fiber and aligned on a Bruker SMART APEX CCD X-ray diffractometer. Intensity measurements were performed using graphite monochromated Mo Kα radiation from a

sealed tube and monocapillary collimator. SMART (v 5.624) was used for preliminary determination of the cell constants and data collection control. The intensities of reflections of a sphere were collected by a combination of 3 sets of exposures (frames). Each set had a different ϕ angle for the crystal and each exposure covered a range of 0.3° in ω. A total of 1800 frames were collected with an exposure time per frame of 30 s.

For **1** and **2** determination of integrated intensities and global refinement were performed with the Bruker SAINT (v 6.02) software package using a narrow-frame integration algorithm. Face-indexed analytical absorption corrections were initially applied using XPREP, where individual shells of unmerged data were corrected analytically.[28] These files were subsequently treated with a semiempirical absorption correction by SADABS.[29] The program suite SHELXTL (v 6.12) was used for space group determination (XPREP), direct methods structure solution (XS), and least-squares refinement (XL).[28] The final refinements included anisotropic displacement parameters for all atoms. Secondary extinction was not noted. Some crystallographic details are given in Table 2.1.

RESULTS AND DISCUSSION

Structures. $(C_2H_{10}N_2)Np_2F_{10}$ (1) is isostructural with both U(IV)[1] and Ce(IV)[2] variants of $(enH_2)M_2F_{10}$ (M = U and Ce; enH_2 = ethylenediammonium dication). The structure of $(C_2H_{10}N_2)Np_2F_{10}$ consists of one crystalographically unique neptunium in a nine-coordinate tricapped trigonal prism bound by fluoride anions (Figure 2.1).

The nine fluoride anions of each neptunium polyhedra form three edge-sharing and two corner-sharing interactions to adjacent neptunium atoms, with a single fluoride

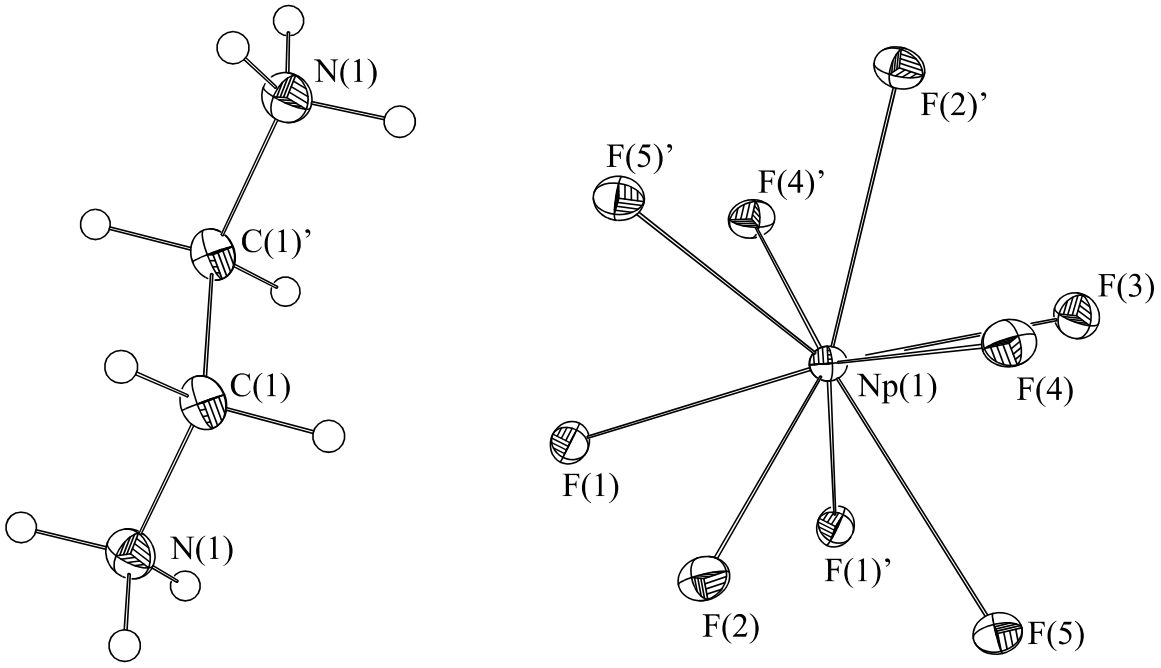

Figure 2.1. Thermal ellipsoid plot of $(C_2H_{10}N_2)Np_2F_{10}$ (**1**) shown at 50% probability.

being terminal. These interactions are the foundation of the formation of infinite $[Np_2F_{10}]^{2-}$ sheets (Figure 2.2) that are separated by ethylenediammonium dications (Figure 2.3). Np–F bond distances (2.209(2) to 2.434(2)Å) (Table 2.2) are within the normal range with F(3) having the shortest Np–F bond distance owing to the terminal nature of the F(3) atom. The terminal fluorides are directed between the layers and form hydrogen bonds with the enH_2^{2+} cations. Hydrogen bonding distances for enH_2^{2+} nitrogen atoms to the fluoride anions within the layers range from 2.714(7) to 3.133(7)Å (N(1) to nearest F(3) atoms 2.714(7), 2.873(7), 3.133(7)Å). Each nitrogen atom has the possibility of forming hydrogen bonding interactions with six different fluoride anions, totaling twelve potential interactions for each enH_2^{2+} cation.

$(C_4H_{12}N_2)_2Np_2F_{12}\cdot H_2O$ (2) was determined to be isostructural with $(C_4H_{12}N_2)_2U_2F_{12}\cdot H_2O$[3]. The structure of $(C_4H_{12}N_2)_2Np_2F_{12}\cdot H_2O$ consists of one crystallographically unique neptunium in an eight-coordinate dodecahedron bound by fluoride atoms (Figure 2.4). Of the eight fluoride atoms with each Np polyhedron, four are terminal. Two of the remaining fluoride atoms form an edge-sharing interaction with an adjacent neptunium atom, forming the $[Np_2F_{12}]^{2-}$ dimer. This dimer then uses the last of the fluorides to link to two adjacent dimers, through edge sharing, leading to the formation of the one-dimentional structure (Figure 2.5).

Neptunium to fluoride bond distances (2.167 Å to 2.427 Å) (Table 2.3) are within the normal range. The terminal fluorides, F(1), F(4), F(5), F(5)', have the shortest bond lengths to Np1 with 2.212(1) Å, 2.208(1) Å, and 2.167(1) Å, respectively, due to their terminal nature. The $[Np_2F_{12}]^{2-}$ chains are separated by the piperazinium dications as well as uncoordinated water molecules.

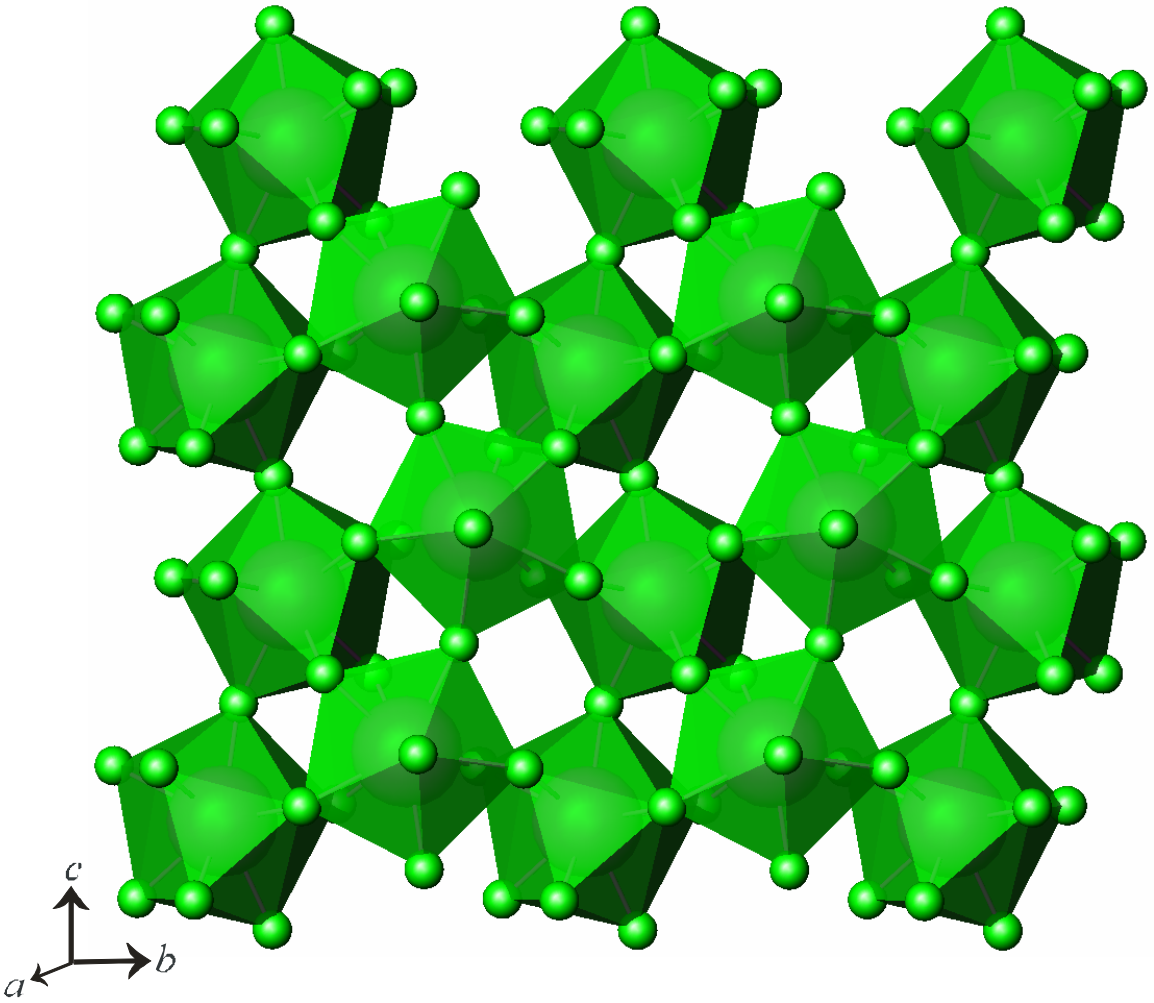

Figure 2.2. A view down the *a*-axis depicting the $[Np_2F_{10}]^{2-}$ sheets extended along the *b/c* plain. One NpF_9 tricapped trigonal prism is connected to neighboring neptunium fluorides through three edge-sharing and two corner-sharing interactions. The terminal F(3) atoms are aligned along the a axis.

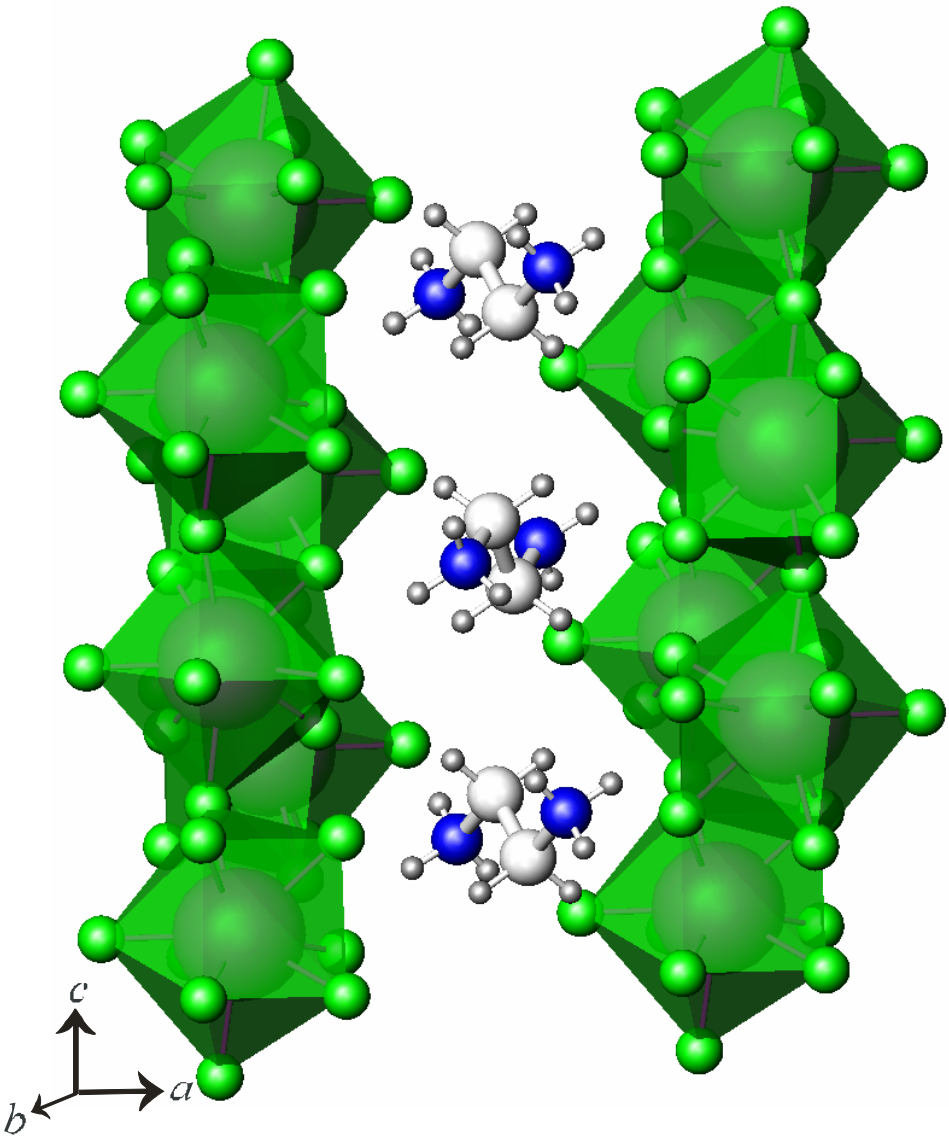

Figure 2.3. A view of $(C_2H_{10}N_2)Np_2F_{10}$ down the *b*-axis showing $[Np_2F_{10}]^{2-}$ sheets separated by enH_2^{2+} dications.

Table 2.1. Crystallographic Data for $(C_2H_{10}N_2)Np_2F_{10}$ (**1**) and $(C_4H_{12}N_2)_2Np_2F_{12}\cdot H_2O$ (**2**).

Formula	$(C_2H_{10}N_2)Np_2F_{10}$	$(C_4H_{12}N_2)_2Np_2F_{12}\cdot H_2O$
Formula Mass	363.11	910.38
Color and habit	green plate	green prism
Crystal System	monoclinic	monoclinic
Space group	*C2/c* (No. 15)	*C2/m* (No. 12)
a (Å)	16.0190(11)	12.8670(10)
b (Å)	7.0570(5)	12.4790(10)
c (Å)	8.7203(6)	6.5671(5)
β (º)	91.536(1)	107.0950(10)
V (Å^3)	985.44(12)	1007.87(14)
Z	4	2
T (K)	193	193
λ (Å)	0.71073	0.71073
Maximum 2θ (deg.)	56.58	56.62
ρ_{calcd} (g cm^{-3})	4.894	3.000
μ(Mo *K*α) (cm^{-1})	211.0	103.72
R(*F*) for $F_o^2 > 2\sigma(F_o^2)$	0.0144	0.0315
$R_w(F_o^2)$ [b]	0.0331	0.1072

[a] $R(F) = \sum \left| |F_o| - |F_c| \right| / \sum |F_o|$. [b] $R_w\left(F_o^2\right) = \left[\sum \left[w\left(F_o^2 - F_c^2\right)^2 \right] / \sum wF_o^4 \right]^{1/2}$.

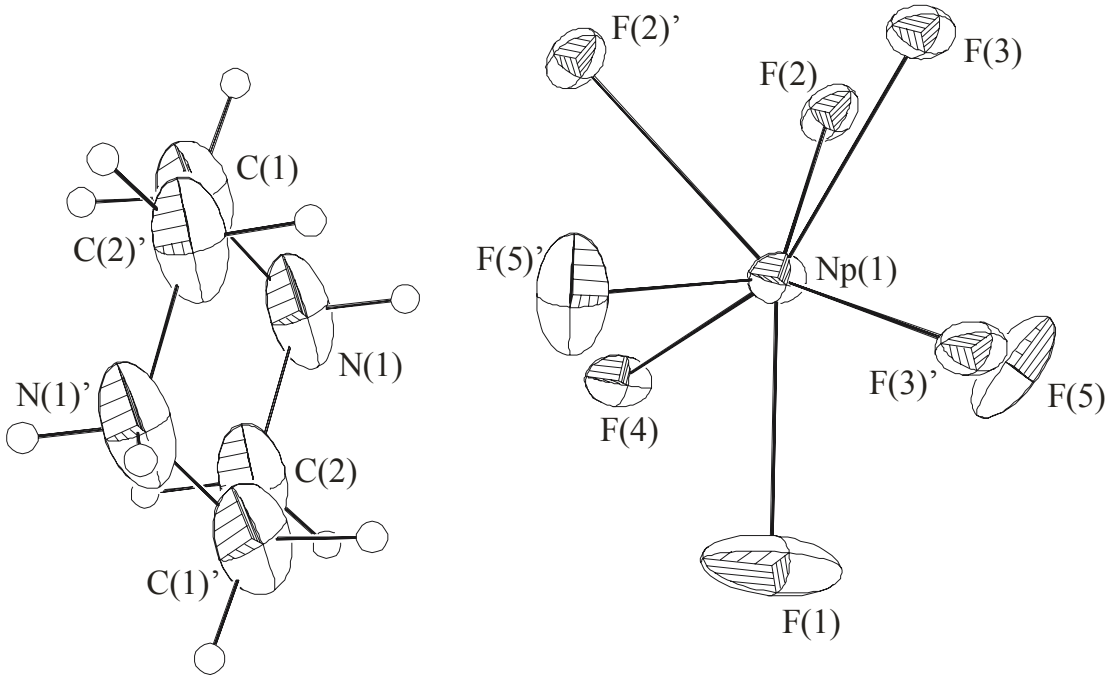

Figure 2.4. Thermal ellipsoid plot of $(C_4H_{12}N_2)_2Np_2F_{12}\cdot H_2O$ (**2**) shown at 50% probability.

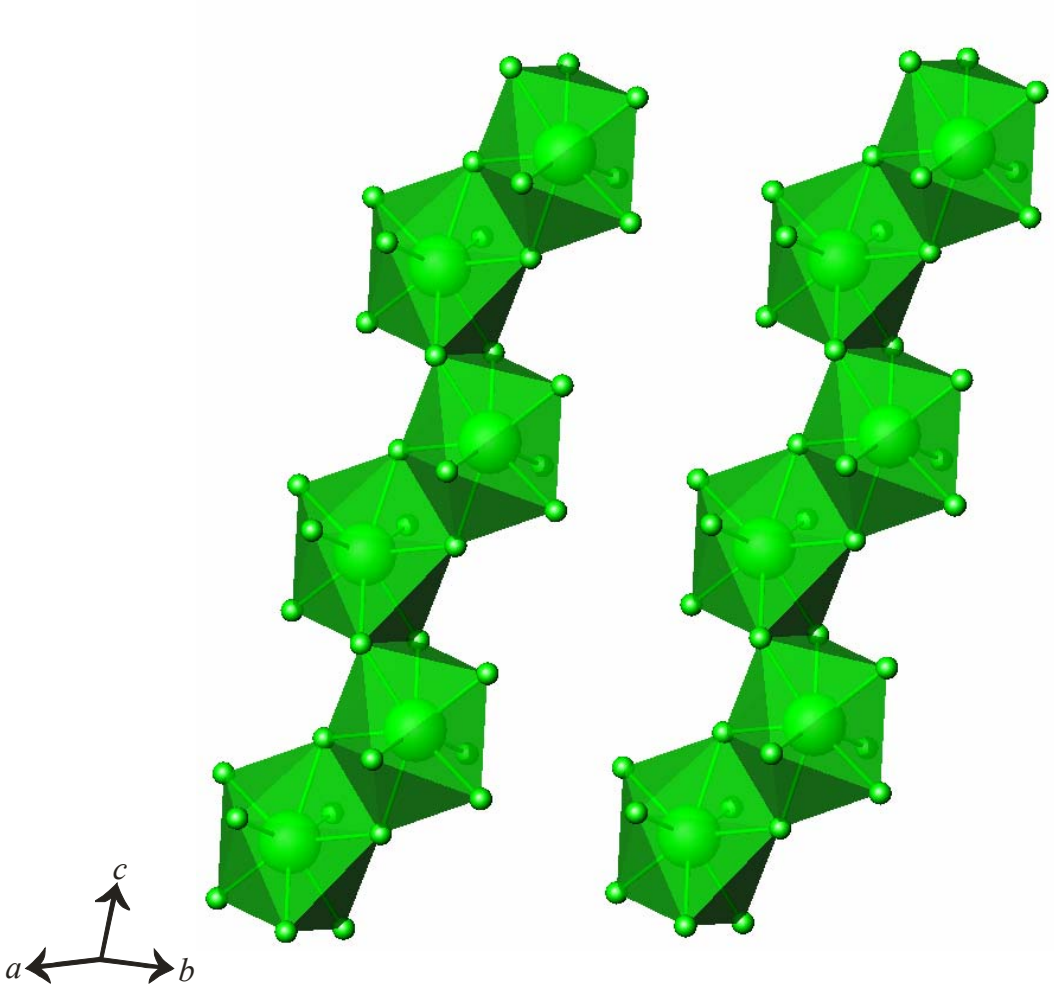

Figure 2.5. A depiction of the one-dimensional neptunium fluoride chains that form in **2**. These chains are a result of corner-sharing interactions between the NpF_8 polyhedra and extend down the *c*-axis.

Table 2.2. Selected Bond Distances (Å) and Angles (º) for $(C_2H_{10}N_2)Np_2F_{10}$ (**1**).

Distances (Å)			
Np(1)–F(1)	2.298(2)	Np(1)–F(4)’	2.347(2)
Np(1)–F(1)’	2.305(2)	Np(1)–F(5)	2.434(2)
Np(1)–F(2)	2.303(2)	Np(1)–F(5)’	2.311(2)
Np(1)–F(2)’	2.343(2)	Np(1)–Np(1)’	3.8487(3)
Np(1)–F(3)	2.209(2)	Np(1)–Np(1)”	3.9086(3)
Np(1)–F(4)	2.312(2)		
Angles (°)			
F(1)–Np(1)–F(1)’	66.54(8)	F(2)–Np(1)–F(4)’	138.45(7)
F(1)–Np(1)–F(2)	69.77(7)	F(2)–Np(1)–F(5)	63.28(7)
F(1)–Np(1)–F(2)’	121.57(7)	F(2)–Np(1)–F(5)’	76.61(7)
F(1)–Np(1)–F(4)’	68.85(7)	F(2)’–Np(1)–F(3)	71.52(7)
F(1)–Np(1)–F(5)	106.56(7)	F(2)’–Np(1)–F(4)	72.20(7)
F(1)–Np(1)–F(5)’	73.28(7)	F(2)’–Np(1)–F(4)’	71.16(7)
F(1)’–Np(1)–F(2)	96.16(7)	F(2)’–Np(1)–F(5)’	64.61(7)
F(1)’–Np(1)–F(2)’	132.88(7)	F(3)–Np(1)–F(4)	80.67(8)
F(1)’–Np(1)–F(4)	133.96(7)	F(3)–Np(1)–F(5)	74.40(7)
F(1)’–Np(1)–F(4)’	70.58(7)	F(3)–Np(1)–F(5)’	136.06(7)
F(1)’–Np(1)–F(5)	66.28(7)	F(4)–Np(1)–F(4)’	142.40(5)
F(1)’–Np(1)–F(5)’	139.06(7)	F(4)–Np(1)–F(5)	69.56(7)
F(2)–Np(1)–F(2)’	130.88(5)	F(4)–Np(1)–F(5)’	83.66(7)
F(2)–Np(1)–F(3)	136.20(7)	F(4)’–Np(1)–F(5)’	88.23(7)
F(2)–Np(1)–F(4)	74.76(7)	F(5)–Np(1)–F(5)’	136.01(3)

Table 2.3. Selected Bond Distances (Å) and Angles (º) for $(C_4H_{12}N_2)_2Np_2F_{12}\cdot H_2O$ (**2**).

Distances (Å)			
Np(1)–F(1)	2.212(9)	Np(1)–F(4)	2.208(6)
Np(1)–F(2)	2.366(3)	Np(1)–F(5)	2.167(6)
Np(1)–F(2)’	2.366(3)	Np(1)–F(5)’	2.167(6)
Np(1)–F(3)	2.427(6)	Np(1)–Np(1)’	4.0085(7)
Np(1)–F(3)’	2.292(6)	Np(1)–Np(1)”	4.0088(7)
Angles (°)			
F(1)–Np(1)–F(2)	137.32(16)	F(2)’–Np(1)–F(3)	79.14(12)
F(1)–Np(1)–F(2)’	137.32(16)	F(2)’–Np(1)–F(3)	76.23(13)
F(1)–Np(1)–F(3)	69.0(3)	F(2)’–Np(1)–F(3)	137.92(19)
F(1)–Np(1)–F(3)’	132.6(3)	F(2)’–Np(1)–F(3)	73.67(19)
F(1)–Np(1)–F(4)	76.6(3)	F(3)–Np(1)–F(3’)	63.6(2)
F(1)–Np(1)–F(5)	77.09(18)	F(3)–Np(1)–F(3’)	145.6(2)
F(1)–Np(1)–F(5)’	77.09(18)	F(3)–Np(1)–F(3’)	76.86(14)
F(2)–Np(1)–F(2)’	64.3(2)	F(3)–Np(1)–F(3’)	76.86(14)
F(2)–Np(1)–F(3)	130.95(12)	F(3)’–Np(1)–F(4)	150.8(2)
F(2)–Np(1)–F(3)’	79.14(12)	F(3)’–Np(1)–F(4)	92.01(19)
F(2)–Np(1)–F(4)	76.23(13)	F(3)’–Np(1)–F(4)	92.01(19)
F(2)–Np(1)–F(5)	73.67(19)	F(4)–Np(1)–F(5)	95.84(17)
F(2)–Np(1)–F(5)’	137.92(19)	F(4)–Np(1)–F(5)	95.84(17)
F(2)’–Np(1)–F(3)	130.95(12)	F(5)–Np(1)–F(5’)	148.3(3)

Stability and endurance of the crystal structure can be attributed to an extensive hydrogen bonding network between the organic molecules and the $[Np_2F_{12}]^{2-}$ chains. Hydrogen bonding distances for $C_4H_{12}N_2$ nitrogen to the nearest fluorides, F(1), F(3), F(4)', and F(5), range from 2.770(1) to 2.982(1) Å, with F(4)' being the nearest. Based on these atom distances, each nitrogen atom has the possibility of forming hydrogen bonding interactions with four different fluoride anions, totaling eight potential interactions for each piperazinium dication. The hydrating water also has the prospect of hydrogen bonding with an O(1) to O(1)' distance of 2.658(1) Å and an O(1) to F(1) distance of 2.601(1) Å (Figure 2.6).

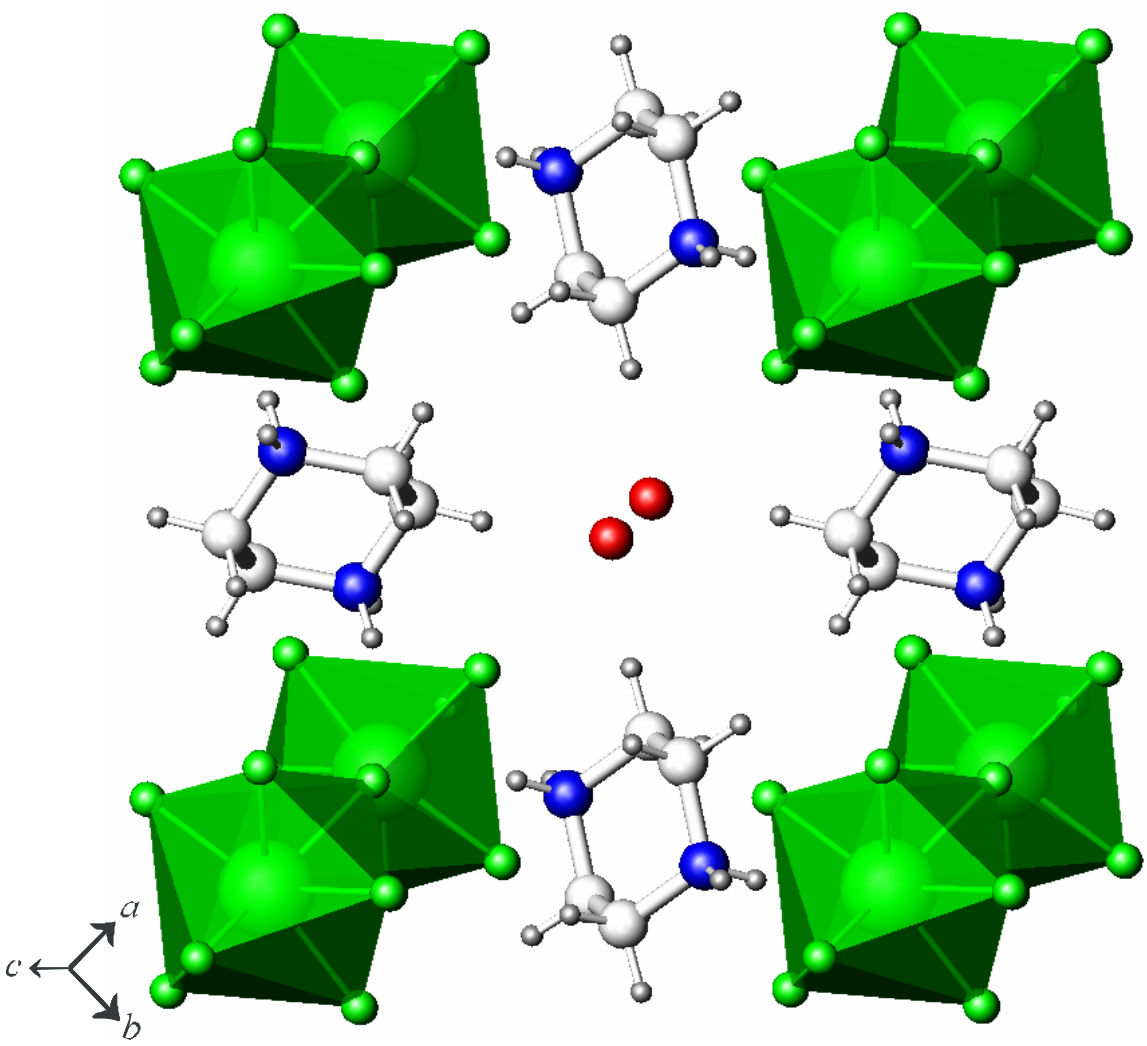

Figure 2.6. A view down the *c*-axis showing the separation of the neptunium fluoride chains by the piperazinium dications, as well as the proximity of the chains to the nitrogen atoms caused by the hydrogen bonding interactions. Due to the extent of the interaction between the chains and the dications, a large void is formed in the extended structure, which is then filled with the hydrating water molecule.

Table 2.4. Atomic Coordinates and Equivalent Isotropic Displacement Parameters for $(C_2H_{10}N_2)Np_2F_{10}$ (**1**).

Atom	*x*	*y*	*z*	U_{eq} (Å^2)[a]
Np1	0.219411(7)	0.09331(17)	0.670144(13)	0.00792(7)
F1	0.32224(12)	0.1783(3)	0.5047(2)	0.0121(4)
F2	0.31883(12)	0.2760(3)	0.7957(2)	0.0128(4)
F3	0.08169(13)	0.0751(3)	0.6639(2)	0.0151(4)
F4	0.19746(13)	0.0471(3)	0.9285(2)	0.0130(4)
F5	0.17109(13)	0.3849(3)	0.7876(2)	0.0125(4)
N1	0.54642(18)	0.2430(4)	0.4833(3)	0.0153(6)
H1a	0.5617	0.3304	0.5554	0.023
H1b	0.5065	0.2931	0.4191	0.023
H1c	0.5917	0.2099	0.4284	0.023
C1	0.5127(2)	0.0725(5)	0.5599(4)	0.0148(7)
H1d	0.4637	0.1080	0.6206	0.018
H1e	0.5557	0.0182	0.6307	0.018

[a] U_{eq} is defined as one-third of the trace of the orthogonalized $\mathbf{U}_{ij}$ tensor.

Table 2.5. Atomic Coordinates and Equivalent Isotropic Displacement Parameters for $(C_4H_{12}N_2)_2Np_2F_{12}\cdot H_2O$ (**2**).

Atom	*x*	*y*	*z*	U_{eq} (Å^2)[a]
Np1	0.90651(3)	0.5000	0.19614(5)	0.01785(17)
F1	0.7436(7)	0.5000	-0.0404(14)	0.073(4)
F3	0.9208(5)	0.5000	-0.1643(10)	0.0219(13)
F5	0.8836(6)	0.6671(5)	0.1045(9)	0.0476(17)
F2	1	0.6007(5)	0.5	0.0237(13)
F4	0.7941(5)	0.5000	0.3937(10)	0.0237(13)
N1	0.7758(10)	0.6670(8)	-0.3411(13)	0.055(3)
H1a	0.8052	0.6147	-0.4063	0.066
H1b	0.7772	0.6423	-0.2083	0.066
C1	0.8432(11)	0.7662(11)	-0.3176(15)	0.053(3)
H1c	0.9198	0.7490	-0.2404	0.063
H1d	0.817	0.8196	-0.2325	0.063
C2	0.6627(13)	0.6864(11)	-0.4671(19)	0.058(4)
H2a	0.6283	0.5000	-0.3889	0.07
H2b	0.6219	0.5000	-0.4872	0.07
O1	0.968(2)	0.5000	0.174(6)	0.33(4)

[a] U_{eq} is defined as one-third of the trace of the orthogonalized $\mathbf{U}_{ij}$ tensor.

REFERENCES

1. Almond, P. M.; Deakin, L.; Porter, M. J.; Mar, A.; Albrecht-Schmitt, T. E. *Chem. Mater.* **2000**, *12*, 3208.
2. Sykora, R. E. & Albrecht-Schmitt, T. E. *Chem. Mater.* **2001**, *13*, 4399.
3. Walker, S. M., Halasyamani, P. S., Allen, A., & O'Hare, D. *J. Am. Chem. Soc.* **1999,** *121*, 10513.
4. Wilson, S. T.; Lok, B. M.; Messina, C. A.; Cannan, T. R.; Flanigen, E. M. *J. Am. Chem. Soc.* **1982**, *104*, 1146.
5. Gier, T. E.; Stucky, G. D. *Nature* **1991**, *349*, 508.
6. Xu, R.; Chen, J.; Feng, C. *Stud. Surf. Sci. Catal.* **1991**, *60*, 63.
7. Clearfield, A. *Chem. Rev.* **1988**, *88*, 125.
8. Fogg, A. M.; Dunn, J. S.; Shyu, S.-G.; Cary, D. R.; O'Hare, D. *Chem. Mater.* **1998**, *10*, 351.
9. Davis, M. E.; Lobo, R. F. *Chem. Mater.* **1992**, *4*, 756.
10. Fahey, Ja. A. Neptunium. In *The Chemistry of the Actinide Elements*, 2nd ed.; Katz, J. J., Seaborg, G. T., Morss, L. R., Eds.; Chapman and Hall: London, 1986; Chapter 6, pp 443-498.
11. Albrecht-Schmitt, T. E., Almond, P. M., & Sykora, R. E. *Inorg. Chem.* **2003**, *42*, 3788.
12. Almond, P. M.; Sykora, R. E.; Skanthakumar, S.; Soderholm, L.; Albrecht-Schmitt, T. E.; *Inorg. Chem* **2004**, *43*, 958.
13. Albrecht-Schmitt, T. E.; Almond, P. M.; Sykora, R. E.; *Inorg. Chem.* **2003**, *42*, 3788.

14. Eller, G. P.; Asprey, L. B.; Kinkead, S. A.; Swanson, B. I.; Kissane, R. J.; *J. Alloys and Comp.* **1998**, *269*, 63.

15. Shevchenko, A. P.; Serezhkin, V. N.; *Radiochem* **2002**, *44*, 5.

16. Francis, R. J.; Halasyamani, P. S.; O'Hare, D. *Chem. Mater.* **1998**, *10*, 3131.

17. Francis, R. J.; Halasyamani, P. S.; O'Hare, D. *Angew. Chem., Int. Ed.* **1998**, *37*, 2214.

18. Walker, S. M.; Halasyamani, P. S.; Allen, S.; O'Hare, D. *J. Am. Chem. Soc.* **1999**, *121*, 10513.

19. Almond, P. M.; Talley, C. E.; Bean, A. C.; Peper, S. M.; Albrecht-Schmitt, T. E. *J. Solid State Chem.* **2000**, *154*, 635.

20. Francis, R. J.; Halasyamani, P. S.; Bee, J. S.; O'Hare, D. *J. Am. Chem. Soc.* **1999**, *121*, 1609.

21. Halasyamani, P. S.; Walker, S. M.; O'Hare, D. *J. Am. Chem. Soc.* **1999**, *121*, 7415.

22. Talley, C. E.; Bean, A. C.; Albrecht-Schmitt, T. E. *Inorg. Chem.* **2000**, *39*, 5174.

23. Almond, P. M.; Deakin, L.; Mar, A.; Albrecht-Schmitt, T. E. *Inorg. Chem.* **2001**, *40*, 866.

24. Allen, S.; Barlow, S.; Halasyamani, P. S.; Mosselmans, J. F. W.; O'Hare, D.; Walker, S. M.; Walton, R. I. *Inorg. Chem.* **2000**, *39*, 3791.

25. Kolis, J. W.; Korzenski, M. B. In *Chemical Synthesis Using Supercritical Fluids*; Jessop, P. G., Leitner, W., Eds.; Wiley-VCH: New York, 1999; pp 213-241.

26. Cheetham, A. K.; Férey, G.; Loiseau, T. *Angew. Chem., Int. Ed. Engl.* **1999**, *38*, 3268.

27. Almond, P. M., Deakin, L., Porter, M. J., Mar, A., & Albrecht-Schmitt, T. E. *Inorg. Chem.*, **2001**, *40*, 886.

28. Sheldrick, G. M. SHELXTL PC, Version 6.12, An Integrated System for Solving, Refining, and Displaying Crystal Structures from Diffraction Data; Siemens Analytical X-Ray Instruments, Inc.: Madison, WI 2001.

29. Sheldrick, G. M. *SADABS* 2001, Program for absorption correction using SMART CCD based on the method of Blessing: Blessing, R. H. *Acta Cryst.* **1995**, *A51*, 33.

Chapter 3

HYDROTHERMAL PREPARATION OF Ni(II)/U(IV) FLUORIDES WITH ONE-, TWO-, AND THREE-DIMENSIONAL TOPOLOGIES

ABSTRACT

A modified compositional diagram for the reactions of $Ni(C_2H_3O_2)_2{\cdot}4H_2O$ with $UO_2(C_2H_3O_2)_2{\cdot}2H_2O$ and HF in aqueous media under mild hydrothermal conditions (200 °C) has been completed to yield three Ni(II)/U(IV) fluorides, $Ni(H_2O)_4UF_6{\cdot}1.5H_2O$ (**1**), $Ni_2(H_2O)_6U_3F_{16}{\cdot}3H_2O$ (**2**), and $Ni(H_2O)_2UF_6(H_2O)$ (**3**). The structure of **1** consists of one-dimensional columns constructed from two parallel chains of edge-sharing dodecahedral [UF_8] units. The sides of the columns are terminated by octahedral Ni(II) that occur as *cis*-[$Ni(H_2O)_4F_2$] polyhedra. In contrast, the crystal structure of **2** reveals a two-dimensional Ni(II)/U(IV) architecture built from edge-sharing tricapped trigonal prismatic [UF_9] units. The top and bottom of the sheets are capped by *fac*-[$Ni(H_2O)_3F_3$] octahedra. The structure of **3** is formed from [$UF_8(H_2O)$] tricapped trigonal prisms that edge-share with one another to form one-dimensional chains. These chains are then joined together into a three-dimensional network by corner-sharing with *trans*-[$Ni(H_2O)_2F_4$] octahedra. Crystallographic data: **1**, orthorhombic, space group *Cmcm*, a = 14.3383(8) Å, b = 15.6867(8) Å, c = 8.0282(4) Å, Z = 8; **2**, hexagonal, space group

*P*6$_3$/*mmc*, *a* = 7.9863(5) Å, *c* = 16.566(1) Å, *Z* = 2; **3**, monoclinic, space group *C*2/*c*, *a* = 12.059(1) Å, *b* = 6.8895(6) Å, *c* = 7.9351(7) Å, β = 92.833(2)°, *Z* = 4.

INTRODUCTION

In recent years the synthesis of organically templated uranium fluorides has been the focus of considerable interest owing to both the diversity of structures observed and the physicochemical properties that these compounds display.[1-11] For instance, the one-dimensional homopiperazinium-templated U(IV) fluoride, $(C_5H_{14}N_2)_2U_2F_{12}\cdot 2H_2O$, exhibits metamagnetic behavior.[7] Likewise, unusual short-range ferromagnetic coupling is found in two-dimensional $(C_2H_{10}N_2)U_2F_{10}$.[7] Ion-exchange properties are also known for a series of U(IV) fluorides with sheet topologies similar to those observed in $(C_2H_{10}N_2)U_2F_{10}$.[1,12] In addition, several porous and three-dimensional network structures with U(VI) have been isolated with fluoride and other hard anions. These compounds include $[C_6H_{14}N_2][(UO_2)_2F_6]$,[11] $[(C_4H_{12}N_2][U_2O_4F_6]$,[4,5] $[(C_2H_5)_2NH_2]_2[(UO_2)_5(PO_4)_4]$,[13] $Na_2(UO_2)(Si_4O_{10})\cdot 2.1H_2O$,[14] $RbNa(UO_2)(Si_2O_6)\cdot H_2O$,[14] $[C_4H_{12}N_2][(UO_2)_2(PO_3H)_2\{PO_2(OH)H\}_2]$,[15] and $[NH_4]_3[(UO_2)_{10}O_{10}(OH)][(UO_4(H_2O)_2]\cdot 2H_2O$.[16] Based on these works, the possibility of preparing uranium-based materials with zeolitic topologies is starting to become a reality.

In spite of these widespread efforts to understand the hydrothermal chemistry of uranium, mixed-metal compounds derived from hydrothermal conditions are lacking. In fact, they are largely restricted to U(VI) chromates and molybdates that are known with both organic structure-directing agents[17] and inorganic cations.[18-29] In the latter case, however, the transition metal does not impart desirable electronic properties associated

with unpaired electrons on the metal centers. Therefore, the preparation of mixed-metal uranium compounds with transition metals bearing *d*-electrons can be viewed as an important synthetic challenge that may give rise to mixed-metal compounds with atypical electronic properties. The majority of well-characterized representatives of transition metal/uranium fluorides are found to contain transition metals in the +2 oxidation state, especially Ni(II), and U(VI) in the form of uranyl, UO_2^{2+}, cations. Members of this group include $[Ni(H_2O)_6]_2[(UO_2)_2F_8]\cdot 2H_2O$,[30] $[Ni(H_2O)_6]_3[(UO_2)_4F_{14}]$,[31] and $[NH_4]_2[Ni(H_2O)_6][(UO_2)_2F_8]$.[32] Limited crystallographic information has also been reported for the mixed-metal U(IV) fluorides $[M(H_2O)_6][U_2F_{10}]\cdot 2H_2O$ (M = Co, Ni, Cu).[33] The common feature of both of these Ni(II)/U(IV)/F and Ni(II)/U(VI)/F systems is that the transition metals are fully hydrated and are essentially serving as counterions that are not directly incorporated into the uranium fluoride extended or molecular structures.

In this report we detail the preparation of three new Ni(II)/U(IV) fluorides, $Ni(H_2O)_4UF_6\cdot 1.5H_2O$ (**1**), $Ni_2(H_2O)_6U_3F_{16}\cdot 3H_2O$ (**2**), and $Ni(H_2O)_2UF_6(H_2O)$ (**3**) under mild hydrothermal conditions. These compounds display dimensionalities ranging from one-dimensional chains to two-dimensional layers to three-dimensional networks created through the combination of a variety of U(IV) polyhedra with various isomers of $Ni(H_2O)_{6-x}F_x$ octahedra where there are linkages between Ni(II) and U(IV) via bridging fluoride anions.

EXPERIMENTAL

Syntheses. $UO_2(C_2H_3O_2)_2{\cdot}2H_2O$ (98%, Alfa-Aesar), $Ni(C_2H_3O_2)_2{\cdot}4H_2O$ (98%, Aldrich), and HF (48 wt.%, Aldrich) were used as received. Distilled and Millipore filtered water was used in all reactions. The resistance of the water was 18.2 MΩ·cm. The PTFE liners used to contain these reactions were cleaned of contaminants by heating with distilled and Millipore-filtered water at 200 °C for 3 d prior to use. *While the UO_3 contains depleted U, standard precautions for handling radioactive materials should be followed. Old sources of depleted U should not be used, as the daughter elements of natural decay are highly radioactive and present serious health risks.* SEM/EDX analyses were performed using a JEOL 840/Link Isis instrument. The reported preparations given herein are taken from a modified compositional diagram and represent the highest yields of pure phases obtained where possible.

$Ni(H_2O)_4UF_6{\cdot}1.5H_2O$ (1) and $Ni(H_2O)_2UF_6(H_2O)$ (3). $UO_2(C_2H_3O_2)_2{\cdot}2H_2O$ (212 mg, 0.500 mmol) and $Ni(C_2H_3O_2)_2{\cdot}4H_2O$ (373 mg, 1.5 mmol) were loaded in a 23-mL PTFE-lined autoclave. Water (1 mL) was then added to the solids, followed by the drop-wise addition of HF (0.73 mL, 20 mmol). The autoclave was sealed and placed in a box furnace and heated to 200 °C. After 72 h the furnace was cooled at 9 °C/h to 23 °C. The product consisted of an aquamarine colored solution over pale green tablets of **1** and large, dark green, roughly hexagonal blocks of **3**. The mother liquor was decanted from the crystals, which were then washed with water and methanol, and allowed to dry. Yield of **1**, 150 mg (62% yield based on U). Yield of **3**, 30 mg (12% yield based on U). EDX analysis for $Ni(H_2O)_4UF_6{\cdot}1.5H_2O$ (**1**) and $Ni(H_2O)_2UF_6(H_2O)$ (**3**) both provided a Ni:U ratio of 1:1.

$Ni_2(H_2O)_6U_3F_{16}\cdot 3H_2O$ (2). $UO_2(C_2H_3O_2)_2\cdot 2H_2O$ (170 mg, 0.4 mmol) and $Ni(C_2H_3O_2)_2\cdot 4H_2O$ (299 mg, 1.2 mmol) were loaded in a 23-mL PTFE-lined autoclave. Water (1 mL) was then added to the solids, followed by the drop-wise addition of HF (0.73 mL, 20 mmol). The autoclave was sealed and placed in a box furnace and heated to 200 °C. After 72 h the furnace was cooled at 9 °C/h to 23 °C. The product consisted of a green solution over light green hexagonal tablets of **2**. The mother liquor was decanted from the crystals, which were then washed with water and methanol, and allowed to dry. Yield, 333 mg (67% yield based on U). EDX analysis for $Ni_2(H_2O)_6U_3F_{16}\cdot 3H_2O$ provided a Ni:U ratio of 2:3.

Crystallographic Studies. Single crystals of $Ni(H_2O)_4UF_6\cdot 1.5H_2O$ (**1**), $Ni_2(H_2O)_6U_3F_{16}\cdot 3H_2O$ (**2**), and $Ni(H_2O)_2UF_6(H_2O)$ (**3**) were carefully selected and mounted on thin glass fibers with epoxy. The mounted crystals were cooled to –80 °C using an Oxford Cryostream, and optically aligned on a Bruker SMART APEX CCD X-ray diffractometer. Intensity measurements were performed using graphite monochromated Mo-Kα radiation from a sealed tube with a monocapillary collimator. SMART was used for preliminary determination of the cell constants and data collection control. For all compounds, the intensities of reflections of a sphere were collected by a combination of 3 sets of exposures (frames). Each set had a different ϕ angle for the crystal and each exposure covered a range of 0.3° in ω. A total of 1800 frames were collected with an exposure time per frame of 30 s.

For all compounds, determination of integral intensities and global cell refinement were performed with the Bruker SAINT (v 6.02) software package using a narrow-frame integration algorithm. A face-indexed analytical absorption correction was initially

applied using XPREP.[34] Individual shells of unmerged data were corrected analytically and exported in the same format. These files were subsequently treated with a semi-empirical absorption correction with SADABS.[35] The program suite SHELXTL (v 5.1) was used for space group determination (XPREP), direct methods structure solution (XS), and least-squares refinement (XL).[34] Hydrogen atom positions were not located from the difference maps and were not included in the final refinements. The final refinements included anisotropic displacement parameters for all non-hydrogen atoms and a secondary extinction parameter.

RESULTS AND DISCUSSION

Syntheses. The preparation of $Ni(H_2O)_4UF_6 \cdot 1.5H_2O$ (**1**), $Ni_2(H_2O)_6U_3F_{16} \cdot 3H_2O$ (**2**), and $Ni(H_2O)_2UF_6(H_2O)$ (**3**) was accomplished by reacting $Ni(C_2H_3O_2)_2 \cdot 4H_2O$ with $UO_2(C_2H_3O_2)_2 \cdot 2H_2O$ and HF in aqueous media at 200 °C for 3 d followed by slow cooling to promote the growth of high-quality single crystals. In this system use was made of a modified compositional diagram[5,7-10,36-39] to determine the conditions under which various U(IV) solids crystallize. In the course of these studies it was determined that the formation of **1-3** is remarkably sensitive to scale, and consistent isolation of solid U(IV) products could only be ensured by maintaining 20 mmol of HF in the reaction mixtures. The most commonly observed crystalline solids were the less interesting U(IV) fluorides $UF_4 \cdot \frac{1}{3}H_2O$ and $[Ni(H_2O)_6][U_2F_{10}] \cdot 2H_2O$.[33] When the reactions were run at increased temperatures or with increased duration, the occurrence of these latter two compounds dominated compositional space, implying that these may be the result of

thermodynamic control, whereas **1-3** are likely kinetic products. There is no obvious correlation between product and reaction stoichiometry.

A series of control reactions were conducted to determine that the reduction of U(VI) to U(IV) in these syntheses is acid and acetate dependent, and likely corresponds to a decarboxylation reaction of the acetate anion. The reduction of U(VI) to U(IV) has previously been observed in the hydrothermal synthesis of organically templated U(IV) fluorides.[1-3,5,6,8,9,11] In these latter syntheses, aliphatic amines are apparently the reducing agents.[7] For example, the reaction of excess ethylenediamine with UO_3 and HF under hydrothermal conditions results in the reduction of U(VI) to U(IV) and the crystallization of $(C_2H_{10}N_2)U_2F_{10}$ in a nearly quantitative yield.[6] Crystallographic data for **1-3** are shown in Table 3.1.

Structures. $Ni(H_2O)_4UF_6 \cdot 1.5H_2O$ (1). The structure of **1** consists of one-dimensional columns constructed from two interconnected, zigzagging chains of edge-sharing dodecahedral $[UF_8]$ units as shown in Figure 3.1. The sides of the columns are terminated by octahedral *cis*-$[Ni(H_2O)_4F_2]$ polyhedra. The individual chains that edge-share to form the columns of **1** are similar to the one-dimensional $^{1}_{\infty}[MF_{4/1}F_{4/2}]^{4-}$ (M = Zr, U) chains found in several inorganic and organically templated U(IV) and Zr(IV) fluorides.[5,40-46]

The nature of the edge-sharing of the $[UF_8]$ units is such that opposite edges are shared to create the one-dimensional chains running along the *c*-axis, and a single edge approximately orthogonal to the direction of chain propagation is shared to link two such chains together. Therefore, six of the eight fluoride anions surrounding each U(IV)

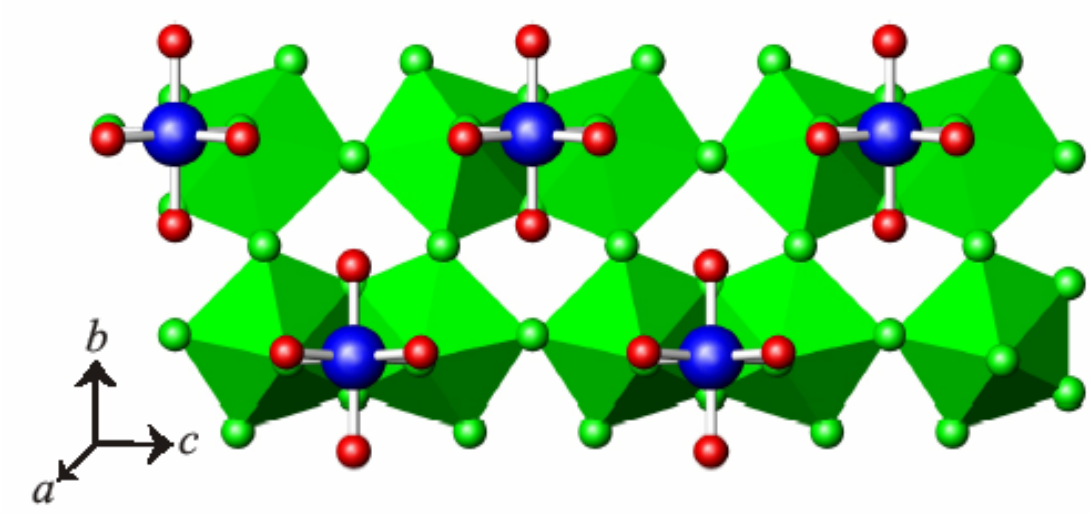

Figure 3.1. A view of the zigzagging chains of edge-sharing dodecahedral [UF_8] units that are linked to form columns in $Ni(H_2O)_4UF_6{\cdot}2.5H_2O$ (**1**). The periphery of these U(IV) fluoride columns are lined with *cis*-[$Ni(H_2O)_2F_4$] octahedra.

Table 3.1. Crystallographic data for $Ni(H_2O)_4UF_6 \cdot 2.5H_2O$ (**1**), $Ni_2(H_2O)_6U_3F_{16} \cdot 3H_2O$ (**2**), and $Ni(H_2O)_2UF_6(H_2O)$ (**3**).

Compound	$Ni(H_2O)_4UF_6 \cdot 2.5H_2O$	$Ni_2(H_2O)_6U_3F_{16} \cdot 3H_2O$	$Ni(H_2O)_2UF_6(H_2O)$
Formula mass	527.84	1297.65	464.79
Crystal system	Orthorhombic	Hexagonal	Monoclinic
Space group	*Cmcm* (No. 63)	$P6_3/mmc$ (No. 194)	$C2/c$ (No. 15)
a (Å)	14.3383(8)	7.9863(5)	12.059(1)
b (Å)	15.6867(8)	7.9863(5)	6.8895(6)
c (Å)	8.0282(4)	16.566(1)	7.9351(7)
α (deg.)	90	90	90
β (deg.)	90	90	92.833(2)
γ (deg.)	90	120	90
V (Å^3)	1805.7(2)	915.0(1)	658.5(1)
Z	8	2	4
T (°C)	–80	–80	–80
λ (Å)	0.71073	0.71073	0.71073
ρ_{calcd} (g cm^{-3})	3.883	4.644	4.689
μ (Mo *K*α, cm^{-1})	201.13	286.67	275.07
R(*F*) for $F_o^2 > 2\sigma(F_o^2)$ [a]	0.0252	0.0237	0.0330
$R_w(F_o^2)$ [b]	0.0692	0.0648	0.0878

[a] $R(F) = \sum \left| |F_o| - |F_c| \right| / \sum |F_o|$. [b] $R_w\left(F_o^2\right) = \left[\sum \left[w\left(F_o^2 - F_c^2\right)^2 \right] / \sum wF_o^4 \right]^{1/2}$.

center are utilized in the formation of the uranium fluoride columns. The two remaining fluoride anions are used to bind the octahedral Ni(II) atoms to the periphery of the columns. The remaining four sites around the Ni(II) centers are occupied by terminal water molecules. This requires the $[Ni(H_2O)_4F_2]$ polyhedra to have a *cis* geometry. The $^{1}_{\infty}[Ni(H_2O)_4UF_6]$ columns are packed together in an interdigitated fashion, and combine to form a channel structure where the channels are filled with occluded water molecules. A view of the channel structure of **1** is shown in Figure 3.2. There are two crystallographically unique water molecules within the channels; one of these is ordered and the other is disordered. The U–F bond distances are within normal ranges and occur from 2.220(4) to 2.425(2) Å. The Ni–O(H_2O) distances of 2.072(5), 2.056(3) (× 2), and 2.081(4) Å are uniformly longer than the two Ni–F distances of 2.003(3) Å, and compare well with those found in $[Ni(H_2O)_6][M_2F_{10}]\cdot 2H_2O$ (M = Ce, U).[104,125] Selected bond distances are summarized in Table 3.2. These bond distances were used to calculate the bond valence sums for the Ni(II) and U(IV) atoms with values of 1.98 and 4.07 being found, respectively.[47,48]

$Ni_2(H_2O)_6U_3F_{16}\cdot 3H_2O$ (2). In contrast to the one-dimensional features found for **1**, the crystal structure of **2** reveals a highly symmetric two-dimensional Ni(II)/U(IV) architecture built from edge-sharing tricapped trigonal prismatic $[UF_9]$ units. The sheets are capped on both sides by $[Ni(H_2O)_3]$ moieties. In this compound a hexagonal planar $[U_3F_3]$ ring is found to repeat throughout the layers. In the center of this ring is a μ_3-F atom residing on a –6*m*2 special position. This central atom also represents the core atom utilized in the simultaneous edge-sharing of three $[UF_9]$ tricapped trigonal prisms where

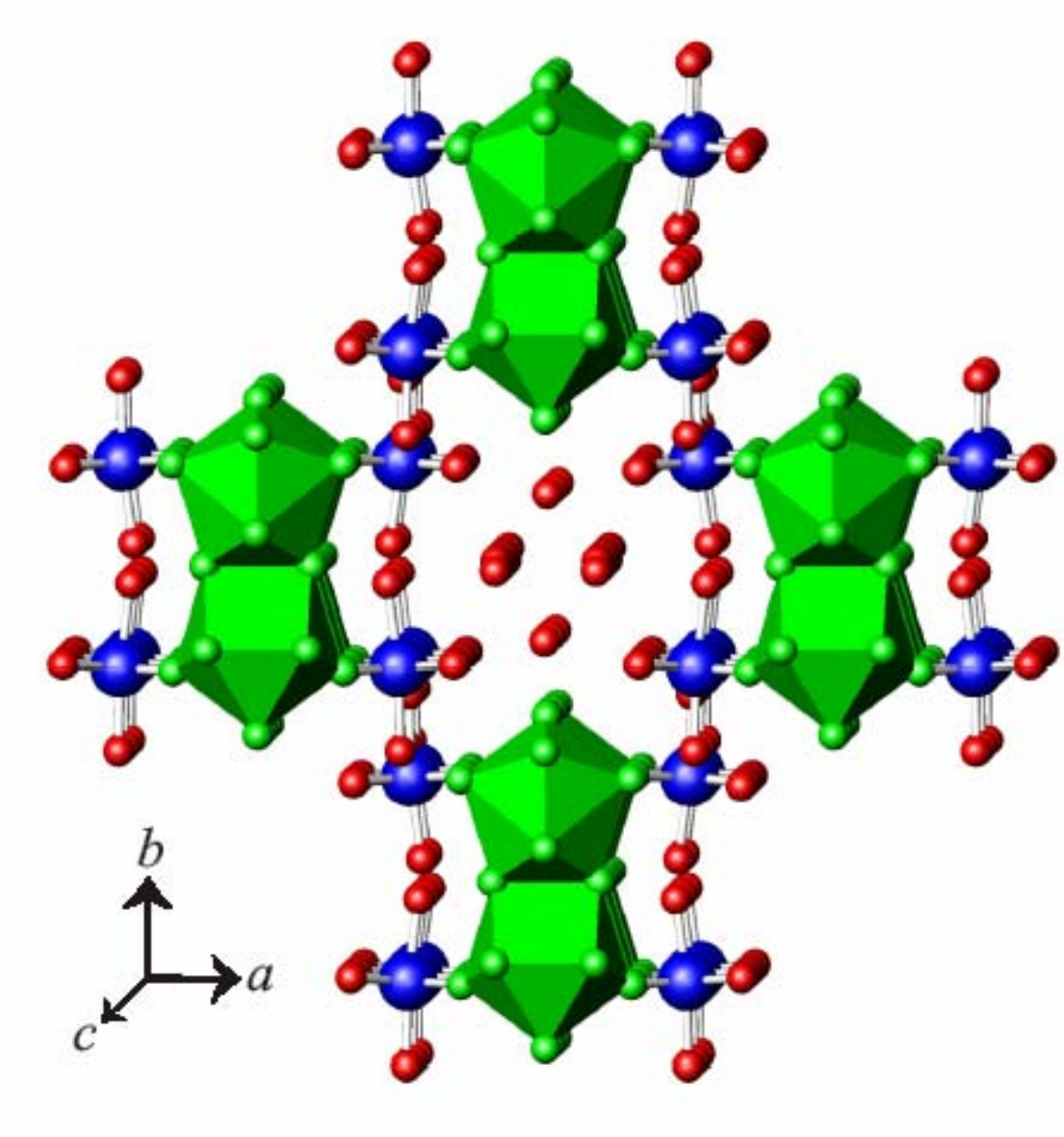

Figure 3.2. A view of the channel structure of $Ni(H_2O)_4UF_6 \cdot 2.5H_2O$ (**1**) formed by the interdigitation of the $Ni(H_2O)_4UF_6$ columns. Ordered and disordered water molecules fill the channels in this compound.

Table 3.2. Selected Bond Distances (Å) for $Ni(H_2O)_4UF_6 \cdot 2.5H_2O$ (**1**).

U(1)–F(1) (× 2)	2.252(3)	Ni(1)–F(1) (× 2)	2.003(3)
U(1)–F(2)	2.357(3)	Ni(1)–O(1)	2.072(5)
U(1)–F(3)	2.220(4)	Ni(1)–O(2) (× 2)	2.056(3)
U(1)–F(4) (× 2)	2.425(2)	Ni(1)–O(3)	2.081(4)
U(1)–F(5)	2.303(3)		
U(1)–F(6) (× 2)	2.390(2)		

each of these units shares two common edges with each other to form a trimer as shown in Figure 3.3. Therefore, while the structure is derived from a single $[UF_9]$ tricapped trigonal prism, the trimer is more useful for visualizing the repeating pattern in the layers. The formation of this fluoride centered ring utilizes three of the nine fluoride anions surrounding each U(IV) center. For each $[UF_9]$ unit an additional four fluoride ligands are occupied in edge-sharing with two neighboring trimers to form the two-dimensional $^{2}_{\infty}[U_3F_{16}]^{4-}$ sheets depicted in Figure 3.4.

The remaining two fluoride ligands in each $[UF_9]$ tricapped trigonal prism are directed above and below each layer. The trimer of edge-sharing $[UF_9]$ therefore has three fluoride ions arranged above and below the rings for the binding of the Ni(II) centers. This necessitates that the $[Ni(H_2O)_3F_3]$ octahedra have a *fac* geometry. The Ni(II) atoms reside directly above and below the μ_3-F atoms in the center of $[UF_{2/1}F_{6/2}F_{1/3}]_3$ trimers and are located on 3*m* sites. A view down the *c*-axis showing the capping of a $^{2}_{\infty}[U_3F_{16}]^{4-}$ sheet with *fac*-$[Ni(H_2O)_3F_3]$ octahedra is shown in Figure 3.5. The remaining water molecules in **2** are located between the layers in channels that run along the *c*-axis. The U–F bond distances range from 2.222(4) to 2.354(3) Å. The three Ni–O(H_2O) distances of 2.061(5) Å are again longer than the three Ni–F bond distances of 2.017(4) Å. Selected bond distances for **2** are summarized in Table 3.3. The bond valence sums for the Ni(II) and U(IV) atoms in **2** were calculated to be 1.97 and 4.14, respectively.[139,140]

$Ni(H_2O)_2UF_6(H_2O)$ (3). The tricapped trigonal prismatic geometry observed for U(IV) in **2** is observed again in **3**. However, one of the fluoride anions has been replaced by a water molecule to yield $[UF_8(H_2O)]$ units. The assignment of this ligand as

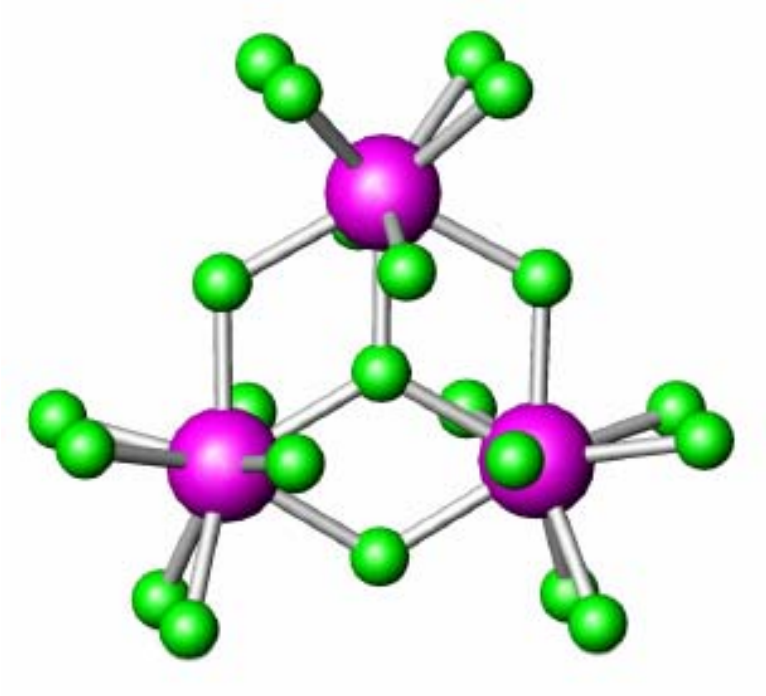

Figure 3.3. A depiction of the cyclic trimer formed from the edge-sharing of three [UF_9] tricapped trigonal prisms in $Ni_2(H_2O)_6U_3F_{16}\cdot 3H_2O$ (**2**).

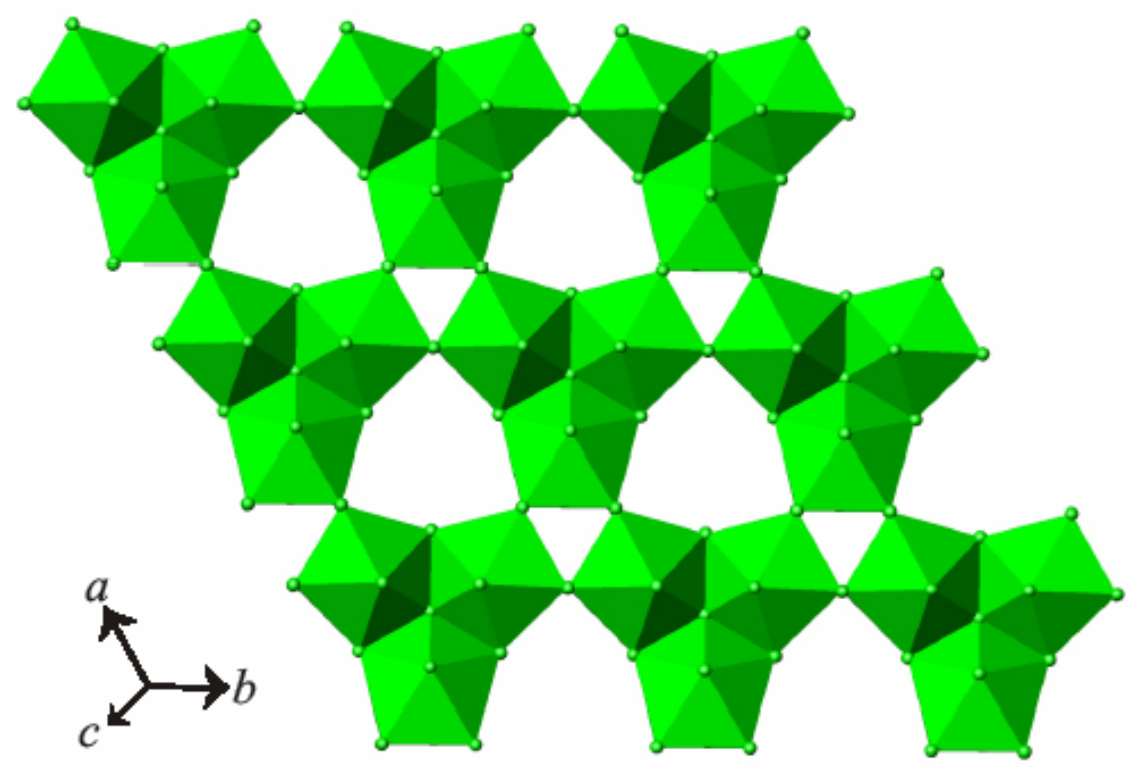

Figure 3.4. A representation of the two-dimensional $^{2}_{\infty}[U_3F_{16}]^{4-}$ sheets created from the edge-sharing of [UF_9] tricapped trigonal prisms with two neighboring trimers formed from these same [UF_9] units in $Ni_2(H_2O)_6U_3F_{16}\cdot 3H_2O$ (**2**).

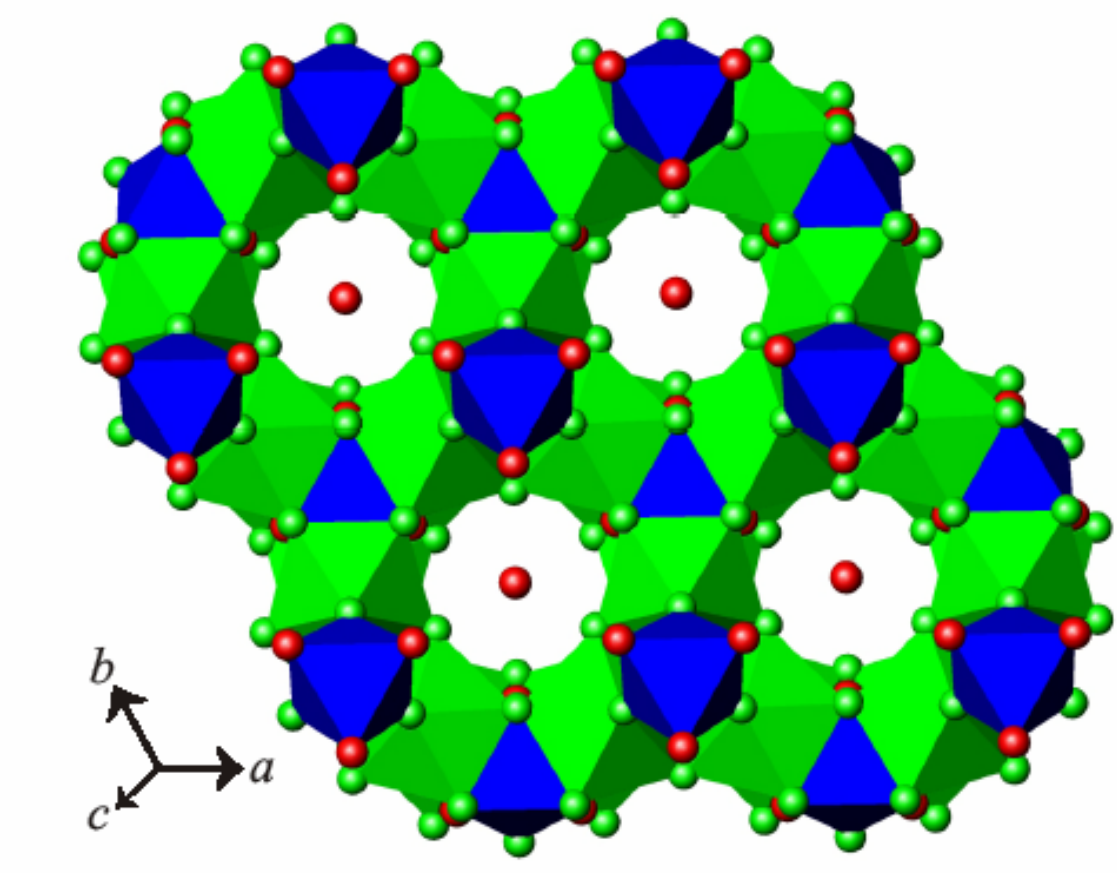

Figure 3.5. A view down the *c*-axis showing the capping of a $^{2}_{\infty}[U_3F_{16}]^{4-}$ sheet with *fac*-$[Ni(H_2O)_3F_3]$ octahedra. Occluded water molecules in **2** are located between the layers in channels that run along the *c*-axis.

Table 3.3. Selected Bond Distances (Å) for $Ni_2(H_2O)_6U_3F_{16}\cdot 3H_2O$ (**2**).

U(1)–F(1) (× 2)	2.354(3)	Ni(1)–F(4) (× 3)	2.017(4)
U(1)–F(2)	2.3261(3)	Ni(1)–O(1) (× 3)	2.061(5)
U(1)–F(3) (× 4)	2.363(2)		
U(1)–F(4) (× 2)	2.222(4)		

water can be inferred from its U–O bond distance of 2.543(9) Å, which is considerably longer than the average U–F distance of 2.309(4) Å in this compound. This designation is also supported by the bond valence sum of the O atom at 0.31, which is well within normal range for bound water molecules. The $[UF_8(H_2O)]$ tricapped trigonal prisms edge-share with one another to form one-dimensional chains as shown in Figure 3.6. Unlike the zigzagging one-dimensional chains found in **1**, the chains of **3** are approximately linear. These chains are in turn linked together by corner-sharing with *trans*-$[Ni(H_2O)_2F_4]$ octahedra into a three-dimensional network.

When viewed down the *c*-axis, as shown in Figure 3.7, it can be seen that both the water molecules bound to the Ni(II) centers and the water molecule ligating the U(IV) atoms are located within channels running down the *c*-axis. The water molecules are sufficiently separated from one another to preclude hydrogen bonding being the driving force behind the formation of this particular structure type. Selected bond distances for **3** are summarized in Table 3.4. The bond valence sums for the Ni(II) and U(IV) atoms in **3** were calculated to be 2.01 and 4.16, respectively.[47,48] An analysis of the bond valence sums for **1-3** reveals little variance in the sums for Ni(II) and U(IV) and supports their assignment in these oxidation states.

CONCLUSIONS

This present study represents the first in a series of investigations that have demonstrated that mixed-metal 3*d* transition metal-U(IV) fluorides with a wide range of structures can be prepared under mild hydrothermal conditions. This preparative and

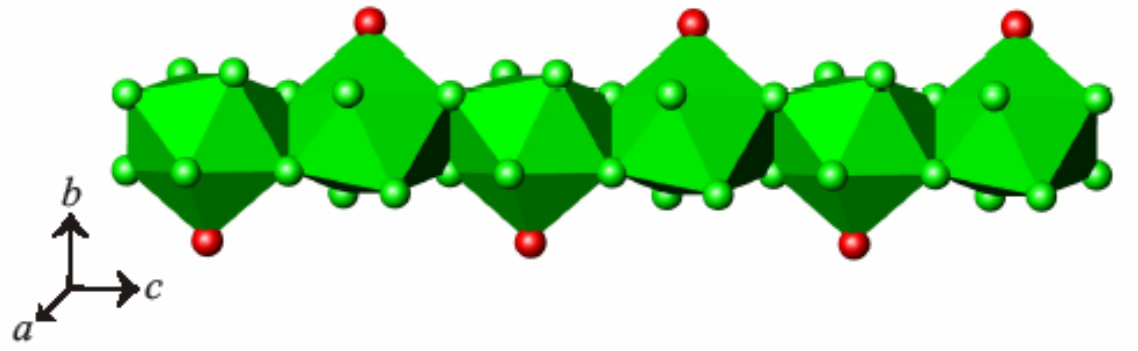

Figure 3.6. The $[UF_8(H_2O)]$ tricapped trigonal prisms in $Ni(H_2O)_2UF_6(H_2O)$ (**3**) edge-share with one another to form one-dimensional chains.

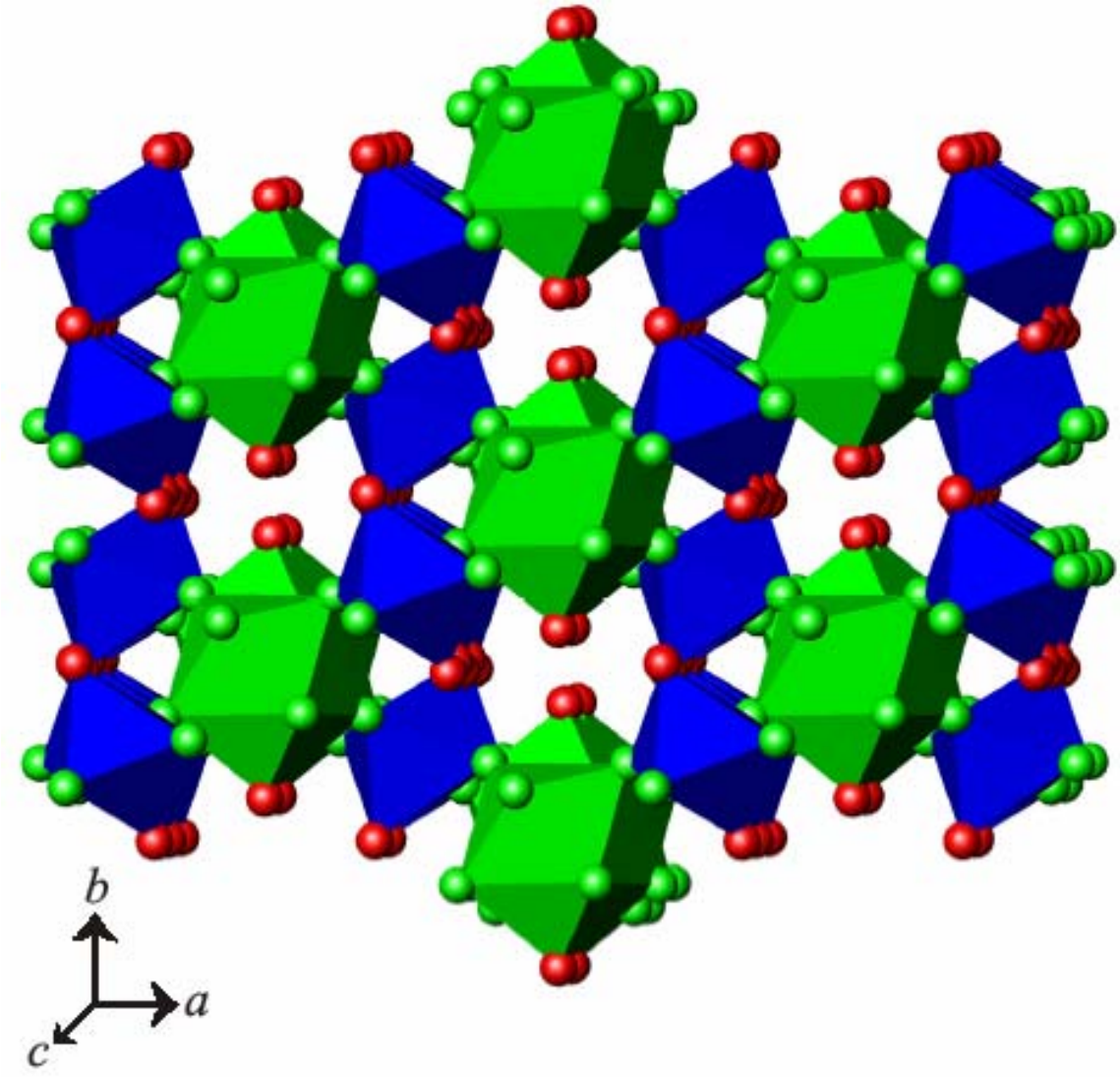

Figure 3.7. A view down the *c*-axis of the three-dimensional network structure of $Ni(H_2O)_2UF_6(H_2O)$ (**3**) demonstrating that both the water molecules bound to the Ni(II) centers and the water molecules ligating the U(IV) atoms reside within channels running along this same axis.

Table 3.4. Selected Bond Distances (Å) for $Ni(H_2O)_2UF_6(H_2O)$ (**3**).

U(1)–F(1) (× 2)	2.244(4)	Ni(1)–F(1) (× 2)	1.990(3)
U(1)–F(2) (× 2)	2.292(4)	Ni(1)–F(2) (× 2)	2.006(3)
U(1)–F(3) (× 2)	2.306(3)	Ni(1)–O(1) (× 2)	2.070(6)
U(1)–F(3)' (× 2)	2.392(4)		
U(1)–O(2)	2.543(9)		

structural study has given rise to ongoing magnetic susceptibility measurements whose goal is to determine whether coupling between the expanded 5*f* orbitals of uranium and n*d* orbitals of transition metals can be mediated by bridging fluoride anions.

Table 3.5. Atomic Coordinates and Equivalent Isotropic Displacement Parameters for $Ni(H_2O)_4UF_6 \cdot 2.5H_2O$ (**1**).

Atom	*x*	*y*	*z*	U_{eq} (Å^2)[a]
U1	0.5	0.129032(13)	0.9968(2)	0.00753(12)
Ni1	0.25783(5)	0.16054(5)	0.75	0.00977(19)
F1	0.35193(18)	0.16476(16)	0.9342(3)	0.0128(5)
F2	0.5	0.2104(3)	0.75	0.0139(10)
F3	0.5	0.2649(2)	0.0739(4)	0.0137(7)
F4	0.5931(3)	0	0	0.0107(8)
F5	0.5	0.0542(3)	0.75	0.0140(10)
F6	0.4124(3)	0.1280(2)	0.25	0.0108(7)
O1	0.2769(3)	0.0296(3)	0.75	0.0147(9)
O2	0.1606(2)	0.1536(2)	0.9378(4)	0.0159(6)
O3	0.2555(3)	0.2932(3)	0.75	0.0128(8)
O4	0.5	0.386(2)	0.75	0.216(15)
O5	0.0878(7)	0.0074(5)	0.0620(12)	0.035(2)

[a] U_{eq} is defined as one-third of the trace of the orthogonalized $\mathbf{U}_{ij}$ tensor.

Table 3.6. Atomic Coordinates and Equivalent Isotropic Displacement Parameters for $Ni_2(H_2O)_6U_3F_{16}\cdot 3H_2O$ (**2**).

Atom	*x*	*y*	*z*	U_{eq} (Å^2)[a]
U1	0.49851(2)	0.50149(2)	0.75	0.00786(18)
Ni1	0.6667	0.3333	0.55152(8)	0.0115(3)
F1	0.3223(8)	0.1612(4)	0.75	0.0163(12)
F2	0.6667	0.3333	0.75	0.0108(18)
F3	0.5599(7)	0.7799(3)	0.6763(2)	0.0179(8)
F4	0.5482(3)	0.4518(3)	0.6224(2)	0.0164(8)
O1	0.4145(8)	0.2073(4)	0.4852(3)	0.0182(10)
O2	0	0	0.6115(11)	0.079(6)
O3	0	0	0.75	0.021(4)

[a] U_{eq} is defined as one-third of the trace of the orthogonalized $\mathbf{U}_{ij}$ tensor.

Table 3.7. Atomic Coordinates and Equivalent Isotropic Displacement Parameters for $Ni(H_2O)_2UF_6(H_2O)$ (**3**).

Atom	*x*	*y*	*z*	U_{eq} (Å^2)[a]
U1	0	0.51807(5)	0.75	0.0053(2)
Ni1	0.25	0.25	1	0.0064(3)
F1	0.1196(3)	0.2862(6)	0.8394(4)	0.0096(8)
F2	0.8294(3)	0.6442(7)	0.8036(4)	0.0106(8)
F3	0.9313(3)	0.6364(7)	0.4938(4)	0.0109(8)
O1	0.1834(7)	0.985(7)	1.0650(10)	0.0121(13)
O2	0	0.88721(3)	0.75	0.021(2)

[a] U_{eq} is defined as one-third of the trace of the orthogonalized $\mathbf{U}_{ij}$ tensor.

REFERENCES

1. Francis, R. J.; Halasyamani, P. S.; O'Hare, D. *Chem. Mater.* **1998**, *10*, 3131.
2. Francis, R. J.; Halasyamani, P. S.; O'Hare, D. *Angew. Chem., Int. Ed. Engl.* **1998**, *37*, 2214.
3. Francis, R. J.; Halasyamani, P. S.; Bee, J. S.; O'Hare, D. *J. Am. Chem. Soc.* **1999**, *121*, 1609.
4. Halasyamani, P. S.; Walker, S. M.; O'Hare, D. *J. Am. Chem. Soc.* **1999**, *121*, 7415.
5. Walker, S. M.; Halasyamani, P. S.; Allen, S.; O'Hare, D. *J. Am. Chem. Soc.* **1999**, *121*, 10513.
6. Almond, P. M.; Deakin, L.; Porter, M. J.; Mar, A.; Albrecht-Schmitt, T. E. *Chem. Mater.* **2000**, *12*, 3208.
7. Talley, C. E.; Bean, A. C.; Albrecht-Schmitt, T. E. *Inorg. Chem*. **2000**, *39*, 5174.
8. Almond, P. M.; Deakin, L.; Mar, A.; Albrecht-Schmitt, T. E. *J. Solid State Chem.* **2001**, *158*, 87.
9. Almond, P. M.; Deakin, L.; Mar, A.; Albrecht-Schmitt, T. E. *Inorg. Chem.* **2001**, *40*, 866.
10. Almond, P. M.; Talley, C. E.; Bean, A. C.; Peper, S. M.; Albrecht-Schmitt, T. E. *J. Solid State Chem.* **2000**, *154*, 635.
11. Cahill, C. L.; Burns, P. C. *Inorg. Chem.* **2001**, *40*, 1347.
12. Sykora, R. E.; Albrecht-Schmitt, T. E. *Chem. Mater.* **2001**, *13*, 4399.
13. Danis, J. A.; Runde, W. H. Scott, B.; Fettinger, J.; Eichhorn, B. *Chem. Comm.* **2001**, *22*, 2378.

14. a) Li, Y.; Burns, P. C. *J. Nucl. Mater.* **2001**, *299*, 219. b) Wang, X.; Haung, J.; Liu, L.; Jacobson, A. J. *J. Mater. Chem.* **2002**, *12*, 406.

15. Doran, M.; Walker, S. M.; O'Hare, D. *Chem. Commun.* **2001**, 1988.

16. Li, Y.; Cahill, C. L.; Burns, P. C. *Chem. Mater.* **2001**, *13*, 4026.

17. Halasayamani, P. S.; Francis, R. J.; Walker, S. M.; O'Hare, D. *Inorg. Chem*. **1999**, *38*, 271.

18. Rastsvetaeva, R. K.; Barinova, A. V.; Fedoseev, A. M.; Budantseva, N. A.; Nekrasov, Yu. V. *Dokl. Akad. Nauk* **1999**, *365*, 68.

19. Krivovichev, S. V.; Burns, P. C. *Can. Mineral*. **2000**, *38*, 847.

20. Khrustalev, V. N.; Andreev, G. B.; Antipin, M. Yu.; Fedoseev, A. M.; Budantseva, N. A.; Shirokova, I. B. *Zh. Neorg. Khim*. **2000**, *45*, 1996.

21. Andreev, G. B.; Antipin, M. Yu.; Fedoseev, A. M.; Budantseva, N. A. *Koord. Khim*. **2001**, *27*, 227.

22. Krivovichev, S. V.; Burns, P. C. *Can. Mineral*. **2001**, *39*, 207.

23. Krivovichev, S. V.; Burns, P. C. *Can. Mineral*. **2001**, *39*, 197.

24. Krivovichev, S. V.; Finch, R. J.; Burns, P. C. *Can. Mineral*. **2002**, *40*, 193.

25. Krivovichev, S. V.; Burns, P. C. *Can. Mineral*. **2002**, *40*, 201.

26. Krivovichev, S. V.; Cahill, C. L.; Burns, P. C. *Inorg. Chem*. **2002**, *41*, 34.

27. Krivovichev, S. V.; Burns, P. C. *Inorg. Chem*. **2002**, *41*, 4108.

28. Sykora, R. E.; Wells, D. M.; Albrech-Schmitt, T. E. *Inorg. Chem*. **2002**, *41*, 2304.

29. Sykora, R. E.; McDaniel, S. M.; Wells, D. M.; Albrecht-Schmitt, T. E. *Inorg. Chem*. **2002**, *41*, 5126.

30. Ivanov, S. B.; Mikhailov, Y. N.; Davidovich, R. L. *Koord. Khim.* **1982**, *8*, 1250.

31. Ivanov, S. B.; Mikhailov, Y. N.; Kuznetsov, V. G.; Davidovich, R. L. *J. Struct. Chem.* **1981**, *22*, 302.

32. Mikhailov, Y. N.; Udovenko, A. A.; Kuznetsov, V. G.; Butman, L. A.; Kokh, L. A. *Zh. Strukt. Khim.* **1973**, *14*, 170.

33. Charpin, P.; Montoloy, F.; Nierlich, M. C. R. *Acad. Sci., Paris, Ser. C* **1968**, *266*, 1685.

34. Sheldrick, G. M. SHELXTL PC, Version 5.0, An Integrated System for Solving, Refining, and Displaying Crystal Structures from Diffraction Data; Siemens Analytical X-Ray Instruments, Inc.: Madison, WI 1994.

35. *SADABS*. Program for absorption correction using SMART CCD based on the method of Blessing: Blessing, R. H. *Acta Crystallogr.* **1995**, *A51*, 33.

36. Halasyamani, P. S.; Willis, M. J.; Lundquist, P. M.; Stern, C. L.; Wong, G. K.; Poeppelmeier, K. R. *Inorg. Chem.* **1996**, *35*, 1367.

37. Harrison, W. T. A.; Dussack, L. L.; Jacobson, A. J. *J. Solid State Chem.* **1996**, *125*, 234.

38. Norquist, A. J.; Heier, K. R.; Stern, C. L.; Poeppelmeier, K. R. *Inorg. Chem.* **1998**, *37*, 6495.

39. Welk, M. E.; Norquist, A. J.; Stern, C. L.; Poeppelmeier, K. R. *Inorg. Chem.* **2000**, *39*, 3946.

40. Ross, C. R., II; Paulsen, B.; Nielson, R. M.; Abrahams, S. C. *Acta Crystallogr.* **1998**, *B54*, 417.

41. Gerasimenko, A. V.; Bukvetskii, B. V.; Davidovich, R. L.; Kondratyuk, N. P. *Koord. Khim.* **1989**, *15*, 130.

42. Penneman, R. A.; Ryan, R. R.; Rosenzweig, A. *Struct. Bonding* **1973**, *13*, 1.

43. Laval, J. P.; Mercurio-Lavaud, D.; Gaudreau, B. *Rev. Chim. Mineral.* **1974**, *11*, 742.

44. Hoppe, R.; Mehlhorn, B. *Z. Anorg. Allg. Chem.* **1976**, *425*, 200.

45. Sykora, R. E.; Ruf, M.; Albrecht-Schmitt, T. E. *J. Solid State Chem.* **2001**, *159*, 198.

46. Laval, J. P.; Papiernik, R.; Frit, B. *Acta Crystallogr.* **1978**, *B34*, 1070.

47. Brown, I. D.; Altermatt, D. *Acta Crystallogr.* **1985**, *B41*, 244.

48. Brese, N. E.; O'Keeffe, M. *Acta Crystallogr.* **1991**, *B47*, 192.

Chapter 4

STRUCTURE AND PROPERTIES OF THE THORIUM VANADYL TELLURATE, $Th(VO_2)_2(TeO_6)(H_2O)_2$

ABSTRACT

The hydrothermal reaction of $Th(NO_3)_4 \cdot xH_2O$ with V_2O_5 and H_6TeO_6 at 200 °C under autogenous pressure results in the formation of $Th(VO_2)_2(TeO_6)(H_2O)_2$ as a pure phase. The single crystal X-ray data indicates that $Th(VO_2)_2(TeO_6)(H_2O)_2$ possesses a three-dimensional structure constructed from ThO_9 tricapped trigonal prisms, VO_5 distorted square pyramids, VO_4 distorted tetrahedra, and TeO_6 distorted octahedra. Both of the vanadium polyhedra contain VO_2^+ vanadyl units with two short V=O bond distances. The tellurate octahedron is tetragonally distorted, and utilizes all of its oxygen atoms to bond to adjacent metal centers, sharing edges with ThO_9 and VO_5 units, and corners with two ThO_9, one VO_5, and two VO_4 polyhedra. Crystallographic data: $Th(VO_2)_2(TeO_6)(H_2O)_2$, orthorhombic, space group *Pbca*, a = 12.6921(7), b = 11.5593(7), c = 13.0950(8) Å, Z = 8 (T = 193 K). The UV-vis diffuse reflectance spectrum of $Th(VO_2)_2(TeO_6)(H_2O)_2$ shows vanadyl-based charge-transfer absorption features. $Th(VO_2)_2(TeO_6)(H_2O)_2$ decomposes primarily to $Th(VO_3)_4$ when heated at 600 °C in air.

INTRODUCTION

Periodate, IO_6^{5-}, and tellurate, TeO_6^{6-}, have played pivotal roles in the isolation of transition metal complexes with unusually high oxidation states.[1] The tellurate anion has been shown to stabilize Ru(VI) and Os(VI) in $Na_6[RuO_2\{TeO_4(OH)_2\}_2]\cdot 16H_2O$[2] and $Rb_2Na_4[OsO_2\{TeO_4(OH)_2\}_2]\cdot 18H_2O$,[3] Pd(IV) in $Na_8K_2H_4[Pd_2Te_4O_{24}H_2]\cdot 20H_2O$,[4] Cu(III) in $Na_5[Cu\{TeO_4(OH)_2\}_2]\cdot 16H_2O$,[5] Ag(III) in $Na_5[Ag\{TeO_4(OH)_2\}_2]\cdot 16H_2O$,[2] and Au(III) in $Na_5[Au\{TeO_4(OH)_2\}_2]\cdot 16H_2O$.[6] By comparison, well-characterized examples of actinide periodate and tellurate complexes are sparse.[1] There are only two known uranyl periodates, $A[(UO_2)_3(HIO_6)_2(OH)(O)(H_2O)]\cdot 1.5H_2O$ (A = Li – Cs, Ag)[7] and $K_2[(UO_2)_2(VO)_2(IO_6)_2O]\cdot H_2O$,[8] both of which possess polar open-framework structures, and no known examples of actinide tellurate compounds.[1] In addition to offering the possibility of stabilizing high oxidation states in actinides, periodate and tellurate provide the opportunity to build structures with three-dimensional connectivity[9,10] owing to their approximately octahedral geometries and their ability to bind a large number of metal centers.[1,5,6]

In an effort to understand the structural chemistry of tellurate with actinides we have investigated the reaction of Th(IV) salts with a variety of tellurate sources, primarily under mild hydrothermal conditions. These studies have resulted in the isolation of the mixed-metal thorium vanadyl tellurate, $Th(VO_2)_2(TeO_6)(H_2O)_2$, which represents the first actinide tellurate whose constitution is unambiguously defined. This compound also provides information on vanadyl tellurate coordination, which is also absent from the literature. Herein we report the structure and properties of $Th(VO_2)_2(TeO_6)(H_2O)_2$.

EXPERIMENTAL

Syntheses. $Th(NO_3)_4 \cdot xH_2O$ (99%, Alfa-Aesar), V_2O_5 (99.9%, Alfa-Aesar), and H_6TeO_6 (99.5%, Alfa-Aesar) were used as received. Reactions were performed in PTFE-lined Parr 4749 autoclaves. Distilled and Millipore-filtered water with a resistance of 18.2 MΩ·cm was used in all reactions. Standard precautions were performed for handling radioactive materials during work with $Th(NO_3)_4 \cdot xH_2O$ and $Th(VO_2)_2(TeO_6)(H_2O)_2$. Semi-quantitative SEM/EDX analyses were performed using a JEOL 840/Link Isis instrument. Th, V, and Te percentages were calibrated against standards. The IR spectrum was collected on a Nicolet 5PC FT-IR spectrometer from a KBr pellet.

$Th(VO_2)_2(TeO_6)(H_2O)_2$. $Th(NO_3)_4 \cdot xH_2O$ (0.2812 g, 0.5857 mmol), V_2O_5 (0.1061 g, 0.5834 mmol), and H_6TeO_6 (0.1128 g, 0.4912 mmol) were loaded into a 23-mL PTFE-lined autoclave. Water (1 mL) was then added to the reaction mixture. The autoclave was sealed and placed into a box furnace and heated to 200 °C. After 6 d the reaction was cooled at a rate of 9 °C/h to 23 °C. The product mixture consisted of clusters of acicular yellow crystals in a green mother liquor. The mother liquor was decanted, and the crystals were then washed with water and methanol and allowed to dry. Yield, 299 mg (79% based on Th). Phase purity was confirmed by powder X-ray diffraction measurements. The measured powder pattern was compared with a pattern calculated from single crystal X-ray data using ATOMS (v. 5, Shape Software). No extraneous diffraction peaks were observed. IR (KBr, cm^{-1}): 1613 (δ, H_2O, w), 979 (ν, VO_2^+, s), 964 (ν, VO_2^+, s), 955 (ν, VO_2^+, s), 930 (ν, VO_2^+, s), (ν, V–O, Te–O, Th–O) 862

(s), 843 (m), 821 (w), 796 (w, sh), 760 (s), 724 (w, sh), 695 (s). EDX measurements show a Th:V:Te ratio of approximately 1(27%):2(47%):1(26%).

Thermal Analysis. Thermal data for $Th(VO_2)_2(TeO_6)(H_2O)_2$ were collected using a TA Instruments, Model 2920 Differential Scanning Calorimeter (DSC) and a TA Q50 Thermogravimetric Analyzer (TGA). Samples (~20 mg) were encapsulated in aluminum or platinum pans and heated at 10 °C/min from 25 °C to 600 °C under a nitrogen atmosphere.

UV-vis Diffuse Reflectance Spectra. The diffuse reflectance spectrum of $Th(VO_2)_2(TeO_6)(H_2O)_2$ was measured from 1800 to 200 nm using a Shimadzu UV3100 spectrophotometer equipped with an integrating sphere attachment with $BaSO_4$ being used as the standard. The Kubelka-Monk function was used to convert diffuse reflectance data to absorbance spectra.[11]

X-ray Powder Diffraction Data. Powder diffraction data were collected using a Rigaku Miniflex powder diffractometer using Cu Kα (λ = 1.54056 Å) radiation. Data were compared with patterns from the ICDD database or with those calculated directly from single crystal data using ATOMS.

Crystallographic Studies. A single crystal of $Th(VO_2)_2(TeO_6)(H_2O)_2$ was mounted on a glass fiber and aligned on a Bruker SMART APEX CCD X-ray diffractometer. Intensity measurements were performed using graphite monochromated Mo Kα radiation from a sealed tube and monocapillary collimator. SMART (v 5.624) was used for preliminary determination of the cell constants and data collection control. The intensities of reflections of a sphere were collected by a combination of 3 sets of exposures (frames). Each set had a different ϕ angle for the crystal and each exposure

covered a range of 0.3° in ω. A total of 1800 frames were collected with an exposure time per frame of 30 s.

For $Th(VO_2)_2(TeO_6)(H_2O)_2$ determination of integrated intensities and global refinement were performed with the Bruker SAINT (v 6.02) software package using a narrow-frame integration algorithm. A face-indexed analytical absorption correction was initially applied using XPREP, where individual shells of unmerged data were corrected analytically.[12] These files were subsequently treated with a semiempirical absorption correction by SADABS.[13] The program suite SHELXTL (v 6.12) was used for space group determination (XPREP), direct methods structure solution (XS), and least-squares refinement (XL).[12] The final refinements included anisotropic displacement parameters for all atoms. Secondary extinction was not noted. Some crystallographic details are given in Table 4.1.

RESULTS AND DISCUSSION

Synthesis. The challenge in preparing actinide tellurates and periodates is that these anions oxidize water and are reduced by two electrons from Te(VI) or I(VII) to Te(IV) or I(V). Under hydrothermal conditions these processes occur quite rapidly, and coincidentally are a convenient method for crystallizing tellurite and iodate compounds.[14-18] During the preparation of $K_2[(UO_2)_2(VO)_2(IO_6)_2O]\cdot H_2O$[8] it was discovered that the presence of V_2O_5 inhibits the reduction of periodate. We therefore applied this method to the synthesis of thorium tellurates and found that the reaction of $Th(NO_3)_4\cdot xH_2O$ with V_2O_5 and telluric acid results in the isolation of a desired product,

Table 4.1. Crystallographic Data for $Th(VO_2)_2(TeO_6)(H_2O)_2$.

Formula	$Th(VO_2)_2(TeO_6)(H_2O)_2$
Formula Mass	657.55
Color and habit	yellow needle
Crystal System	orthorhombic
Space group	*Pbca* (No. 61)
a (Å)	12.6921(7)
b (Å)	11.5593(7)
c (Å)	13.0950(8)
V (Å^3)	1921.2(2)
Z	8
T (K)	193
λ (Å)	0.71073
Maximum 2θ (deg.)	56.58
ρ_{calcd} (g cm^{-3})	4.519
μ(Mo *K*α) (cm^{-1})	203.83
R(*F*) for F_o^2 >	0.0250
$R_w(F_o^2)$ [b]	0.0622

[a] $R(F) = \sum \left| |F_o| - |F_c| \right| / \sum |F_o|$. [b] $R_w\left(F_o^2\right) = \left[\sum \left[w\left(F_o^2 - F_c^2\right)^2 \right] / \sum wF_o^4 \right]^{1/2}$.

$Th(VO_2)_2(TeO_6)(H_2O)_2$, that contains Th(IV), V(V), and Te(VI), in both high yield and purity.

Structure of $Th(VO_2)_2(TeO_6)(H_2O)_2$. The structure of $Th(VO_2)_2(TeO_6)(H_2O)_2$ is three-dimensional in nature, and is constructed from ThO_9 tricapped trigonal prisms, VO_5 distorted square pyramids, VO_4 distorted tetrahedra, and TeO_6 distorted octahedra. An ORTEP diagram showing these building units is shown in Figure 4.1. The oxidation states can be assigned in this compound as Th(IV), V(V) at both sites, and Te(VI). The Th–O bond distances range from 2.282(4) to 2.601(5) Å. The ThO_9 units share one edge with the VO_5 polyhedra and a second edge with the TeO_6 octahedra. This unit has six additional corner-sharing interactions: two with the VO_5 distorted square pyramids, two with the VO_4 distorted tetrahedra, and two more with the TeO_6 octahedra. These interactions result in three μ_3-O atoms (O(3), O(4), and O(5)), and four μ_2-O atoms (O(2), O(6), O(7), and O(10)). The two remaining oxygen atoms (O(11) and O(12)) are concluded to be water molecules based on their long Th–O bond distances of 2.564(5) and 2.601(5) Å, their bond valence sums of 0.34 and 0.31, charge balance requirements, and the presence of water stretching and bending modes in the IR spectrum. Selected bond distances and angles are given in Table 4.2.

There are two crystallographically unique vanadium atoms in $Th(VO_2)_2(TeO_6)(H_2O)_2$ in two different coordination environments. V(1) is in a five-coordinate distorted square pyramidal geometry. V(2) meanwhile is found in a distorted tetrahedral environment. Both of the V(V) polyhedra contain a VO_2^+ vanadyl unit with two short V=O bond distances. V(1) has vanadyl oxygen bond lengths of 1.628(5) and

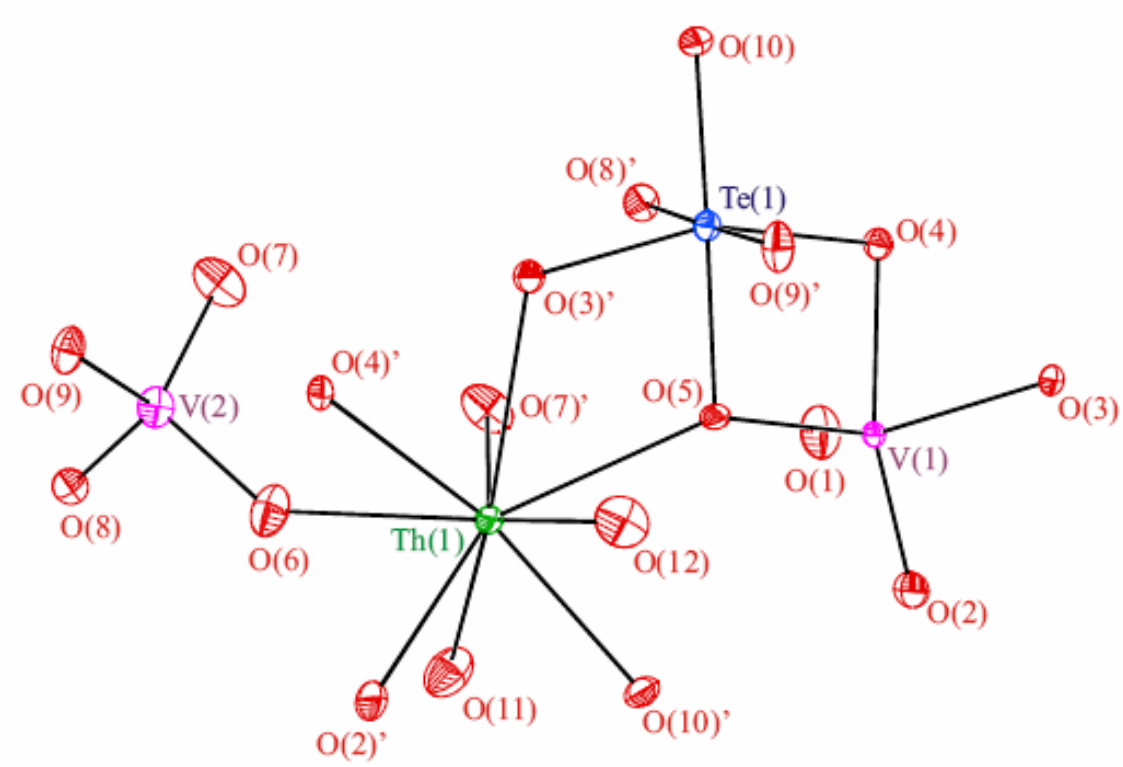

Figure 4.1. A view of the ThO_9 tricapped trigonal prisms, VO_5 distorted square pyramids, VO_4 distorted tetrahedra, and TeO_6 distorted octahedra in $Th(VO_2)_2(TeO_6)(H_2O)_2$. 50% probability ellipsoids are depicted.

Table 4.2. Selected Bond Distances (Å) and Angles (°) for $Th(VO_2)_2(TeO_6)(H_2O)_2$.

Distances (Å)			
Th(1)–O(2)	2.384(4)	V(1)–O(4)	2.044(4)
Th(1)–O(3)	2.479(4)	V(1)–O(5)	1.929(4)
Th(1)–O(4)	2.430(4)	V(2)–O(6)	1.654(5)
Th(1)–O(5)	2.528(4)	V(2)–O(7)	1.654(5)
Th(1)–O(6)	2.455(5)	V(2)–O(8)	1.771(4)
Th(1)–O(7)	2.400(5)	V(2)–O(9)	1.801(4)
Th(1)–O(10)	2.282(4)	Te(1)–O(3)	1.921(4)
Th(1)–O(11)	2.564(5)	Te(1)–O(4)	1.907(4)
Th(1)–O(12)	2.601(5)	Te(1)–O(5)	1.943(4)
V(1)–O(1)	1.628(5)	Te(1)–O(8)	1.948(4)
V(1)–O(2)	1.671(5)	Te(1)–O(9)	1.953(4)
V(1)–O(3)	1.945(4)	Te(1)–O(10)	1.829(4)
Angles (°)			
O(1)–V(1)–O(2)	106.3(3)	O(6)–V(2)–O(7)	111.2(3)
O(10)–Te(1)–O(4)	101.61(17)	O(3)–Te(1)–O(4)	159.49(17)
O(10)–Te(1)–O(3)	98.90(17)	O(10)–Te(1)–O(5)	178.60(19)
O(4)–Te(1)–O(5)	78.98(17)	O(3)–Te(1)–O(5)	80.51(17)
O(10)–Te(1)–O(8)	88.04(19)	O(4)–Te(1)–O(8)	88.73(17)
O(3)–Te(1)–O(8)	91.61(17)	O(5)–Te(1)–O(8)	90.71(18)
O(10)–Te(1)–O(9)	90.20(19)	O(4)–Te(1)–O(9)	92.84(17)
O(3)–Te(1)–O(9)	87.44(17)	O(5)–Te(1)–O(9)	91.04(18)
O(8)–Te(1)–O(9)	177.84(18)		

1.671(5) Å to O(1) and O(2), respectively, and an O(1)–V(1)–O(2) bond angle of 106.3(3)°. The shorter V(1)–O(1) bond distance reflects its terminal nature. The remaining four oxygen atoms in the $V(1)O_5$ units are bridging. The distortion of the $V(1)O_5$ unit is evident in the bond angles of the square base of the unit. The O(3)–V(1)–O(4) angle is 74.84(17)°, which is close to that of the adjacent O(4)–V(1)–O(5) angle of 76.02(16)°. An examination of the remaining base angles shows this distortion with O(2)–V(1)–O(3) and O(2)–V(1)–O(5) having bonding angles of 94.97(19)° and 99.47(19)° degrees, respectively. The VO_5 polyhedron contains several interactions to adjacent polyhedra. There are two edge-sharing interactions: one with a ThO_9 unit and a second with a TeO_6 unit, both involving μ_3-O(4). The O(3) and O(5) atoms are also μ_3 because the VO_5 unit utilizes O(3) and O(5) to edge-share or corner-share with either a ThO_9 tricapped trigonal prism or a TeO_6 octahedron. A depiction of these complex combinations is shown in Figure 4.2a.

The tetrahedral VO_4 units containing V(2) are distorted from ideality. The bond distances observed within the vanadyl unit of VO_4 tetrahedron are similar to those found within VO_5 unit with a distance of 1.654(5) Å to both O(6) and O(7), and a bond angle of 111.2(3)°. The remaining V–O bond lengths are V(2)–O(8) at 1.771(4) Å, and V(2)–O(9) at 1.801(4) Å. The bond angles range from 105.3(2)° to 119.2(2)°. The VO_4 units only corner-share with adjacent polyhedra, leaving all oxygen atoms as bridging: O(6) and O(7) to Th(1) and O(8) and O(9) to Te(1). A view of these interactions is shown in Figure 4.2b.

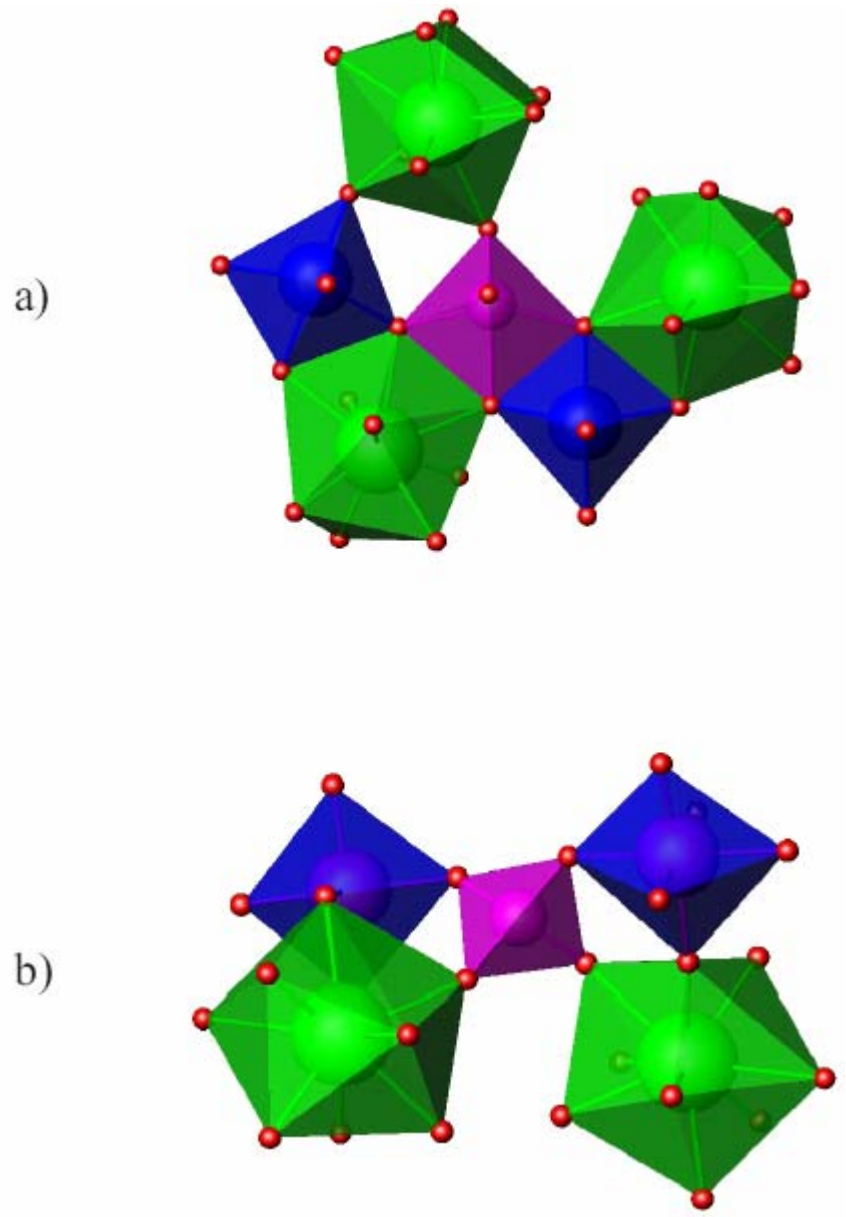

Figure 4.2. a) A depiction of the interactions between the VO_5 distorted square pyramids and neighboring polyhedra in $Th(VO_2)_2(TeO_6)(H_2O)_2$. Edge-sharing occurs with one ThO_9 unit and one TeO_6 unit. Corner-sharing occurs with two additional ThO_9 tricapped trigonal prisms and one TeO_6 octahedron. b) The VO_4 units corner-share with two ThO_9 units and two TeO_6 units. Vanadium polyhedra are shown in magneta, thorium in green, and tellurium in blue.

The tellurate anions, containing Te(VI), are highly distorted from idealized octahedral symmetry with Te–O bond distances ranging from 1.829(4) to 1.953(4) Å. The distortion is approximately tetragonal in nature and is in the direction of O(10), this being the shortest Te–O bond distance of 1.829(4) Å. The O–Te–O bond angles given in Table 4.2 also demonstrate the deviation of the tellurate anion from octahedral symmetry. The TeO_6^{6-} anion utilizes all of its oxygen atoms to bond to adjacent polyhedra with one edge-sharing interaction with a ThO_9 unit and another with a VO_5 unit. Corner-sharing interactions also occur with two ThO_9, one VO_5, and two VO_4 polyhedra as shown in Figure 4.3. These bonds result in three μ_2-O atoms (O(3), O(4), and O(5)) as well as three μ_3-O atoms (O(8), O(9), and O(10)).

The triad that forms from the ThO_9, VO_5, and TeO_6 through edge-sharing is the essential building block of part of the structure of $Th(VO_2)_2(TeO_6)(H_2O)_2$. These units form a continuum of edge-sharing interactions to create Th-V-Te oxide chains, which extend along the *b*-axis as shown in Figure 4.4. Corner-sharing interactions between the TeO_6 and VO_5 units and the Th centers of adjacent chains lead to the formation of two-dimensional sheets in the [*ab*] plane. The three-dimensional network is formed by the linkage of these sheets through the VO_4 units, as in shown in Figure 4.5. The VO_4 tetrahedra bridge the Th and Te centers from one sheet to thorium and tellurium in an adjacent sheet in the *c* direction.

Optical Properties. The optical properties of $Th(VO_2)_2(TeO_6)(H_2O)_2$ have been evaluated using UV-vis diffuse reflectance spectroscopy (Figure 4.6). This compound displays a weak absorption band near 387 nm that is followed by strong absorption at approximately 600 nm. The spectrum is similar that of other vanadyl oxoanion

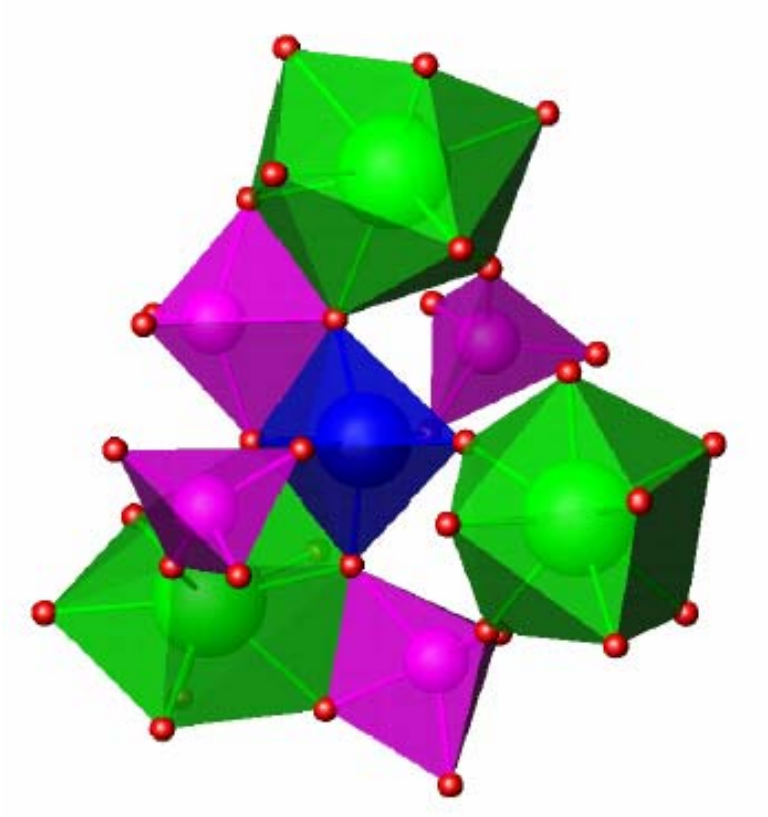

Figure 4.3. An illustration of the bonding for the tellurate, TeO_6^{6-}, anion in $Th(VO_2)_2(TeO_6)(H_2O)_2$. All six oxygen atoms are used to bind neighboring metal centers resulting in two edge-sharing interactions with a ThO_9 unit and one with a VO_5 unit. Corner-sharing interactions also occur with one ThO_9, one VO_5, and two VO_4 polyhedra. Vanadium polyhedra are shown in magenta, thorium in green, and tellurium in blue.

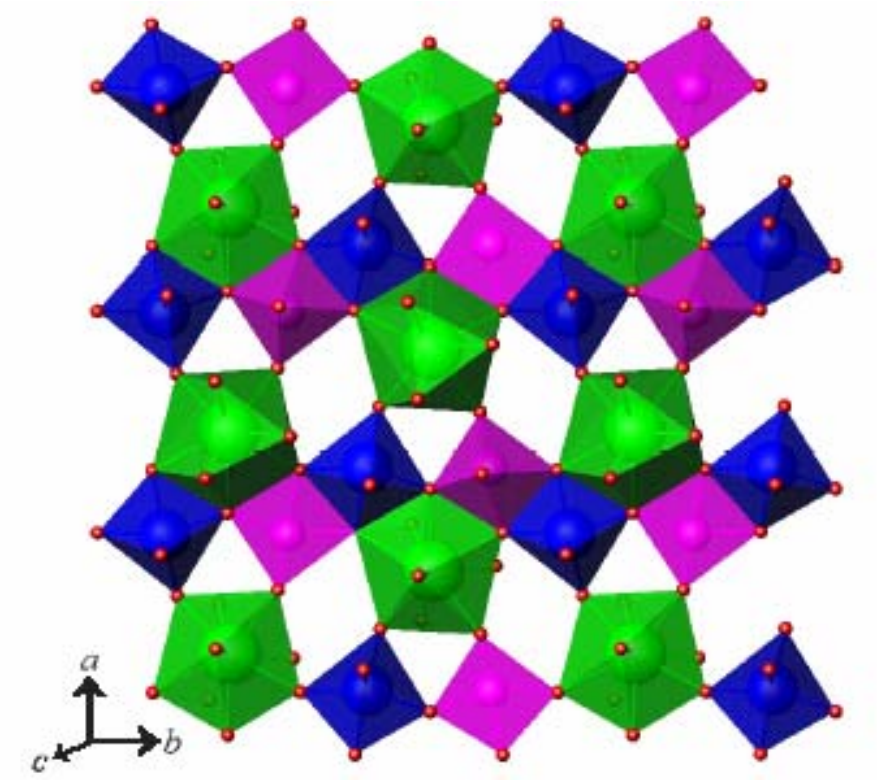

Figure 4.4. A view of the ThO_9, VO_5, and TeO_6 units that form a continuum of edge-sharing interactions to yield Th-V-Te oxide chains that extends along the *b*-axis. Corner-sharing interactions between TeO_6 and VO_5 units and the Th centers of adjacent chains form two-dimensional sheets in the [*ab*] plane.

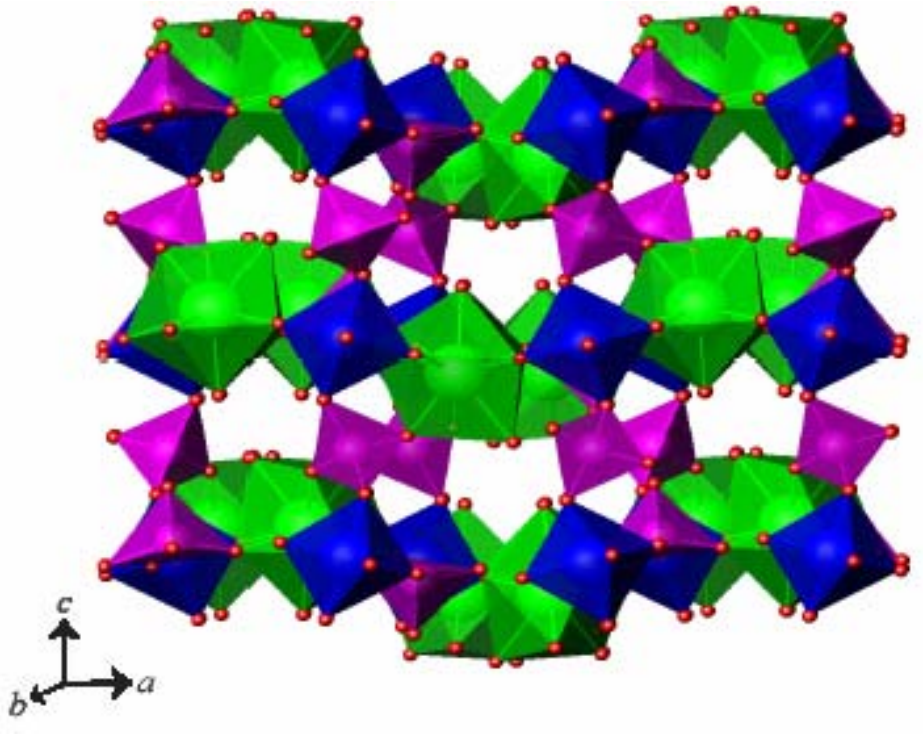

Figure 4.5. The three-dimensional network of $Th(VO_2)_2(TeO_6)(H_2O)_2$ is formed by the linkage of these sheets through the VO_4 units. The VO_4 tetrahedra bridge the Th and Te centers from one sheet to thorium and tellurium in an adjacent sheet in the *c* direction. Vanadium polyhedra are shown in magenta, thorium in green, and tellurium in blue.

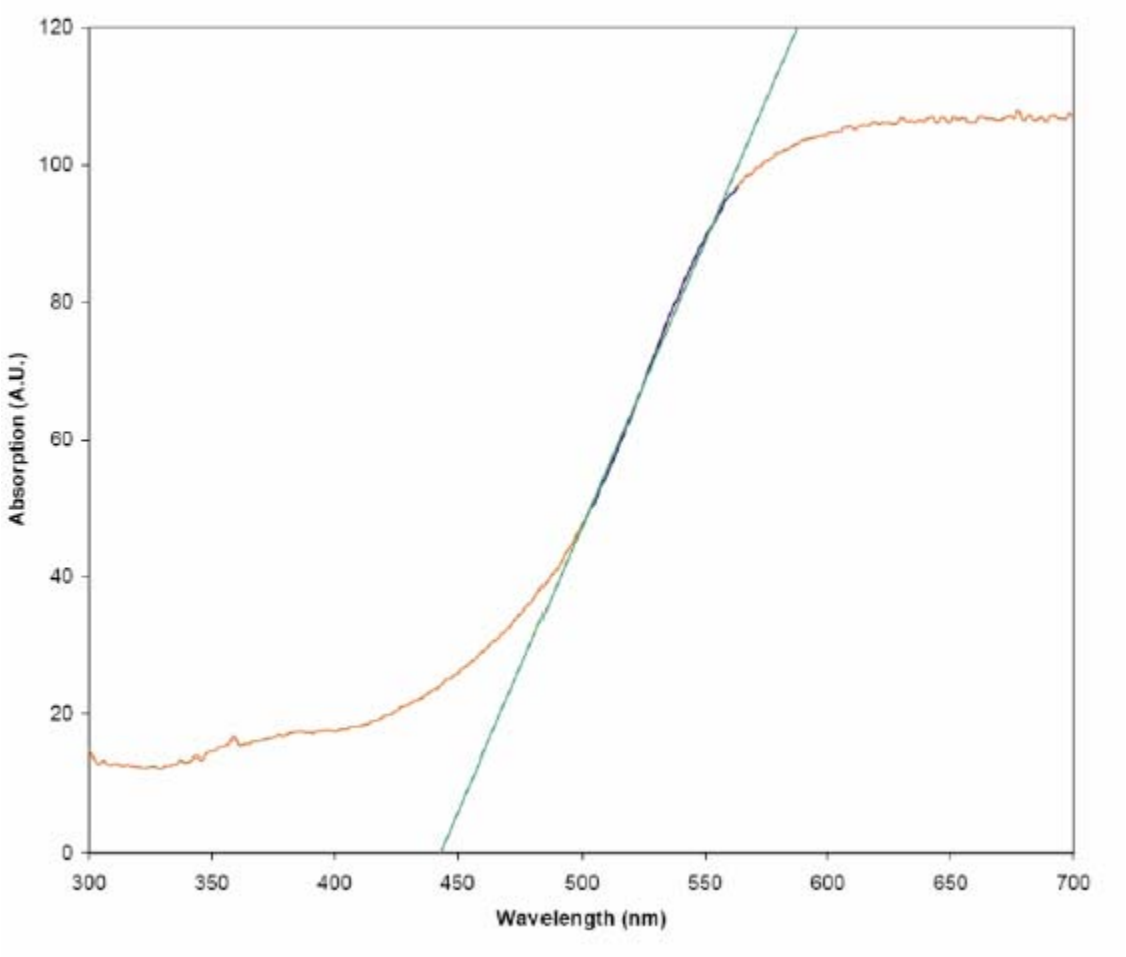

Figure 4.6. The diffuse reflectance absorbance spectrum of $Th(VO_2)_2(TeO_6)(H_2O)_2$ featuring a weak absorption band near 387 nm that is followed by strong absorption feature at approximately 600 nm.

compounds such as $A[VO_2(IO_3)_2]$ (A = K, Rb) and $A[(VO)_2(IO_3)_3O_2]$ (A = NH_4, Rb, Cs).[19] It is likely that the visible absorption for $Th(VO_2)_2(TeO_6)(H_2O)_2$ can be attributed to charge-transfer in the vanadyl units.

Thermal Behavior. Differential scanning calorimetry measurements on $Th(VO_2)_2(TeO_6)(H_2O)_2$ show that the compound is stable to approximately 250 °C, thereafter it begins to lose water with an endotherm centered at 282 °C. This is followed by further decomposition with three endotherms at 418, 456, and 472 °C following by a small exotherm at 534 °C. TGA measurements show that the endotherm near 456 °C is associated with the loss of Te from the sample (Figure 4.7). $Th(VO_2)_2(TeO_6)(H_2O)_2$ decomposes primarily to $Th(VO_3)_4$ when heated at 600 °C in air as determined by X-ray powder diffraction measurements.[20]

CONCLUSIONS

The synthesis of the first actinide tellurate, $Th(VO_2)_2(TeO_6)(H_2O)_2$, has been achieved via the hydrothermal reaction of $Th(NO_3)_4{\cdot}xH_2O$ with V_2O_5 and H_6TeO_6. The remarkably complex three-dimensional structure of $Th(VO_2)_2(TeO_6)(H_2O)_2$ is a direct consequence of the high coordination number of Th combined with the variable coordination of vanadium and the remarkable ability of tellurate to simultaneously bind seven metal centers. This first example of a thorium tellurate points to what is likely to be a large family of structurally diverse actinide tellurate compounds.

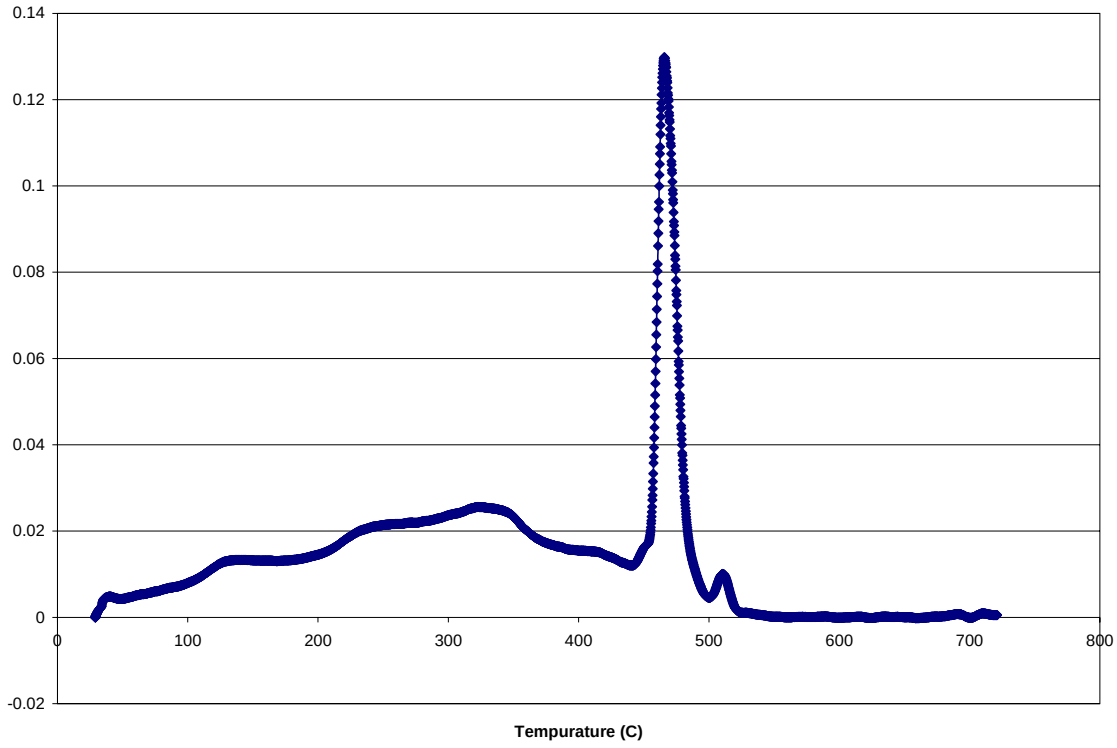

Figure 4.7. Thermogravimetric analysis of $Th(VO_2)_2(TeO_6)(H_2O)_2$ shows that the endotherm centered around 456 ºC is due to a loss of Te, which is confirmed by X-ray powder diffraction.

Table 4.3. Atomic Coordinates and Equivalent Isotropic Displacement Parameters for $Th(VO_2)_2(TeO_6)(H_2O)_2$.

Atom	*x*	*y*	*z*	U_{eq} (Å^2)[a]
Th1	0.156268(15)	0.065122(17)	0.175256(15)	0.00954(7)
Te1	-0.07545(3)	0.22523(3)	0.25827(3)	0.00934(9)
V1	0.07358(7)	0.42168(8)	0.20293(8)	0.00947(19)
V2	0.06217(8)	-0.18383(9)	-0.00118(8)	0.0151(2)
O1	0.0589(4)	0.4391(4)	0.0804(4)	0.0243(10)
O2	0.2011(4)	0.4446(4)	0.2274(4)	0.0188(9)
O3	0.0266(3)	0.5690(3)	0.2583(3)	0.0106(8)
O4	-0.0731(3)	0.3901(3)	0.2609(3)	0.0104(7)
O5	0.0693(3)	0.2557(3)	0.2183(3)	0.0110(8)
O6	0.1467(4)	-0.0897(4)	0.0472(4)	0.0213(10)
O7	-0.0505(4)	-0.1207(4)	-0.0315(4)	0.0246(10)
O8	0.1206(3)	-0.2326(4)	-0.1162(3)	0.0139(8)
O9	0.0342(3)	-0.2868(3)	0.0984(3)	0.0142(8)
O10	-0.2123(3)	0.1950(3)	0.2929(3)	0.0128(8)
O11	0.2723(4)	0.0941(4)	0.0170(4)	0.0269(11)
O12	0.1694(4)	0.0951(4)	0.3717(3)	0.0203(10)

[a] U_{eq} is defined as one-third of the trace of the orthogonalized $\mathbf{U}_{ij}$ tensor.

REFERENCES

1. Levason, W. *Coord. Chem. Rev.* **1997**, *161*, 33.
2. Hector, A. L.; Hill, N. J.; Levason, W.; Webster, M. *Z. Anorg. Allg. Chem.* **2002**, *628*, 815.
3. Levason, W.; Oldroyd, R. D.; Webster, M. *J. Chem., Dalton Trans.,* **1994**, *20*, 2983.
4. Levason, W.; Spicer, M. D.; Webster, M. *Inorg. Chem.* **1991**, *30*, 967.
5. Levason, W.; Spicer, M. D.; Webster, M. *J. Chem., Dalton Trans.,* **1988**, *5*, 1377.
6. Levason, W.; Webster, M. *Acta Crystallogr.* **1998**, *C54*, 1729.
7. Sullens, T. A.; Jensen, R. A.; Shvareva, T. Y.; Albrecht-Schmitt, T. E. *J. Am. Chem. Soc.* **2004**, *126*, 2676.
8. Sykora, R. E.; Albrecht-Schmitt, T. E. *Inorg. Chem.* **2003**, *42*, 2179.
9. Ok, K. M.; Halasyamani, P. S. *Solid State Sci.* **2002**, *4*, 793.
10. Yu, R.; Ok, K. M.; Halasyamani, P. S. *J. Chem., Dalton Trans.,* **2004**, *3*, 392.
11. Wendlandt, W. W.; Hecht, H. G.: *Reflectance Spectroscopy*. Interscience Publishers, New York, 1966.
12. Sheldrick, G. M. SHELXTL PC, Version 6.12, An Integrated System for Solving, Refining, and Displaying Crystal Structures from Diffraction Data; Siemens Analytical X-Ray Instruments, Inc.: Madison, WI 2001.
13. Sheldrick, G. M. *SADABS* 2001, Program for absorption correction using SMART CCD based on the method of Blessing: Blessing, R. H. *Acta Crystallogr.* **1995**, *A51*, 33.
14. Bean, A. C.; Peper, S. M.; Albrecht-Schmitt, T. E. *Chem. Mater.* **2001**, *13*, 1266.

15. Hector, A. L.; Henderson, S. J.; Levason, W.; Webster, M. *Z. Anorg. Allg. Chem.* **2002**, *628*, 198.

16. Douglas, P.; Hector, A. L.; Levason, W.; Light, M. E.; Matthews, M. L.; Webster, M. *Z. Anorg. Allg. Chem.* **2004**, *630*, 479.

17. Brown, I. D.; Altermatt, D. *Acta Crystallogr*. **1985**, *B41*, 244.

18. Brese, N. E.; O'Keeffe, M. *Acta Crystallogr.* **1991**, *B47*, 192.

19. Sykora, R. E.; Ok, K. M.; Halasyamani, P. S.; Wells, D. M.; Albrecht-Schmitt, T. E. *Chem. Mater.* **2002**, *14*, 2741.

20. Quarton, M.; Pages, M.; Freundlich, W. *Comp. Ren. Sean. Acad. Sci., Serie C: Sci. Chim.* **1978**, 286, 369-71.

Chapter 5

CATION-CATION INTERACTIONS BETWEEN URANYL CATIONS IN A POLAR OPEN-FRAMEWORK URANYL PERIODATE

ABSTRACT

Novel open-framework alkali metal and silver uranyl periodates, having the formula $A[(UO_2)_3(HIO_6)(OH)(O)(H_2O)]\cdot 1.5H_2O$ (A = Li, Na, K, Rb, Cs, Ag), have been prepared through mild hydrothermal synthesis. These isostructural compounds contain distorted UO_7 pentagonal bipyramids that are linked through a uranyl (UO_2^{2+}) to uranyl cation-cation interaction. This interaction arises from a single axial uranyl oxygen coordinating at an equatorial site of an adjacent uranyl unit. These uranium oxide polyhedra are further bound by IO_6 distorted octahedra creating an open-framework structure whose channels contain the alkali metal cations.

INTRODUCTION

Cation-cation interactions (CCI's) are an integral part of both the solution and solid-state chemistry of AnO_2^+ (An = U, Np, Pu, Am) cations, which contain actinides in +V oxidation state.[1] These interactions occur via coordination of one actinide metal center by the oxo atom of a second actinyl unit, and can lead to the formation of dimers, oligomers, one-dimensional chains, two-dimensional sheets, and even three-dimensional

networks that do not necessarily require the support of ancillary ligands.[1,2] These interactions are particularly well recognized for Np(V),[3] but have also been identified in U(V),[4] Pu(V),[5] and Am(V) chemistry.[6] CCI's play a critical role in the inner-sphere electron transfer that leads to the disproportionation of U(V) into U(VI) and U(IV),[4] and in interactions in Np(V) compounds that give rise to Ising-type ferromagnetic and metamagnetic behavior.[7] CCI's are rare in compounds that exclusively contain U(VI) in the form of uranyl cations (hereafter uranyl refers to the UO_2^{2+} cation).[8] However, in condensed phases UO_2^{2+} cations are known to interact with alkali and alkaline earth metal cations.[9] Due to the isostructural nature of these compounds, $Cs[(UO_2)_3(HIO_6)(OH)(O)(H_2O)]\cdot 1.5H_2O$ will be used in the forthcoming description and characterizations of these structures.

EXPERIMENTAL

Syntheses. Li_2CO_3 (Alpha Aesar), Na_2CO_3 (Alpha Aesar), K_2CO_3 (Alpha Aesar), Rb_2CO_3 (Alpha Aesar), Cs_2CO_3 (Alpha Aesar), Ag_2CO_3 (Alpha Aesar), $UO_2(NO_3)_2\cdot 6H_2O$ (216 mg, 0.431 mmol), H_5IO_6 (116 mg, 0.509 mmol) were used as received. Distilled and Millipore-filtered water was used in all reactions. The resistance of the water was 18.2 MΩ·cm. The PTFE liners used to contain these reactions were cleaned of contaminants by heating with distilled and Millipore filtered water at 200 °C for 3 d prior to use. *While the UO_3 contains depleted U, standard precautions for handling radioactive materials should be followed. Old sources of depleted U should not be used, as the daughter elements of natural decay are highly radioactive and present serious health risks.* SEM/EDX analyses were performed using a JEOL 840/Link Isis

instrument. The reported preparations given herein are taken from a modified compositional diagram and represent the highest yields of pure phases obtained where possible.

$Li[(UO_2)_3(HIO_6)(OH)(O)(H_2O)]\cdot 1.5H_2O$ (1). Li_2CO_3 (46 mg, 0.629 mmol), $UO_2(NO_3)_2\cdot 6H_2O$ (312 mg, 0.621 mmol), and H_5IO_6 (142 mg, 0.624 mmol) were loaded into a 23 mL PTFE-lined autoclave. Millipore-filtered water (1.5 mL)was then added to the reaction mixture. The autoclave was heated at 185 °C for 120 h and slow cooled at 5 °C/h to 135 °C where it was held for 12 h. After this the autoclave was cooled at 5 °C/h to 22 °C. Yellow prisms of **1** were isolated in 86% yield based on uranium (583 mg). Crystals were shown to contain Li, U, and I in a 1:3:1 ratio as determined from semi-quantitative EDAX measurements.

$Na[(UO_2)_3(HIO_6)(OH)(O)(H_2O)]\cdot 1.5H_2O$ (2). Na_2CO_3 (63 mg, 0.599 mmol), $UO_2(NO_3)_2\cdot 6H_2O$ (300 mg, 0.599 mmol), and H_5IO_6 (136 mg, 0.597 mmol) were loaded into a 23 mL PTFE-lined autoclave. Millipore-filtered water (1.5 mL) was then added to the reaction mixture. The autoclave was heated at 185 °C for 120 h and slow cooled at 5 °C/h to 135 °C where it was held for 12 h. After this the autoclave was cooled at 5 °C/h to 22 °C. Yellow prisms of **2** were isolated in 73% yield based on uranium (484 mg). Crystals were shown to contain Na, U, and I in a 1:3:1 ratio as determined from semi-quantitative EDAX measurements.

$K[(UO_2)_3(HIO_6)(OH)(O)(H_2O)]\cdot 1.5H_2O$ (3). K_2CO_3 (80 mg, 0.574 mmol), $UO_2(NO_3)_2\cdot 6H_2O$ (289 mg, 0.577 mmol), and H_5IO_6 (131 mg, 0.576 mmol) were loaded into a 23 mL PTFE-lined autoclave. Millipore-filtered water (1.5 mL) was then added to the reaction mixture. The autoclave was heated at 185 °C for 120 h and slow cooled at 5

°C/h to 135 °C where it was held for 12 h. After this the autoclave was cooled at 5 °C/h to 22 °C. Yellow prisms of **3** were isolated in 89% yield based on uranium (577 mg). Crystals were shown to contain K, U, and I in a 1:3:1 ratio as determined from semi-quantitative EDAX measurements.

$Rb[(UO_2)_3(HIO_6)(OH)(O)(H_2O)]\cdot 1.5H_2O$ (4). Rb_2CO_3 (120 mg, 0.520 mmol), $UO_2(NO_3)_2\cdot 6H_2O$ (261 mg, 0.521 mmol), and H_5IO_6 (118 mg, 0.521 mmol) were loaded into a 23 mL PTFE-lined autoclave. Millipore-filtered water (1.5 mL) was then added to the reaction mixture. The autoclave was heated at 185 °C for 120 h and slow cooled at 5 °C/h to 135 °C where it was held for 12 h. After this the autoclave was cooled at 5 °C/h to 22 °C. Yellow prisms of **4** were isolated in 82% yield based on uranium (499 mg). Crystals were shown to contain Rb, U, and I in a 1:3:1 ratio as determined from semi-quantitative EDAX measurements.

$Cs[(UO_2)_3(HIO_6)(OH)(O)(H_2O)]\cdot 1.5H_2O$ (5). Cs_2CO_3 (154 mg, 0.473 mmol), $UO_2(NO_3)_2\cdot 6H_2O$ (238 mg, 0.473 mmol), and H_5IO_6 (108 mg, 0.475 mmol) were loaded into a 23 mL PTFE-lined autoclave. Millipore-filtered water (1.5 mL) was then added to the reaction mixture. The autoclave was heated at 185 °C for 120 h and slow cooled at 5 °C/h to 135 °C where it was held for 12 h. After this the autoclave was cooled at 5 °C/h to 22 °C. Yellow prisms of **5** were isolated in 91% yield based on uranium (523 mg). Crystals were shown to contain Cs, U, and I in a 1:3:1 ratio as determined from semi-quantitative EDAX measurements.

$Ag[(UO_2)_3(HIO_6)(OH)(O)(H_2O)]\cdot 1.5H_2O$ (6). Ag_2CO_3 (137 mg, 0.496 mmol), $UO_2(NO_3)_2\cdot 6H_2O$ (250 mg, 0.497 mmol), H_5IO_6 (113 mg, 0.498 mmol) were loaded into a 23 mL PTFE-lined autoclave. Millipore-filtered water (1.5 mL) was then added to the

reaction mixture. The autoclave was heated at 185 °C for 120 h and slow cooled at 5 °C/h to 135 °C where it was held for 12 h. After this the autoclave was cooled at 5 °C/h to 22 °C. Yellow prisms of **6** were isolated in 85% yield based on uranium (503 mg). Crystals were shown to contain Ag, U, and I in a 1:3:1 ratio as determined from semi-quantitative EDAX measurements.

X-ray structural analysis. $Li[(UO_2)_3(HIO_6)(OH)(O)(H_2O)]\cdot 1.5H_2O$ (1): yellow prism, dimensions 0.192 x 0.048 x 0.048 mm, monoclinic, *Cc*, $Z = 4$, a = 13.087(1), b = 10.120(1), c = 11.119(1) Å, β = 102.229(2)°, V = 1439.1(3) $Å^3$ (T = 193 K), $\mu = 359.04\ cm^{-1}$, $R_1 = 0.0444$, wR2 = 0.0980.[15] Bruker APEX CCD diffractometer: $\theta_{max} = 56.62°$, MoKα, $\lambda = 0.71073$ Å, 0.3° ω scans, 7227 reflections measured, 3464 independent reflections, all of which were included in the refinement. The data were corrected for Lorentz-polarization effects and for absorption (analytical and SADABS). The structure was solved by direct methods, followed by a refinement of F^2 by full-matrix least-squares with 181 parameters.[15] Anisotropic displacement parameters were included for all heavy atoms and most oxygen atoms.

$Na[(UO_2)_3(HIO_6)(OH)(O)(H_2O)]\cdot 1.5H_2O$ (2): yellow prism, dimensions 0.120 x 0.064 x 0.050 mm, monoclinic, *Cc*, $Z = 4$, a = 13.093(2), b = 10.0755(7), c = 11.034(2) Å, β = 102.073(2)°, V = 1428.0(5) $Å^3$ (T = 193 K), $\mu = 332.59\ cm^{-1}$, $R_1 = 0.0549$, wR2 = 0.1223.[15] Bruker APEX CCD diffractometer: $\theta_{max} = 56.54°$, MoKα, $\lambda = 0.71073$ Å, 0.3° ω scans, 7364 reflections measured, 3485 independent reflections, all of which were included in the refinement. The data were corrected for Lorentz-polarization effects and for absorption (analytical and SADABS). The structure was solved by direct methods, followed by a refinement of F^2 by full-matrix least-squares with 181 parameters.[15]

Anisotropic displacement parameters were included for all heavy atoms and most oxygen atoms.

$K[(UO_2)_3(HIO_6)(OH)(O)(H_2O)]\cdot 1.5H_2O$ (3): yellow prism, dimensions 0.258 x 0.042 x 0.040 mm, monoclinic, *Cc*, $Z = 4$, $a = 13.009(1)$, $b = 10.1144(9)$, $c = 11.152(1)$ Å, $\beta = 102.289(2)°$, $V = 1433.7(2)$ Å^3 (T = 193 K), $\mu = 363.34$ cm^{-1}, $R_1 = 0.0367$, wR2 = 0.0892.[15] Bruker APEX CCD diffractometer: $\theta_{max} = 56.54°$, MoKα, $\lambda = 0.71073$ Å, 0.3° ω scans, 6976 reflections measured, 3383 independent reflections, all of which were included in the refinement. The data were corrected for Lorentz-polarization effects and for absorption (analytical and SADABS). The structure was solved by direct methods, followed by a refinement of F^2 by full-matrix least-squares with 181 parameters.[15] Anisotropic displacement parameters were included for all heavy atoms and most oxygen atoms.

$Rb[(UO_2)_3(HIO_6)(OH)(O)(H_2O)]\cdot 1.5H_2O$ (4): yellow prism, dimensions 0.098 x 0.034 x 0.028 mm, monoclinic, *Cc*, $Z = 4$, $a = 13.231(3)$, $b = 10.095(2)$, $c = 11.150(3)$ Å, $\beta = 103.003(4)°$, $V = 1451.1(6)$ Å^3 (T = 193 K), $\mu = 389.34$ cm^{-1}, $R_1 = 0.0513$, wR2 = 0.1120.[15] Bruker APEX CCD diffractometer: $\theta_{max} = 56.54°$, MoKα, $\lambda = 0.71073$ Å, 0.3° ω scans, 7133 reflections measured, 3579 independent reflections, all of which were included in the refinement. The data were corrected for Lorentz-polarization effects and for absorption (analytical and SADABS). The structure was solved by direct methods, followed by a refinement of F^2 by full-matrix least-squares with 181 parameters.[15] Anisotropic displacement parameters were included for all heavy atoms and most oxygen atoms.

$Cs[(UO_2)_3(HIO_6)(OH)(O)(H_2O)]\cdot 1.5H_2O$ (5): yellow prism, dimensions 0.070 x 0.052 x 0.048 mm, monoclinic, *Cc*, $Z = 4$, $a = 13.0960(9)$, $b = 10.0714(7)$, $c = 11.0398(8)$ Å, $\beta = 102.064(1)°$, $V = 1421.0(2)$ Å^3 (T = 193 K), $\mu = 388.78$ cm^{-1}, $R_1 = 0.0239$, wR2 = 0.0478.[15] Bruker APEX CCD diffractometer: $\theta_{max} = 56.54°$, MoKα, $\lambda = 0.71073$ Å, 0.3° ω scans, 7026 reflections measured, 3447 independent reflections, all of which were included in the refinement. The data were corrected for Lorentz-polarization effects and for absorption (analytical and SADABS). The structure was solved by direct methods, followed by a refinement of F^2 by full-matrix least-squares with 181 parameters.[15] Anisotropic displacement parameters were included for all heavy atoms and most oxygen atoms.

$Ag[(UO_2)_3(HIO_6)(OH)(O)(H_2O)]\cdot 1.5H_2O$ (6): yellow prism, dimensions 0.124 x 0.040 x 0.038 mm, monoclinic, *Cc*, $Z = 4$, $a = 13.220(3)$, $b = 9.566(2)$, $c = 10.999(2)$ Å, $\beta = 102.43(3)°$, $V = 1358.3(5)$ Å^3 (T = 193 K), $\mu = 394.35$ cm^{-1}, $R_1 = 0.0548$, wR2 = 0.1098.[15] Bruker APEX CCD diffractometer: $\theta_{max} = 56.54°$, MoKα, $\lambda = 0.71073$ Å, 0.3° ω scans, 6989 reflections measured, 3287 independent reflections, all of which were included in the refinement. The data were corrected for Lorentz-polarization effects and for absorption (analytical and SADABS). The structure was solved by direct methods, followed by a refinement of F^2 by full-matrix least-squares with 181 parameters.[15] Anisotropic displacement parameters were included for all heavy atoms and most oxygen atoms.

Ion-exchange analysis. Ion exchange properties were also investigated under three methods, all involving a ten-fold excess (in total) of alkali chloride salts in solution to establish exchange with either **2**, **3**, **4**, or **6**. The first method involved heating the

solution to 50 ºC with the solid for 3 d. The second had the solution held constant at room temperature for 14 d. The final method had **2** in solution at 120 ºC for 3 d. All semi-quantitative exchange values were measured with either Cs^+ selective electrodes or by EDAX analysis.

Results and Discussion

Synthesis. In an effort to expand solid state-studies on uranyl periodate[10] compounds beyond the single known example of $K_2[(UO_2)_2(VO)_2(IO_6)_2O]\cdot H_2O$,[11] we have explored the hydrothermal reactions of alkali metal and silver carbonates with uranyl nitrate and periodic acid at 185 °C. These reactions result in the formation of $A[(UO_2)_3(HIO_6)_2(OH)(O)(H_2O)]\cdot 1.5H_2O$ (A = Li(**1**) – Cs(**5**), Ag(**6**)) in yields as high as 91%. The primary difficulty in this synthetic procedure is slowing the reduction of the I(VII) to I(V), which results in the formation of $UO_2(IO_3)_2(H_2O)$.[12] Compounds **1**–**6** are isolated as lemon yellow prisms from a colorless mother liquor. The IR vibrational spectra of these compounds show a characteristic δ(IOH) mode near 1071 cm^{-1},[10] as well as strong uranyl symmetric and asymmetric modes.

Structure. $Cs[(UO_2)_3(HIO_6)_2(OH)(O)(H_2O)]\cdot 1.5H_2O$. Single crystal X-ray diffraction studies (Table 5.1-3) on **1**-**6** reveal that all of the compounds are isostructural and crystallize in the polar monoclinic space group *Cc*. The structure of **5**, which will be used to represent all six compounds, results from the assembly of three crystallographically unique uranyl units that are bridged by aquo, hydroxo, oxo, and monoprotonated periodate groups to yield a remarkably complex three-dimensional

Table 5.1. Crystallographic data for $A[(UO_2)_3(HIO_6)(OH)(O)(H_2O)]\cdot 1.5H_2O$ (A = Li(**1**), Na(**2**)).[19]

Compound	**1**	**2**
Formula mass	1117.05	1135.00
Crystal system	Monoclinic	Monoclinic
Space group	*Cc* (No. 9)	*Cc* (No. 9)
a (Å)	13.0874(14)	13.093(2)
b (Å)	10.1197(11)	10.0755(7)
c (Å)	11.1186(12)	11.034(2)
α (deg.)	90	90
β (deg.)	102.229(2)	102.073(2)
γ (deg.)	90	90
V (Å^3)	1439.1(3)	1428.0(5)
Z	4	4
T (°C)	–80	–80
λ (Å)	0.71073	0.71073
ρ_{calcd} (g cm^{-3})	5.711	5.723
μ (Mo *K*α, cm^{-1})	359.04	332.59
R(*F*) for $F_o^2 > 2\sigma(F_o^2)$ [a]	0.0444	0.0548
$R_w(F_o^2)$ [b]	0.0980	0.1223

[a] $R(F) = \sum \left| |F_o| - |F_c| \right| / \sum |F_o|$. [b] $R_w\left(F_o^2\right) = \left[\sum \left[w\left(F_o^2 - F_c^2\right)^2 \right] / \sum wF_o^4 \right]^{1/2}$

Table 5.2. Crystallographic data for $A[(UO_2)_3(HIO_6)(OH)(O)(H_2O)]\cdot 1.5H_2O$ (A = K(**3**), Rb(**4**)).[19]

Compound	**3**	**4**
Formula mass	1117.05	1135.00
Crystal system	Monoclinic	Monoclinic
Space group	*Cc* (No. 9)	*Cc* (No. 9)
a (Å)	13.0090(10)	13.231(3)
b (Å)	10.1144(9)	10.095(2)
c (Å)	11.1520(10)	11.150(3)
α (deg.)	90	90
β (deg.)	102.289(2)	103.003(4)
γ (deg.)	90	90
V (Å^3)	1433.7(2)	1451.1(6)
Z	4	4
T (°C)	–80	–80
λ (Å)	0.71073	0.71073
ρ_{calcd} (g cm^{-3})	5.342	5.384
μ (Mo *K*α, cm^{-1})	363.34	389.34
$R(F)$ for $F_o^2 > 2\sigma(F_o^2)$ [a]	0.0367	0.0513
$R_w(F_o^2)$ [b]	0.0892	0.1120

[a] $R(F) = \sum \left| |F_o| - |F_c| \right| / \sum |F_o|$. [b] $R_w\left(F_o^2\right) = \left[\sum \left[w\left(F_o^2 - F_c^2\right)^2 \right] / \sum wF_o^4 \right]^{1/2}$

Table 5.3. Crystallographic data for $A[(UO_2)_3(HIO_6)(OH)(O)(H_2O)]\cdot 1.5H_2O$ (A = Cs(**5**), Ag(**6**)). [19]

Compound	**5**	**6**
Formula mass	1221.90	1204.86
Crystal system	Monoclinic	Monoclinic
Space group	*Cc* (No. 9)	*Cc* (No. 9)
a (Å)	13.0960(9)	13.220(3)
b (Å)	10.0714(7)	9.566(2)
c (Å)	11.0398(8)	10.999(2)
α (deg.)	90	90
β (deg.)	102.604(1)	102.43(3)
γ (deg.)	90	90
V (Å^3)	1421.0(2)	1358.3(5)
Z	4	4
T (°C)	–80	–80
λ (Å)	0.71073	0.71073
ρ_{calcd} (g cm^{-3})	5.711	5.892
μ (Mo *K*α, cm^{-1})	388.78	394.35
$R(F)$ for $F_o^2 > 2\sigma(F_o^2)$ [a]	0.0239	0.0548
$R_w(F_o^2)$ [b]	0.0478	0.1098

[a] $R(F) = \sum \left| |F_o| - |F_c| \right| / \sum |F_o|$. [b] $R_w\left(F_o^2\right) = \left[\sum \left[w\left(F_o^2 - F_c^2\right)^2 \right] / \sum wF_o^4 \right]^{1/2}$

structure with intersecting channels extending along the *c* axis and approximately down 110 and 1-10, as shown in Figures 5.1 and 5.2. Three-dimensional uranyl compounds are uncommon because uranyl polyhedra typically align in a parallel fashion, and given the terminal nature of the oxo atoms, layered architectures result.[13,14] Alkali metal cations and water molecules fill the channels, which as can be seen in Figure 5.1 are also polar. The structure is apparently quite rigid and the channels show almost no measurable size variance with reduction in the size of the alkali metal cations. However, the displacement parameters for the cations smaller than Rb^+ do show considerable enlargement corresponding to rattling within the confines of the channels. This rattling does not result in splitting or disorder of the alkali metal cation position. However, in the case of **1**, the Li^+ cation had to be refined isotropically owing to the large motion of this cation within the channel.

Each of the three uranyl units in **5** is coordinated by five oxygen atoms in the equatorial plane to yield $[UO_7]$ pentagonal bipyramids. The uranyl U=O distances for U(1) and U(2) are normal and range from 1.769(8) to 1.781(7) Å. The equatorial U-O distances are also within normal limits and occur from 2.181(7) to 2.581(6) Å. The shortest U–O bond length in the equatorial plane is to the μ_3-oxide ion. The uranyl unit for U(3) has U=O distances of 1.829(7) and 1.793(8) Å. The former U=O distance does not correspond to a typical terminal uranyl oxo atom (Figure 5.3), but rather this atom is bridging to a neighboring uranyl unit containing U(1). This bridging distance is within typical limits for donor atoms in the equatorial plane with a distance of 2.379(7) Å, as depicted in Figure 5.4. This interaction effectively turns uranyl polyhedra perpendicular

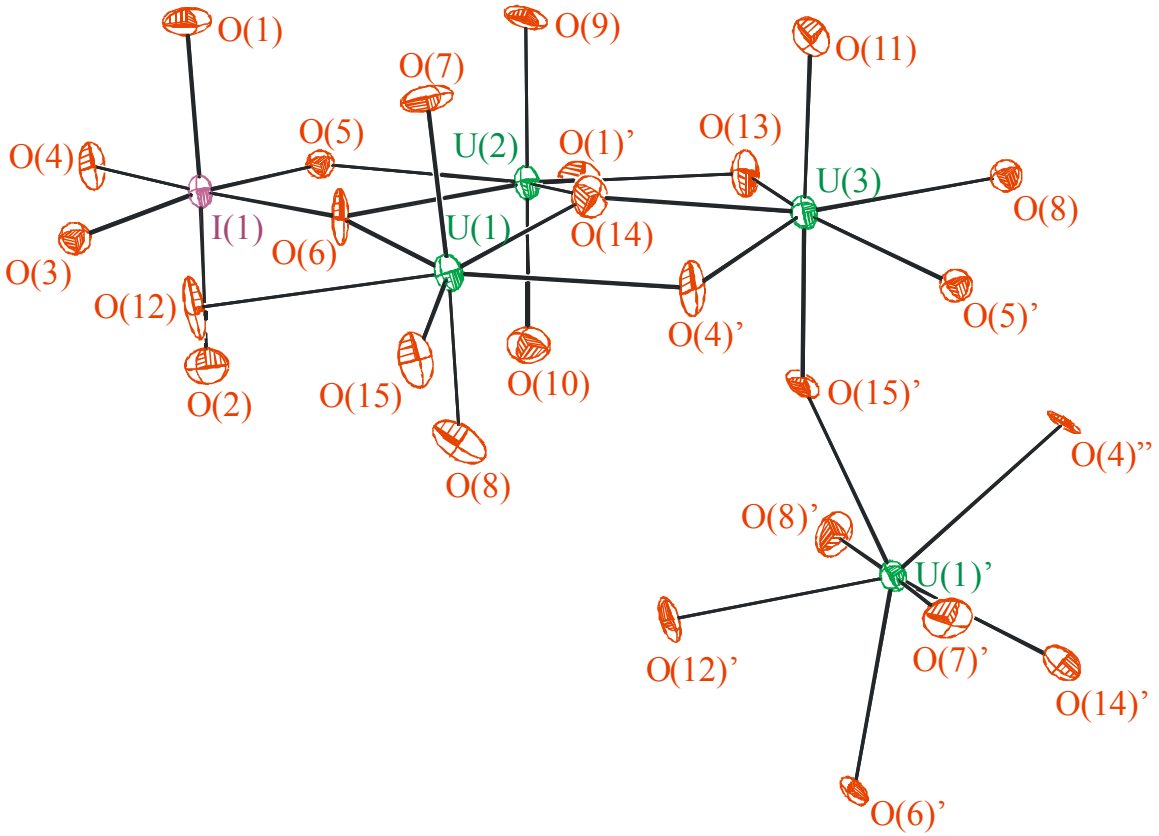

Figure 5.1. Thermal ellipsoid plot of $Cs[(UO_2)_3(HIO_6)_2(OH)(O)(H_2O)]\cdot 1.5H_2O$ at 50% probability. O(15)' acts as both a coordinating equatorial oxygen atom to U(1) and an oxo-atom of the U(3) uranyl (UO_2^{2+}) unit. This dual role is the basis of the cation-cation interaction between U(1) and U(3). Cs^+ is eliminated for clarity.

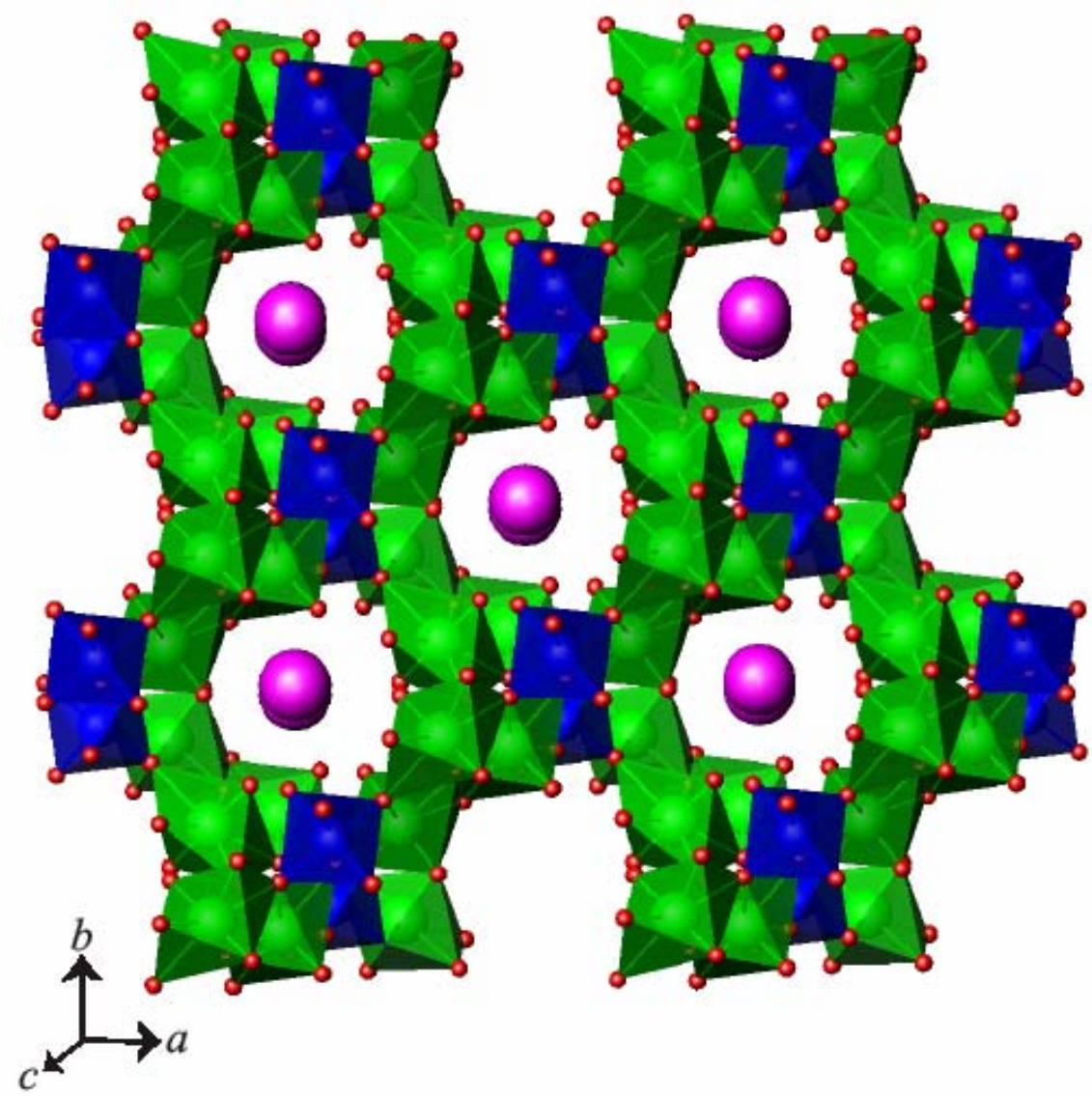

Figure 5.2. A view down the *c* axis showing the polar open-framework structures of $A[(UO_2)_3(HIO_6)(OH)(O)(H_2O)]\cdot 1.5H_2O$ (Li(**1**)-Cs(**5**)). The major channels running down this axis are filled with alkali metal cations. UO_7 pentagonal bipyramids are shown in green and IO_6 octahedra in blue.

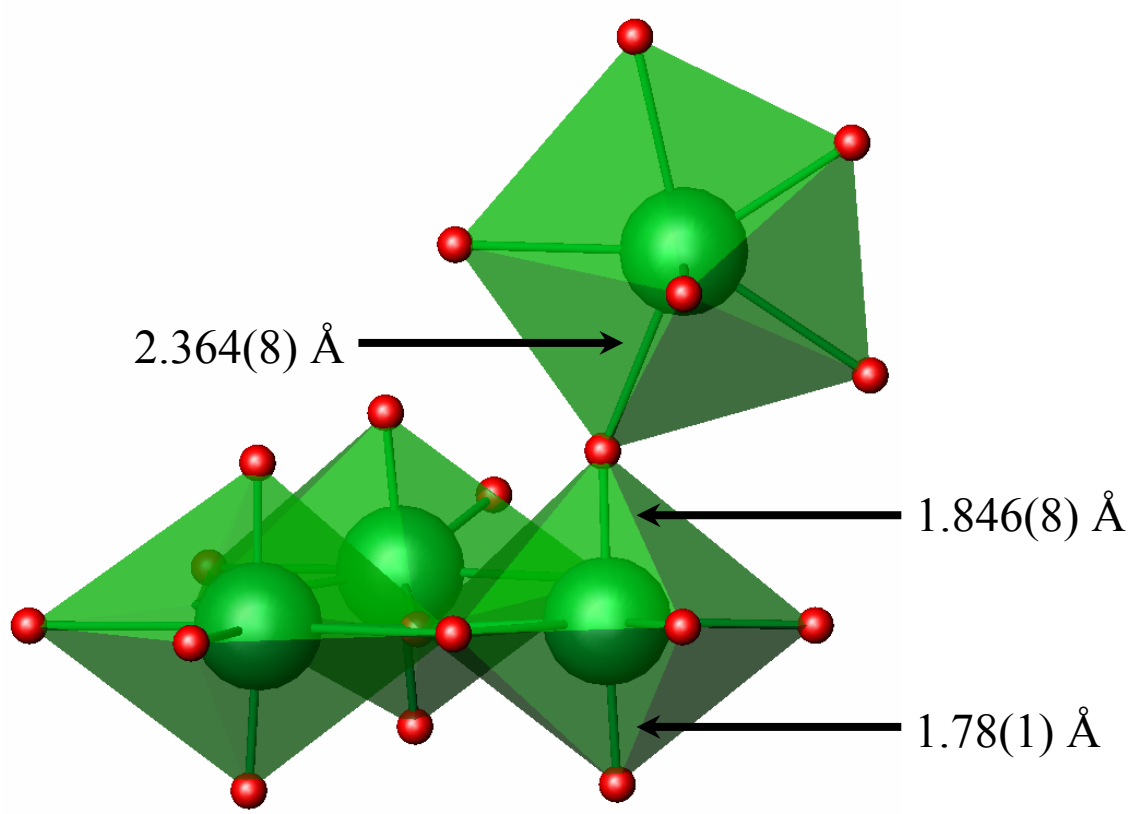

Figure 5.3. An illustration of the cation-cation interaction between the uranyl unit containing U(3) and the uranyl cation containing U(1). The slight elongation of the uranyl bond length between the dual role oxygen atom and the lower uranium atom is also evident.

to one another creating two orthogonal uranium oxide sheets within the structure. This is best viewed in Figure 5.2, thereby leading to a three-dimensional architecture. Bond-valence sum calculations confirm that these three uranium centers are unambiguously U(VI) with values of 6.06, 6.00, and 6.12 for U(1), U(2), and U(3), respectively.[15-17] This is a rare example of cation-cation interactions between uranyl cations, and it provides a structural link between the CCI's in AnO_2^+ compounds and those that contain UO_2^{2+}.[8]

The question then arises: what makes U(3) so different from U(1) and U(2) to make the normally terminal uranyl cation form a cation-cation interaction more similar to that expected for an AnO_2^+ cation instead of UO_2^{2+}? A close look at the individual coordination environments of the uranium centers reveals that U(2) and U(3) are chelated by the HIO_6^{4-} anion. This anion also utilizes its oxo atoms to bridge to an additional four uranium centers. The hydrogen periodate anion has five I–O bond distances ranging from 1.830(7) to 1.894(7) Å and a sixth longer I–O(H) bond length of 1.926(8) Å to the nominal hydroxo group. We suggest that through the chelation of U(3) by the hydrogen periodate anion that significant electron density is transferred from this highly charged anion to the U(3) uranyl cation to make the oxo atoms better Lewis bases than is typically found. We cannot exclude the possibility that this interaction is a consequence of other features of this structure, especially crystal packing forces.

The transfer of charge from the U(3) uranyl unit to an adjacent uranyl cation should result in a strengthening of the interactions with the donor atoms in the equatorial plane. The converse of which is that stronger equatorial bonds results in the formation of CCI's. Unfortunately, the ligand environments for each U center are different, making

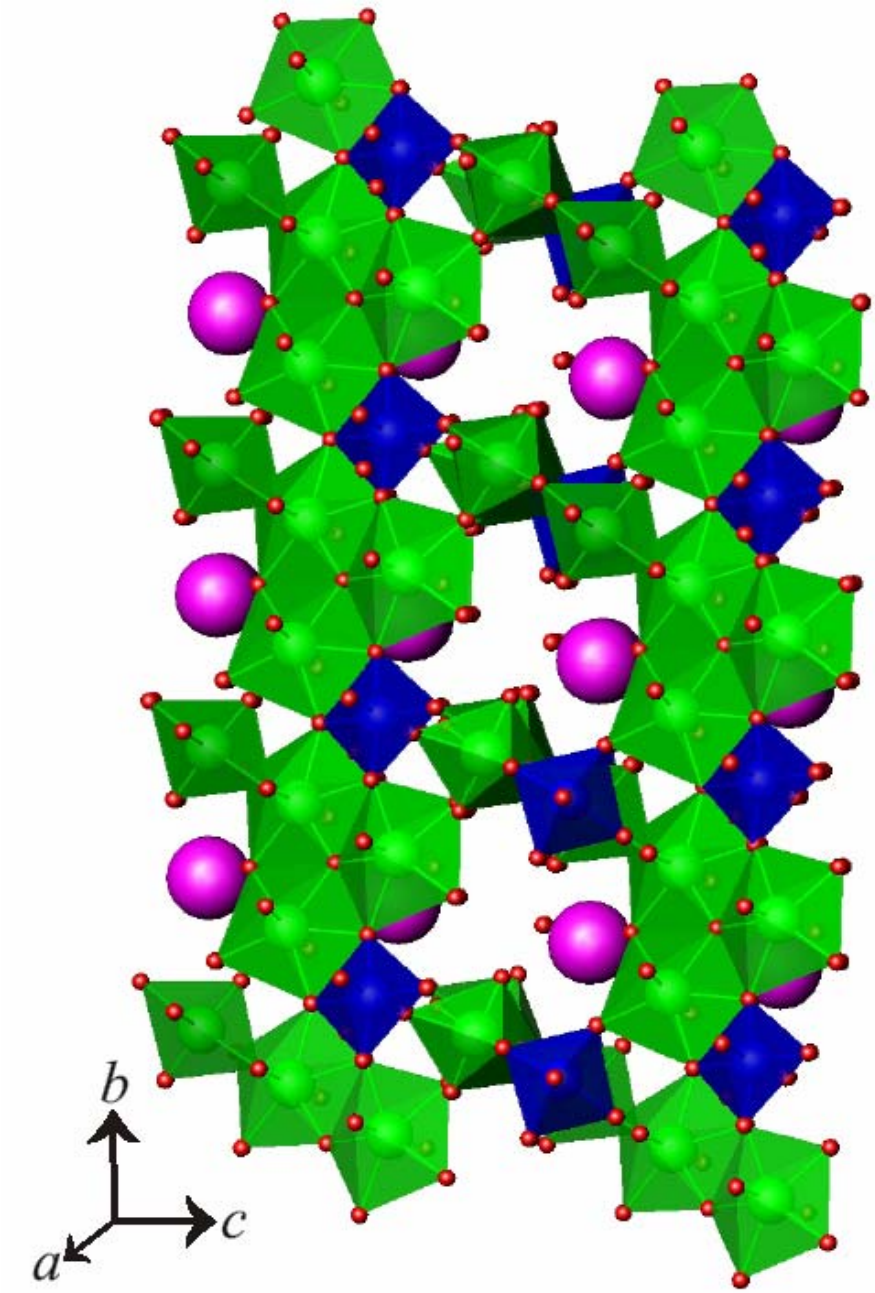

Figure 5.4. A view of $A[(UO_2)_3(HIO_6)(OH)(O)(H_2O)]\cdot 1.5H_2O$ (Li(**1**)-Cs(**5**)) showing the second type of channel that intersects with the channels running down the *c* axis to yield an open-framework structure.

comparisons difficult. However, the average U–O distance to equatorial atoms surrounding U(3) is 2.322(7) Å, whereas statistically longer U–O distances of 2.377(7) Å and 2.389(7) Å are observed for U(1) and U(2), respectively. In a recent, and quite timely, report by Sarsfield and Helliwell, it was shown that uranyl coordination compounds could be rationally prepared that have uranyl oxo atoms of increased Lewis basicity.[18] These oxo atoms are of sufficient basicity to form adducts with $B(C_6F_5)_3$. The charge transfer that results from the formation of this adduct also coincides well with the lengthening of the uranyl oxo distances and shortening the average bond length in the equatorial plane of this complex.

There is a difference in one fundamental aspect of the crystal structure between the alkali- and silver-containing compounds. As illustrated in the text as well as the figures of **1-5,** the channels are filled with the alkali metal cation. The structure of **6** reveals the silver cation and the hydrating water molecule actually change places within the gaps formed in the structure (Figure 5.5). One, and perhaps the only, explanation for this occurrence is the ability of silver to participate in covalent bonding. As seen in Figures 5.5, the silver cation is closer to the surrounding structure by occupying the hydrating water site rather than the alkali metal cation site. In **5** Cs(1) maintains long range interactions with ten oxygen atoms with an average distance of 3.264 Å. Silver in **6** however has but three interactions to neighboring oxygen atoms, but these interactions are 2.490, 2.415, and 2.446 Å in length for an average Ag–O distance of 2.450 Å. This silver-oxygen association also exists in a distorted trigonal planar linkage with the distortion coming primarily from the existing framework surrounding the silver cation. The hydrating water molecule in **6** occupies the prominent position in the center of the

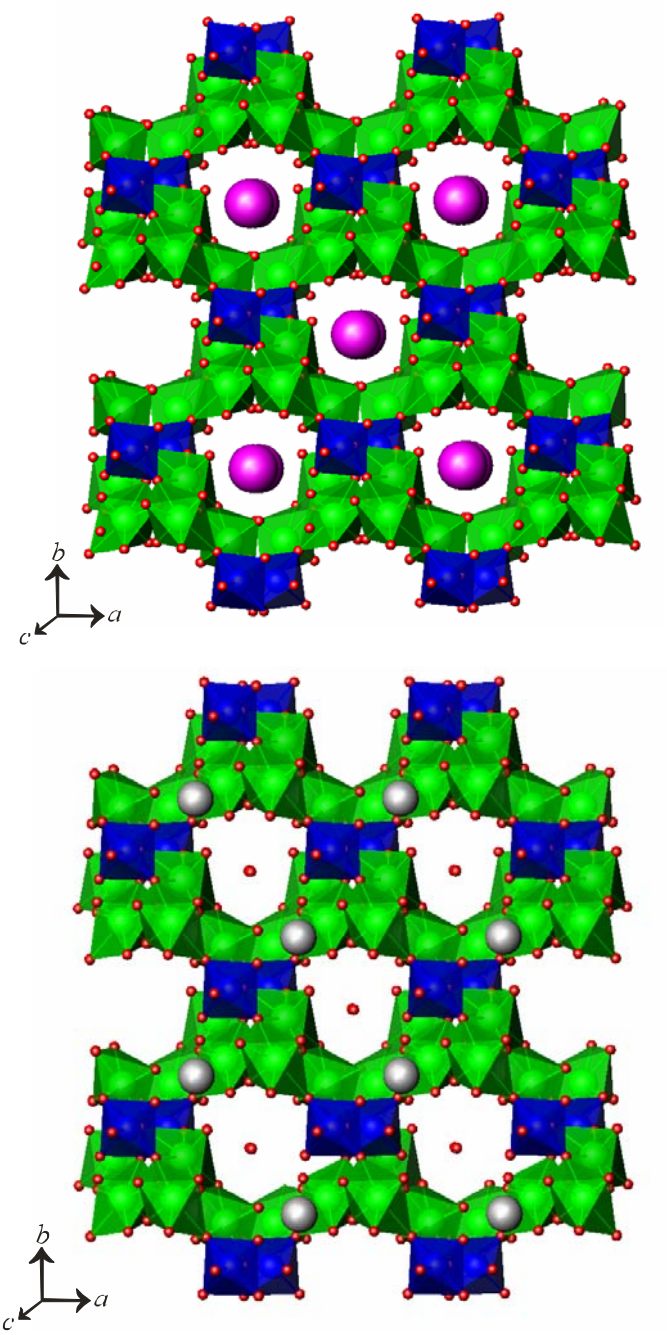

Figure 5.5. An illustration of the difference in location of the counter cation between the alkali (top) and the silver (bottom) analogues of $Ag[(UO_2)_3(HIO_6)(OH)(O)(H_2O)]\cdot 1.5H_2O$ (A = Li(**1**)–Cs(**5**), Ag(**6**)). The Cs^+ analogue is depicted as the representative of the alkali series.

channel running along the *c*-axis. No other structural variations are present between the alkali and silver analogues of $A[(UO_2)_3(HIO_6)_2(OH)(O)(H_2O)]\cdot 1.5H_2O$ (A = Li(**1**) – Cs(**5**), Ag(**6**)).

Ion-exchange. The ion-exchange capabilities of these compounds were examined using a combination of EDAX measurements on the solids as well as Cs^+-selective electrodes of the solutions for Cs^+-exchange reactions. These results were compared with those obtained from $K_2[(UO_2)_2(VO)_2(IO_6)_2O]\cdot H_2O$, which also possesses a three-dimensional structure with large channels occupied by K^+ cations. At 22 °C, the exchange of Na^+ in **2** for larger alkali metal cations is slow and equilibrium was not established after two weeks. However, the complete exchange of Na^+ for Cs^+ can be accomplished at 120 °C in three days. Competing ion-exchange reactions were also carried out whereby **2** was stirred with a tenfold excess of K^+, Rb^+, and Cs^+. These reactions revealed a 3.9:1.3:1 ratio of these cations in the ion-exchanged solids demonstrating an almost fourfold preference for the K^+ cations over Cs^+. The K^+ cations in $K_2[(UO_2)_2(VO)_2(IO_6)_2O]\cdot H_2O$ can also be exchanged for Cs^+, although this exchange occurs more rapidly at 22 °C than it does for **2**. No measurable ion-exchange capabilities were observed by **6** due to covalent interactions of the silver cation. Selected ion exchange data are available in Table 5.4.

Table 5.4. Ion-exchange studies of the various analogues of 1-5. All crystals were within a ten fold excess of dissolved salt solution at the indicated temperature and duration. Atomic percentage was measured by EDAX analysis. A slight selectivity for K^+ over the other cations is observed.

Crystal[a]	Salt	Atomic %		
		K	Rb	Cs
$K[(UO_2)_3(HIO_6)(OH)(O)(H_2O)]\cdot 1.5H_2O$	CsCl	72.80	n/a	1.75*
$K[(UO_2)_3(HIO_6)(OH)(O)(H_2O)]\cdot 1.5H_2O$	RbCl	81.90	22.95	NA
$Rb[(UO_2)_3(HIO_6)(OH)(O)(H_2O)]\cdot 1.5H_2O$	CsCl	n/a	65.40	54.35
Crystal[b]	Salt	Atomic %		
		K	Rb	Cs
$Li[(UO_2)_3(HIO_6)(OH)(O)(H_2O)]\cdot 1.5H_2O$	K, Rb, CsCl	35.50	28.35	36.25
$Na[(UO_2)_3(HIO_6)(OH)(O)(H_2O)]\cdot 1.5H_2O$	K, Rb, CsCl	62.80	21.10	16.10
$K[(UO_2)_3(HIO_6)(OH)(O)(H_2O)]\cdot 1.5H_2O$	CsCl	82.50	n/a	10.30
$K[(UO_2)_3(HIO_6)(OH)(O)(H_2O)]\cdot 1.5H_2O$	RbCl	65.65	31.10	n/a
$Rb[(UO_2)_3(HIO_6)(OH)(O)(H_2O)]\cdot 1.5H_2O$	CsCl	n/a	69.30	18.60
Crystal[c]	Salt	Atomic %		
		K	Rb	Cs
$Na[(UO_2)_3(HIO_6)(OH)(O)(H_2O)]\cdot 1.5H_2O$	CsCl	n/a	n/a	100

a. Mixture was maintained at 50 ºC for 3 days.
b. Mixture was maintained at 22 ºC for 14 days.
c. Mixture was maintained at 120 ºC for 3 days.
* Measured percentage was below EDAX error range of ±5%.

Table 5.5. Atomic Coordinates and Equivalent Isotropic Displacement Parameters for $Cs[(UO_2)_3(HIO_6)(OH)(O)(H_2O)]\cdot 1.5H_2O$ (**5**).

Atom	*x*	*y*	*z*	U_{eq} (Å^2)[a]
U1	0.17720(3)	-0.36938(4)	-0.18082(3)	0.01011(9)
U2	0.26595(3)	-0.13134(4)	0.09972(3)	0.01058(9)
U3	0.02878(3)	-0.34265(4)	0.07958(3)	0.01030(9)
I1	0.41701(5)	-0.09085(7)	-0.12730(6)	0.00924(13)
Cs1	-0.00749(6)	-0.01413(7)	-0.18513(7)	0.02286(17)
O1	0.3294(6)	0.0349(7)	-0.2134(7)	0.0187(17)
O2	0.5101(6)	-0.2273(7)	-0.0455(7)	0.0194(18)
O3	0.4343(6)	-0.1710(7)	-0.2709(6)	0.0110(14)
O4	0.5311(6)	0.0282(7)	-0.1109(7)	0.0148(16)
O5	0.4086(5)	-0.0218(7)	0.0297(6)	0.0097(15)
O6	0.3044(6)	-0.1988(7)	-0.1115(6)	0.0154(17)
O7	0.0921(6)	-0.2592(7)	-0.2818(7)	0.0186(18)
O8	0.2643(6)	-0.4841(8)	-0.0908(7)	0.0220(18)
O9	0.1889(6)	0.0091(7)	0.0398(7)	0.0174(17)
O10	0.3422(6)	-0.2721(8)	0.1589(7)	0.0201(18)
O11	-0.0615(6)	-0.2209(8)	0.0006(8)	0.0224(19)
O12	0.2886(6)	-0.3658(8)	-0.3354(7)	0.0212(18)
O13	0.1322(6)	-0.1894(8)	0.2040(7)	0.0175(17)
O14	0.1435(6)	-0.2666(8)	-0.0195(7)	0.0154(16)
O15	0.1193(5)	-0.5344(7)	-0.3346(6)	0.0134(16)
O16	0.2226(18)	-0.251(2)	-0.564(2)	0.050(6)

[a] U_{eq} is defined as one-third of the trace of the orthogonalized $\mathbf{U}_{ij}$ tensor.

Table 5.6. Atomic Coordinates and Equivalent Isotropic Displacement Parameters for $Ag[(UO_2)_3(HIO_6)(OH)(O)(H_2O)]\cdot 1.5H_2O$ (**6**).

Atom	*x*	*y*	*z*	U_{eq} (Å^2)[a]
U1	0.74267(9)	0.67144(12)	0.75832(9)	0.0084(2)
U2	0.89510(8)	0.62564(12)	0.50163(8)	0.0101(3)
U3	0.98378(8)	0.87792(12)	0.78169(8)	0.0104(3)
I1	0.13837(14)	0.9022(2)	0.55687(15)	0.0088(4)
Ag1	0.4508(2)	0.7347(3)	0.5905(2)	0.0279(7)
O1	0.0117(18)	0.599(2)	0.357(2)	0.028(6)
O2	0.8468(15)	0.8362(19)	0.8882(16)	0.009(4)
O3	0.0318(17)	0.7820(19)	0.5811(18)	0.017(5)
O4	0.0431(18)	0.032(2)	0.478(2)	0.026(6)
O5	0.9256(16)	0.038(2)	0.7183(18)	0.014(5)
O6	0.2459(17)	0.036(2)	0.5659(19)	0.015(5)
O7	0.9710(16)	0.494(2)	0.5941(19)	0.015(5)
O8	0.2390(15)	0.7651(18)	0.6308(18)	0.011(4)
O9	0.1515(15)	0.825(2)	0.4100(17)	0.012(4)
O10	0.8618(16)	0.748(2)	0.6604(18)	0.014(5)
O11	0.8335(16)	0.548(2)	0.8463(18)	0.016(5)
O12	0.8234(16)	0.743(2)	0.3969(18)	0.017(5)
O13	0.1318(15)	0.9696(19)	0.7166(16)	0.006(4)
O14	0.0426(16)	0.723(2)	0.8442(19)	0.016(5)
O15	0.6469(16)	0.786(2)	0.6732(19)	0.014(5)
O16	0.7129(19)	0.004(3)	0.486(2)	0.039(7)

[a] U_{eq} is defined as one-third of the trace of the orthogonalized $\mathbf{U}_{ij}$ tensor.

REFERENCES

1. a) Sullivan, J. C.; Hindman, J. C.; Zielen, A. J. *J. Am. Chem. Soc.* **1961**, *83*, 3373. b) Cousson, A.; Dabos, S.; Abazli, H.; Nectoux, F.; Pagès, M.; Choppin, G. *J. Less-Common Met.* **1984**, *99*, 233. c) Albrecht-Schmitt, T. E.; Almond, P. M.; Sykora, R. E. *Inorg. Chem.* **2003**, *42*, 3788.
2. Andreev, G. B.; Budantseva, N. A.; Antipin, M. Yu. Krot, N. N. *Russ. J. Coord. Chem.* **2002**, *28*, 434.
3. Krot, N. N.; Suglobov, D. N. *Radiokhimiya* **1989**, *31*, 1.
4. Ekstrom, A. *Inorg. Chem.* **1974**, *13*, 2237.
5. Stoyer, N. J.; Hoffman, D. C.; Silva, R. J. *Radiochim. Acta* **2000**, *88*, 279.
6. Guillaume, B.; Hobart, D. E.; Bourges, J. Y. *J. Inorg. Nucl. Chem.* **1981**, *43*, 3295.
7. Nakamoto, T.; Nakada, M.; Nakamura, A.; Haga, Y.; Onuki, Y. *Solid State Commun.* **1999**, *109*, 77.
8. a) Rose, D.; Chang, Y.-D.; Chen, Q.; Zubieta, J. *Inorg. Chem.* **1994**, *33*, 5167. b) Thuéry, P.; Nierlich, M.; Souley, B.; Asfari, Z.; Vicens, J. *J. Chem. Soc., Dalton Trans.* **1999**, *15*, 2589. c) Taylor, J. C.; Ekstrom, A.; Randall, C. H. *Inorg. Chem.* **1978**, *17*, 3285. d) Brandenburg, N. P.; Loopstra, B. *Acta Crystallogr.* **1978**, *B34*, 3734.
9. a) Zachariasen, W. H. *Acta Crystallogr.* **1948**, *1*, 281. b) Zachariasen, W. H. *Acta Crystallogr.* **1954**, *7*, 788. c) Zachariasen, W. H. *Acta Crystallogr.* **1954**, *7*, 795.
10. Levason, W. *Coord. Chem. Rev.* **1997**, *161*, 33.
11. Sykora R. E.; Albrecht-Schmitt, T. E. *Inorg. Chem.* **2003**, *42*, 2179.

12. Bean, A. C.; Peper, S. M.; Albrecht-Schmitt, T. E. *Chem. Mater.* **2001**, *13*, 1266.

13. Burns, P. C.; Miller, M. L.; Ewing, R. C. *Can. Mineral.* **1996**, *34*, 845.

14. Krivovichev, S. V.; Cahill, C. L.; Burns, P. C. *Inorg. Chem.* **2002**, *41*, 34.

15. Burns, P. C.; Ewing, R. C.; Hawthorne, F. C. *Can. Mineral.* **1997**, *35*, 1551.

16. Brown, I. D.; Altermatt, D. *Acta Crystallogr.* **1985**, *B41*, 244.

17. Brese, N. E.; O'Keeffe, M. *Acta Crystallogr.* **1991**, *B47*, 192.

18. Sarsfield, M. J.; Helliwell, M. *J. Am. Chem. Soc.* **2004**, *ASAP*.

19. Sheldrick, G. M. SHELXTL, Version 6.12, Bruker AXS, Inc.: Madison, WI 2001.

Chapter 6

EXTENDED NETWORKS, POROUS SHEETS, AND CHIRAL FRAMEWORKS. THORIUM MATERIALS CONTAINING MIXED GEOMETRY ANIONS: STRUCTURES AND PROPERTIES OF $Th(SeO_3)(SeO_4)$, $Th(IO_3)_2(SeO_4)(H_2O)_3 \cdot H_2O$, and $Th(CrO_4)(IO_3)_2$

ABSTRACT

Three novel Th(IV) compounds containing heavy oxoanions, $Th(SeO_3)(SeO_4)$ (**1**), $Th(IO_3)_2(SeO_4)(H_2O)_3 \cdot H_2O$ (**2**), and $Th(IO_3)_2(CrO_4)$ (**3**), have been synthesized under mild hydrothermal conditions. Each of these three distinct structures contains trigonal-pyramidal and tetrahedral oxoanions. Compound **1** adopts a three-dimensional structure formed from ThO_9 tricapped trigonal prisms, trigonal pyramidal selenite, SeO_3^{2-}, anions containing Se(IV), and tetrahedral selenate, SeO_4^{2-}, anions containing Se(VI). The structure of **2** contains two-dimensional porous sheets and occluded water molecules. The Th centers are found as isolated ThO_9 tricapped trigonal prisms being bound by four trigonal pyramidal iodate anions, two tetrahedral selenate anions, and three coordinating water molecules. In the structure of **3** the Th(IV) cations are found as ThO_9 tricapped trigonal prisms. Each Th center is bound by six IO_3^{1-} anions and three CrO_4^{2-} anions forming a chiral three-

dimensional structure. Second-harmonic generation of 532 nm light from 1064 nm radiation by a polycrystalline sample of **3** was observed. Crystallographic data (193 K, Mo Kα, λ = 0.71073): **1**; monoclinic, $P2_1/c$; a = 7.0351(5) Å, b = 9.5259(7) Å, c = 9.0266(7) Å, β = 103.128(1), Z = 4; **2**, monoclinic, $P2_1/n$, a = 7.4889(9) Å, b = 8.002(1) Å, c = 20.165(3) Å, β = 100.142(2), Z = 4; **3**, orthorhombic, $P2_12_12_1$, a = 7.3672(5) Å, b = 9.3617(6) Å, c = 11.9201(7) Å, Z = 4.

INTRODUCTION

Thorium, lacking f electrons in its normal oxidation state of +4, is ostensibly a rather mundane element compared to the heavier members of the series, but has nevertheless played a number of critical roles in actinide chemistry, particularly in serving as a surrogate for more radioactive elements, especially ^{239}Pu(IV).[1] Recently, thorium has garnered renewed interest because of its high coordination numbers, typically eight or nine, that give rise to rich structural chemistry. Examples of these efforts include the preparation of organically templated thorium fluorides (e.g. $[C_4N_2H_{12}]_{0.5}[ThF_5]$ and $[C_5N_2H_{14}][ThF_6]\cdot 0.5H_2O$),[2] open-framework organic-inorganic hybrids, such as $[(Th_2F_5)(NC_7H_4O_4)_2(H_2O)_2][NO_3]$,[3] and the recent report from our group on the preparation of the first actinide tellurate in the form of the mixed-metal compound, $Th(VO)_2(TeO_6)(H_2O)_2$.[4]

Despite recent efforts in understanding the chemistry of U,[5] Np,[6] Pu,[7] Am,[8] and Cm[9] with oxoanions containing a nonbonding but stereochemically active lone pair of electrons, little is known about the structural chemistry of thorium with anions of this type. This is somewhat surprising given the importance of separating and

quantifying thorium via the precipitation of its iodate salt.[10] There have also been reports on the preparation and properties of thorium selenites and tellurites such as $Th(SeO_3)_2 \cdot H_2O$[11] and $Th(TeO_3)_2$,[12] but no single-crystal X-ray diffraction data exists. The structure of $ThTe_2O_6$ has been solved using X-ray powder methods.[13]

The selenite system is of particular interest because of the possibility of forming mixed-anion compounds containing both SeO_3^{2-} and SeO_4^{2-},[14] which was recently highlighted with the report of $Au_2(SeO_3)_2(SeO_4)$.[15] Given the high coordination numbers of Th and the presence of trigonal pyramidal and tetrahedral anions there is also the distinct possibility that these compounds might adopt acentric structures.[16] Herein we report the preparation, crystal structures, and properties of three Th(IV) compounds that contain both tetrahedral and trigonal pyramidal anions, $Th(SeO_3)(SeO_4)$ (**1**), $Th(IO_3)_2(SeO_4)(H_2O)_3 \cdot H_2O$ (**2**), and $Th(CrO_4)(IO_3)_2$ (**3**). The structures and reactivity of uranyl chromate iodates has been previously described.[17]

EXPERIMENTAL

Syntheses. $Th(NO_3)_4 \cdot xH_2O$ (99%, Alfa-Aesar), H_5IO_6 (Alfa Aesar), $Cr(NO_3)_3 \cdot 9H_2O$ (99.99%, Fisher), and H_2SeO_4 (40% aqueous soln., Alfa Aesar) were used as received. Distilled and Millipore-filtered water with a resistance of 18.2 MΩ·cm was used in all reactions. All reactions were run in PTFE-lined 23-mL Parr 4749 autoclaves. Standard precautions for handling radioactive materials were followed. SEM/EDX analyses were performed using a JEOL 840/Link Isis instrument. Typical EDX analyses are within 4% of ratios determined from single-crystal X-ray diffraction experiments.

$Th(SeO_3)(SeO_4)$ (1). Cs_2CO_3 (0.171 mg, 0.526 mmol) (needed for crystallization to occur), $Th(NO_3)_4{\cdot}xH_2O$ (252 mg, 0.526 mmol), H_2SeO_4 (0.33 mL, 1.28 mmol), and 0.33 mL of water were loaded in a 23-mL PTFE-lined autoclave. The autoclave was sealed and placed in a preheated furnace for 4 d at 210 °C. The furnace was then cooled at 9 °C/h to 23 °C. The product consisted of a colorless solution over clear, colorless crystals. The major product is $Th(SeO_3)_2$. Compound **1** is present only in trace amounts and can be manually separated. The crystals were washed with methanol and allowed to dry. IR (KBr, cm^{-1}): 943 (*v*, SeO_4^{2-}), 911 (*v*, SeO_4^{2-}), 881 (*v*, SeO_4^{2-}), 863 (*v*, SeO_4^{2-}), 820 (*v*, SeO_3^{2-}), 728 (*v*, SeO_3^{2-}), 713 (*v*, SeO_3^{2-}), 530, 470 (*v*, SeO_3^{2-}), 442 (*v*, SeO_3^{2-}), 408 (*v*, SeO_4^{2-}). EDX analysis for $Th(SeO_3)(SeO_4)$ provided a Th:Se ratio of 1:2.

$Th(IO_3)_2(SeO_4)(H_2O)_3{\cdot}H_2O$ (2). $Th(NO_3)_4{\cdot}xH_2O$ (145 mg, 0.291 mmol), H_5IO_6 (69 mg, 0.302 mmol), $Cr(NO_3)_3{\cdot}9H_2O$ (242 mg, 0.605 mmol), H_2SeO_4 (0.1 ml, 0.389 mmol), and 1.0 mL of water were loaded in a 23-mL PTFE-lined autoclave. The autoclave was sealed and placed in a preheated furnace for 3 days at 210 °C. The furnace was then cooled at 9 ºC/h to 23 °C. The product consisted of a yellow solution over clear green-yellow prisms of **2** as well as undefined black and white powders. The crystals were washed with methanol and allowed to dry. The yield was undeterminable due to the mixture of products. IR (KBr, cm^{-1}): 900 (ν, SeO_4^{2-}), 867 (ν, SeO_4^{2-}), 853 (ν, SeO_4^{2-}), 817 (ν, IO_3^{1-}), 802 (ν, IO_3^{1-}), 785 (ν, IO_3^{1-}), 760 (ν, IO_3^{1-}), 715 (ν, IO_3^{1-}), 600 (δ, IO_3^{1-}), 532 (δ, IO_3^{1-}). EDX analysis for $Th(IO_3)_2(SeO_4)(H_2O)_3{\cdot}H_2O$ provided a Th:I:Se ratio of 1:2:1.

$Th(CrO_4)(IO_3)_2$ (3). $Th(NO_3)_4{\cdot}xH_2O$ (217 mg, 0.435 mmol), H_5IO_6 (103 mg, 0.451 mmol), $Cr(NO_3)_3{\cdot}9H_2O$ (181 mg, 0.451 mmol), and 1.0 mL of water were loaded in a 23-mL PTFE-lined autoclave. The autoclave was sealed and placed in a preheated furnace for 3 days at 200 °C. The furnace was then cooled at 9 °C/h to 23 °C. The product consisted of a yellow solution over orange-yellow prisms. Yield 300 mg, near quantitative. The crystals were washed with methanol and allowed to dry. Phase purity was confirmed by PXRD. EDX analysis for $Th(CrO_4)(IO_3)_2$ provided a Th:I:Cr ratio of 1:1:2.

Nonlinear Optical Measurements. Second harmonic generation (SHG) was investigated using a 1064 nm excitation laser pulses from a Q-switched Nd:YAG laser (Continuum Surelite I-10). A Scientech volume absorbing calorimeter was used to measure average laser power. SHG at 532 nm was visually observed in a darkened room from a polycrystalline sample of **3** contained in a glass tube as the intensity of the unfocused laser was increased above a beam cross-section averaged intensity of 4.3 megawatt/cm^2. At a given laser intensity above the SHG threshold, the SHG intensity from **3** was weak compared to that observed from a commercial ceramic frequency doubling laser beam finder (Kentek View-It®).

Crystallographic Studies. Crystals of $Th(SeO_3)(SeO_4)$ (**1**), $Th(IO_3)_2(SeO_4)(H_2O)_3{\cdot}H_2O$ (**2**), and $Th(CrO_4)(IO_3)_2$ (**3**) were mounted on glass fibers and aligned on a Bruker SMART APEX CCD X-ray diffractometer. Intensity measurements were performed using graphite monochromated Mo Kα radiation from a sealed tube and a monocapillary collimator. SMART was used for preliminary determination of the cell constants and data collection control. For all compounds,

the intensities of reflections of a sphere were collected by a combination of three sets of exposures (frames). Each set had a different φ angle for the crystal and each exposure covered a range of 0.3º in ω. A total of 1800 frames were collected with an exposure time per frame of 40 s for **1**, 60 s for **2**, and 30 s for **3**. Longer exposure times for **1** and **2** were necessary due to the small size of the crystals.

For **1**-**3**, determination of integrated intensities and global cell refinement were performed with the Bruker SAINT (v 6.02) software package using a narrow-frame integration algorithm. A face-indexed absorption correction was initially applied using XPREP.[18] Individual shells of unmerged data were corrected and exported in the same format. These files were subsequently treated with a semi-empirical absorption correction by SADABS.[19] The program suite SHELXTL (v 5.1) was used for space group determination (XPREP), direct methods structure solution (XS), and least-squares refinement (XL).[18] Some crystallographic details are listed in Table 6.1.

RESULTS AND DISCUSSION

Syntheses. The reaction of $Th(NO_3)_4{\cdot}xH_2O$ with selenic acid in the presence of Cs^+ results in the reduction of Se(VI) to Se(IV) and the subsequent crystallization of $Th(SeO_3)_2$ with trace amounts of $Th(SeO_3)(SeO_4)$ (**1**). This reaction presumably proceeds via the oxidation of water. Yields of **1** were not improved by changing the reaction conditions, scale, or stoichiometry. The preparation of $Th(IO_3)_2(SeO_4)(H_2O)_3{\cdot}H_2O$ (**2**) is less than straightforward. In this case, $Th(NO_3)_4{\cdot}xH_2O$ is reacted with H_5IO_6, $Cr(NO_3)_3{\cdot}9H_2O$, and H_2SeO_4 to yield the

Table 6.1. Crystallographic Data for $Th(SeO_3)(SeO_4)$ (**1**), $Th(IO_3)_2(SeO_4)(H_2O)_3{\cdot}H_2O$ (**2**), and $Th(CrO_4)(IO_3)_2$ (**3**).

Formula	$Th(SeO_3)(SeO_4)$	$Th(IO_3)_2(SeO_4)(H_2O)_3{\cdot}H_2O$	$Th(CrO_4)(IO_3)_2$
Formula mass (amu)	501.96	796.86	697.84
Space group	$P2_1/c$ (No. 14)	$P2_1/n$ (No. 14)	$P2_12_12_1$ (No. 19)
a (Å)	7.0351(5)	7.4889(9)	7.3672(5)
b (Å)	9.5259(7)	8.002(1)	9.3617(6)
c (Å)	9.0266(7)	20.165(3)	11.9201(7)
α (°)	90	90	90
β (°)	103.128(1)	100.142(2)	90
γ (°)	90	90	90
V (Å^3)	589.11(8)	1189.6(3)	822.12(9)
Z	4	4	4
T (°C)	-80	-80	-80
λ (Å)	0.71073	0.71073	0.71073
ρ_{calcd} (g cm^{-3})	5.660	4.404	5.638
μ(Mo $K\alpha$) (cm^{-1})	376.48	208.56	269.38
$R(F)$ for $F_o^2 > 2\sigma(F_o^2)$ [a]	0.0247	0.0471	0.0204
$R_w(F_o^2)$ [b]	0.0565	0.1165	0.0423

[a] $R(F) = \sum \left| |F_o| - |F_c| \right| / \sum |F_o|$. [b] $R_w\left(F_o^2\right) = \left[\sum \left[w\left(F_o^2 - F_c^2\right)^2 \right] / \sum wF_o^4 \right]^{1/2}$.

desired product. The periodic acid oxidizes water to yield iodate, which is a convenient method for slowly introducing iodate in f-element reactions;[20-22] the Cr(III) is also oxidized to Cr(VI) and remains in solution, and finally the selenic acid remains SeO_4^{2-} in this reaction owing to the presence of the strongly oxidizing IO_6^{5-}. The preparation of $Th(CrO_4)(IO_3)_2$ (**3**) is the most direct, involving the oxidation of Cr(III) to CrO_4^{2-} by IO_6^{5-} with concomitant reduction to IO_3^{1-}. These then crystallize with Th(IV) to yield **3** in near quantitative yield. Crystals of **3** were not obtained by directly reacting chromate and iodate with Th(IV).

Structure of $Th(SeO_3)(SeO_4)$ (1). This compound adopts a three-dimensional structure formed from ThO_9 tricapped trigonal prisms, shown in Figure 6.1, trigonal pyramidal selenite, SeO_3^{2-}, anions containing Se(IV), and tetrahedral selenate, SeO_4^{2-}, anions containing Se(VI). The ThO_9 polyhedra edge-share to form one-dimensional chains that extend down the *a*-axis. Each selenate anion bridges between three such chains. The selenite anion chelates one thorium center in one chain and uses its third oxygen atom to bridge to a second chain. A view of the extended structure is depicted in Figure 6.2.

Th–O bond distances, which range from 2.354(5) to 2.625(5) Å, are within the normal limits, with the two longest Th–O bond distances (2.530(4) and 2.625(5) Å) being with the two μ_3-O atoms of the selenite anions, O(5) and O(6), respectively. The selenate bond distances (Se(1)–O) range from 1.625(5) to 1.638(5) Å, which O–Se(1)–O bond angles being found from 106.9(2) to 113.0(2)°. Se(2)–O bonds occur from 1.677(5) to 1.734(5) Å, with O–Se(2)–O bond angles from 91.1(2) to 103.8(2)°. Selected bond distances and angles for **1** can be found in Table 6.2. Bond valence

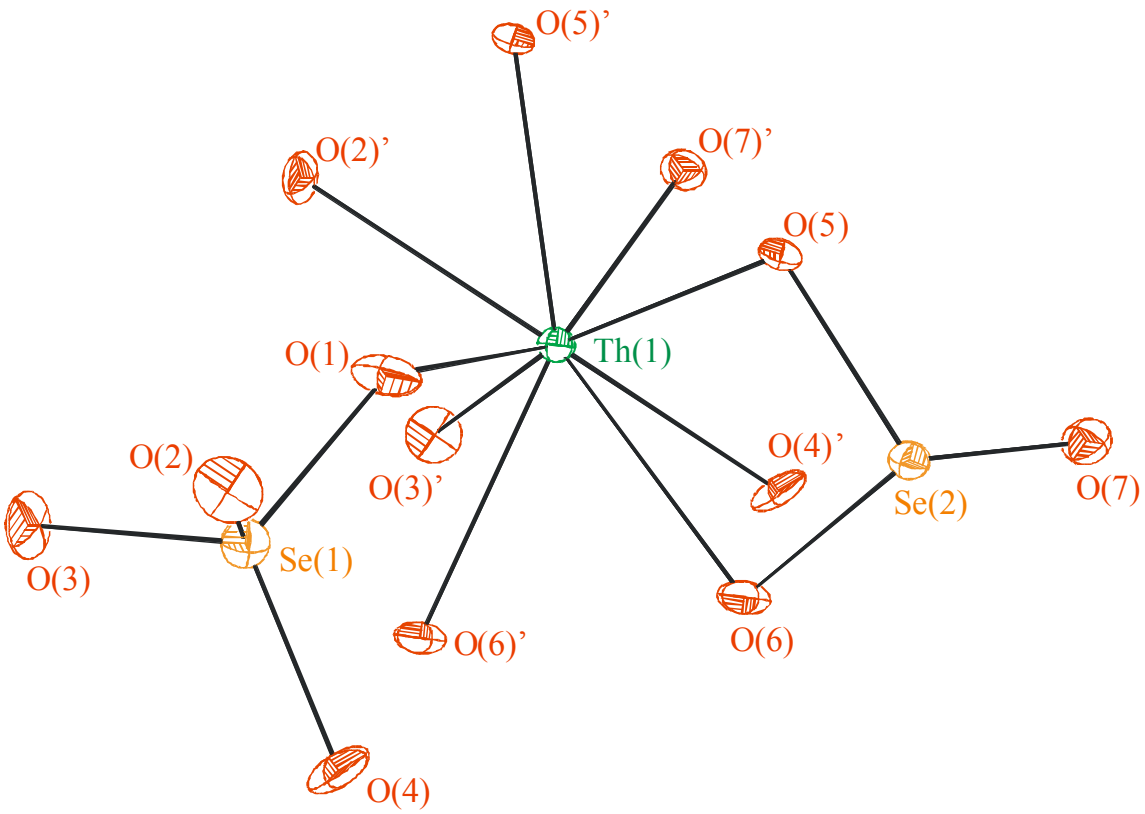

Figure 6.1. A view of the fundamental building units in $Th(SeO_3)(SeO_4)$ (**1**) showing ThO_9 tricapped trigonal prisms, trigonal pyramidal selenite, SeO_3^{2-}, anions containing Se(IV), and tetrahedral selenate, SeO_4^{2-}, anions containing Se(VI). 50% probability ellipsoids are depicted.

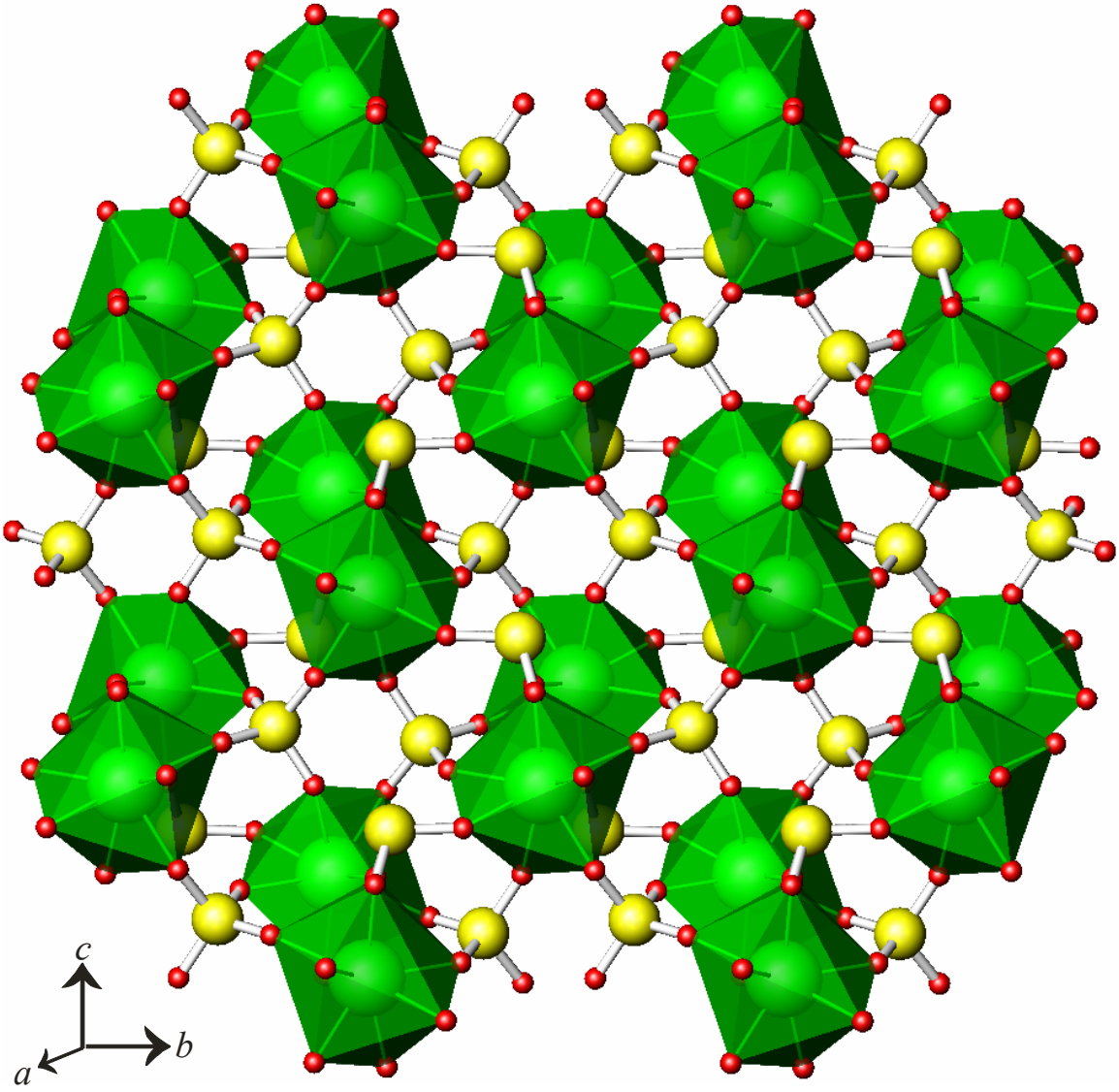

Figure 6.2. A depiction of the extended structure of $Th(SeO_3)(SeO_4)$ (**1**).

Table 6.2. Selected Bond Distances (Å) and Angles (°) for $Th(SeO_3)(SeO_4)$.

Distances (Å)			
Th(1)–O(1)	2.404(5)	Th(1)–O(7)'	2.354(5)
Th(1)–O(2)'	2.426(5)	Se(1)–O(1)	1.625(5)
Th(1)–O(3)'	2.458(5)	Se(1)–O(2)	1.626(5)
Th(1)–O(4)'	2.464(5)	Se(1)–O(3)	1.638(5)
Th(1)–O(5)	2.458(5)	Se(1)–O(4)	1.638(5)
Th(1)–O(5)'	2.530(4)	Se(2)–O(5)	1.677(5)
Th(1)–O(6)	2.625(5)	Se(2)–O(6)	1.725(4)
Th(1)–O(6)’	2.429(5)	Se(2)–O(7)	1.734(5)
Angles (°)			
O(1)–Se(1)–O(2)	106.3(2)	O(3)–Se(1)–O(4)	112.4(3)
O(1)–Se(1)–O(3)	108.5(3)	O(5)–Se(2)–O(6)	91.1(2)
O(1)–Se(1)–O(4)	113.0(2)	O(5)–Se(2)–O(7)	101.0(2)
O(2)–Se(1)–O(3)	109.5(3)	O(6)–Se(2)–O(7)	103.8(2)
O(2)–Se(1)–O(4)	106.9(2)		

sums calculations were performed on all polyhedral central atoms, resulting in a sum of Th(1), 4.14, Se(1), 3.93, and Se(2), 6.10, which are in agreement with the expected oxidation states.[23,24]

$Th(IO_3)_2(SeO_4)(H_2O)_3 \cdot H_2O$ (2). The structure of $Th(IO_3)_2(SeO_4)(H_2O)_3 \cdot H_2O$ contains two-dimensional sheets extending in the [*bc*] plain and occluded water molecules. The Th centers are found as isolated ThO_9 tricapped trigonal prisms beingbound by four trigonal-pyramidal iodate anions, two tetrahedral selenate anions, and three coordinating water molecules. All four IO_3 units coordinate to ThO_9 on the same side in an approximately fourfold pattern through two capping and two *trans* trigonal-prismatic oxygen atoms, as is shown in Figure 6.3. The two remaining trigonal-prismatic oxygen atoms on one side of ThO_9 are a part of two SeO_4 units. Th(1)–O bond distances range from 2.383(7) Å to 2.611(7) Å with the longer three being the bond distances to the coordinating water molecules. These three coordinating water molecules are directed between the layers. The sheets of **2** are porous with gaps on the order of 15.76 x 5.50 Å (Figure 6.4). The hydrating water molecule occupies an optimized position between the sheets and in proximity of the pores in the sheets.

There are two crystallographically unique IO_3^{1-} anions in the structure of **2**. The iodate anion containing I(1) caps the ThO_9 unit, and the iodate containing I(2) occupies some of the sites forming the trigonal prism. Each iodate anion has a terminal oxygen atom, and these have the shortest bond lengths with I(1)–O(3) being 1.797(7) Å, and I(2)–O(6) being 1.800(7) Å. The I(1)–O bond lengths range from 1.797(7) to 1.819(8) Å, while those of I(2) are very similar with distances from

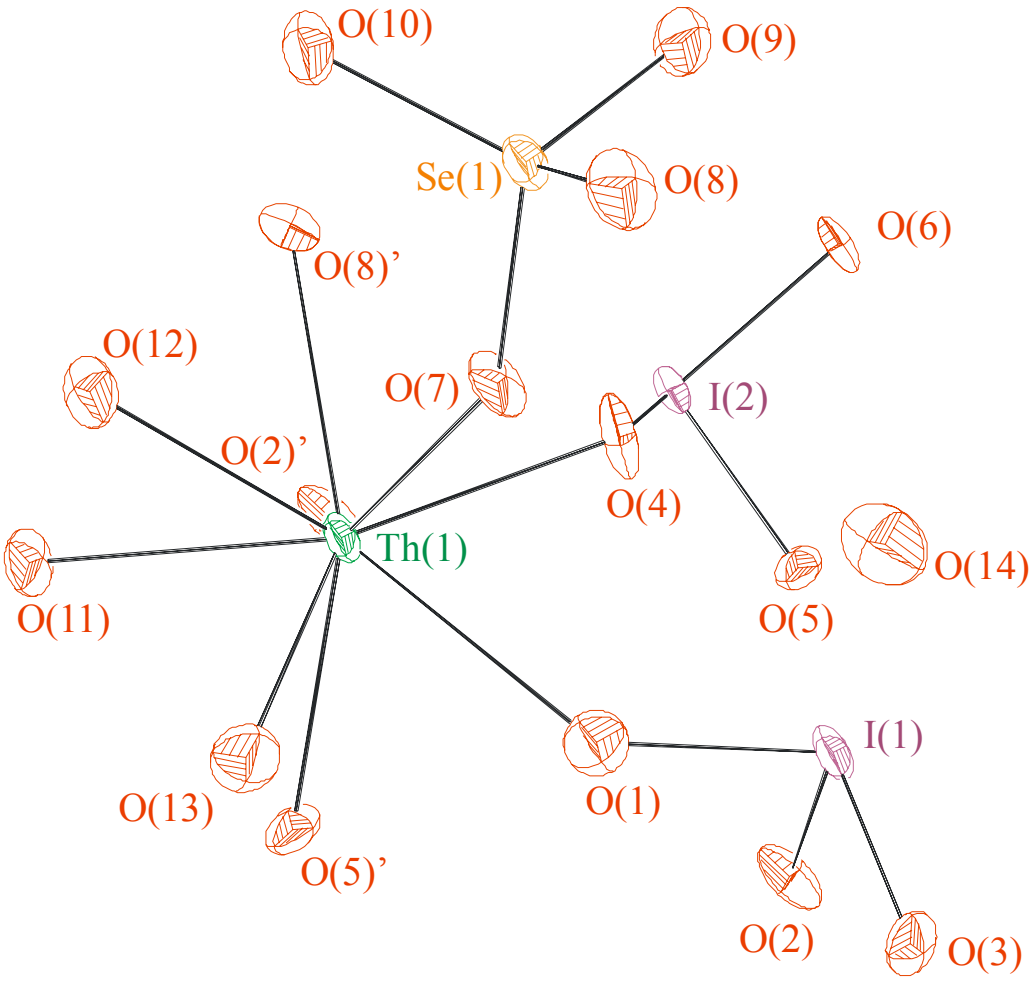

Figure 6.3. An illustration of the ThO_9, IO_3^{1-}, and SeO_4^{2-} units in $Th(IO_3)_2(SeO_4)(H_2O)_3{\cdot}H_2O$ (**2**). 50% probability ellipsoids are depicted.

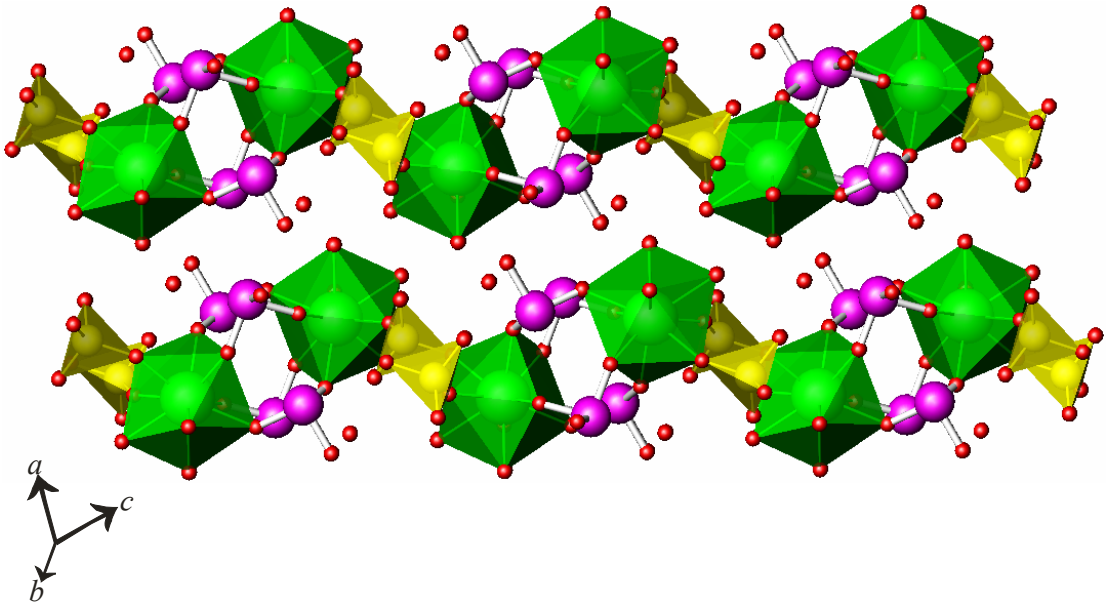

Figure 6.4. A view down [111] of the porous sheets in $Th(IO_3)_2(SeO_4)(H_2O)_3 \cdot H_2O$ (**2**).polyhedral central atoms.

Table 6.3. Selected Bond Distances (Å) and Angles (°) for $Th(IO_3)_2(SeO_4)(H_2O)_3 \cdot H_2O$.

Distances (Å)			
Th(1)–O(1)	2.427(8)	I(1)–O(2)	1.819(8)
Th(1)–O(2)'	2.427(8)	I(1)–O(3)	1.797(7)
Th(1)–O(4)	2.430(8)	I(2)–O(4)	1.817(8)
Th(1)–O(5)'	2.416(8)	I(2)–O(5)	1.810(7)
Th(1)–O(7)	2.383(7)	I(2)–O(6)	1.800(7)
Th(1)–O(8)'	2.385(8)	Se(1)–O(7)	1.644(8)
Th(1)–O(11)	2.463(8)	Se(1)–O(8)	1.608(8)
Th(1)–O(12)	2.611(7)	Se(1)–O(9)	1.624(8)
Th(1)–O(13)	2.496(8)	Se(1)–O(10)	1.621(8)
I(1)–O(1)	1.805(9)		
Angles (°)			
O(1)–I(1)–O(2)	95.7(4)	O(7)–Se(1)–O(8)	106.7(4)
O(1)–I(1)–O(3)	97.5(4)	O(7)–Se(1)–O(9)	110.5(4)
O(2)–I(1)–O(3)	98.9(4)	O(7)–Se(1)–O(10)	109.3(4)
O(4)–I(2)–O(5)	95.4(4)	O(8)–Se(1)–O(9)	107.7(4)
O(4)–I(2)–O(6)	98.0(4)	O(8)–Se(1)–O(10)	110.9(4)
O(5)–I(2)–O(6)	96.8(4)	O(9)–Se(1)–O(10)	111.6(4)

1.800(7) to 1.817(8) Å. The O–I–O bond angles for the two IO_3 units are also nearly identical with ranges of 95.7(4) to 98.9(4)° for I(1) and 95.4(4) to 98.0(4)° for I(2). The SeO_4^{2-} anions bridge two ThO_9 units and also have two terminal oxygen atoms. Bond lengths within this unit range from 1.608(8) to 1.644(8) Å, and the bond angles from 106.7(4) to 111.6(4)°. Selected bond distances and bond angles of **2** can be found in Table 6.3. Bond valence sums calculations were performed on all Th(1) resulted in a sum of 4.27, Se(1) 6.23, I(1) 5.06, and I(2) 5.03; all results are in agreement with stated oxidation states.[23,24]

$Th(CrO_4)(IO_3)_2$ (3). As is **1** and **2** the Th(IV) cations in **3** are found as ThO_9 tricapped trigonal prisms. Each Th center is bound by six IO_3^{1-} anions and three CrO_4^{2-} anions (Figure 6.5). The Th–O distances range from 2.345(5) to 2.670(5) Å, and there is no correlation between Th–O bond length and ligand type. **3** crystallizes in the chiral space group $P2_12_12_1$, probably owing to the presence of the lone pair of electrons on the iodate anions, although this feature is also present in **1** and **2**, and both of these compounds are centrosymmetric. Both the $I(1)O_3^{1-}$ and $I(2)O_3^{1-}$ trigonal pyramidal units bridge between three ThO_9 units. The CrO_4^{2-} anions also corner-shares with three ThO_9 units. The remaining oxygen atom on the CrO_4^{2-} anions is terminal. The coordination of the CrO_4^{2-} anions to Th(IV) yields $[ThCrO_4]$ sheets that propagate in the [*ab*] plane. The thorium atoms are then further coordinated by the iodate anions that link the sheets together to create a three-dimensional structure as shown in Figure 6.6.

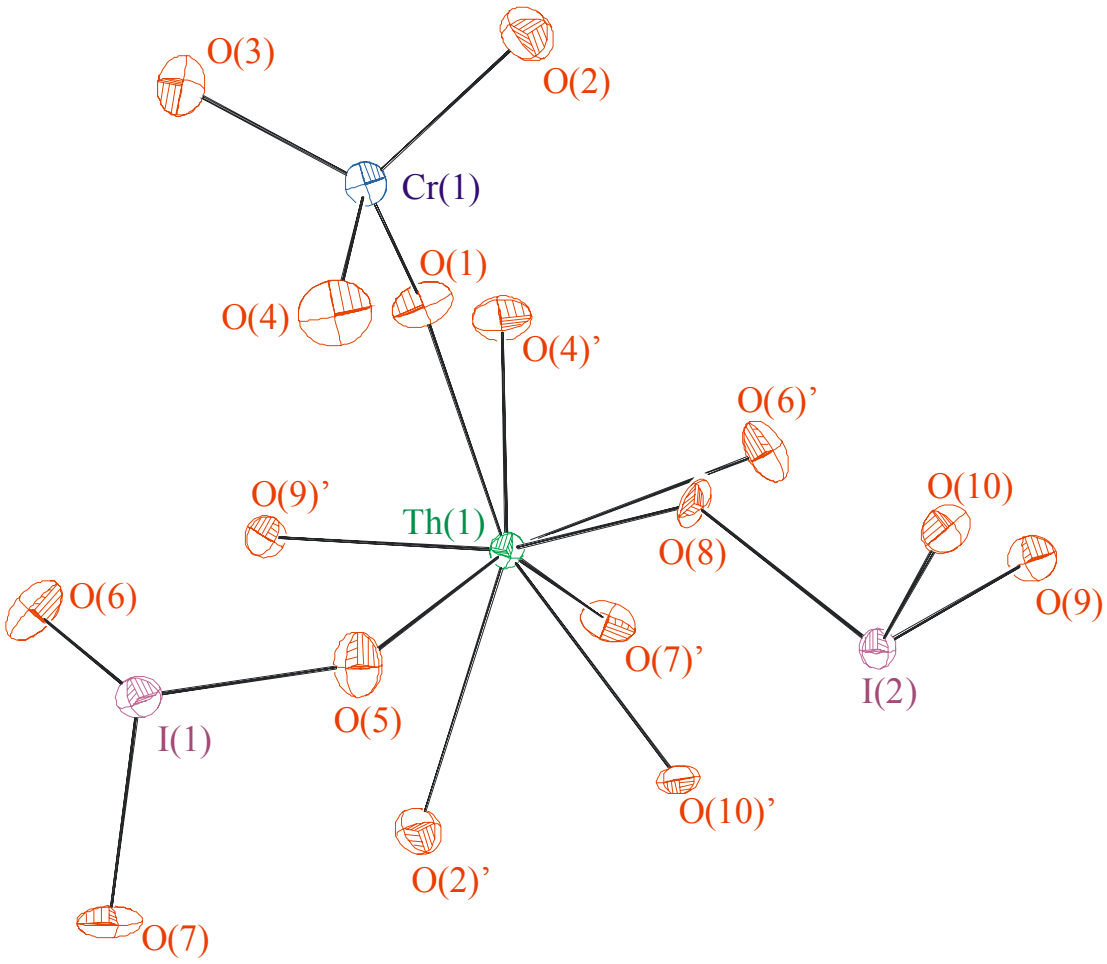

Figure 6.5. A depiction of the fundamental building units in $Th(CrO_4)(IO_3)_2$ (**3**) showing a Th center bound by six IO_3^{1-} anions and three CrO_4^{2-} anions. 50% probability ellipsoids are depicted.

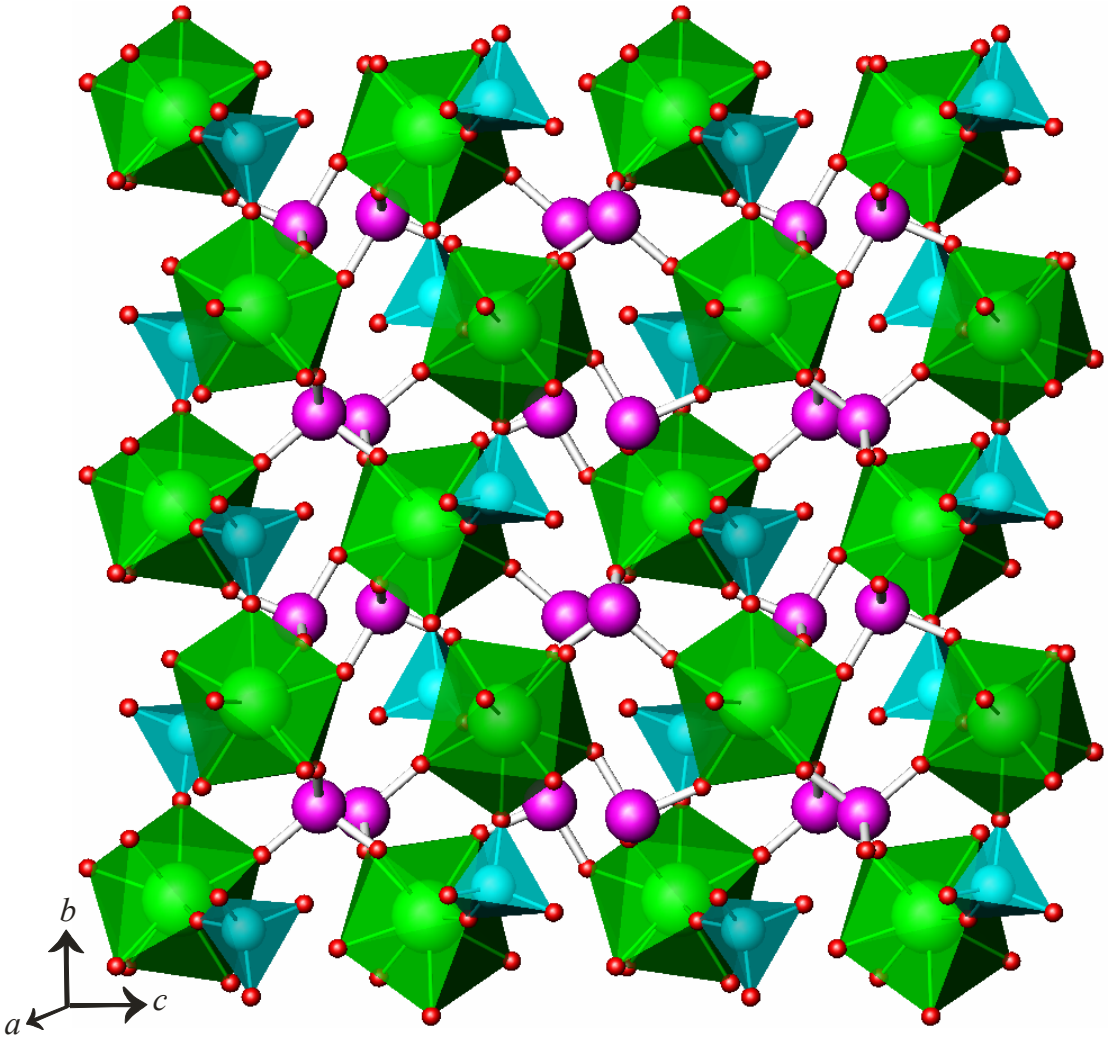

Figure 6.6. An illustration of the extended structure of $Th(CrO_4)(IO_3)_2$ (**3**) showing $[ThCrO_4]$ sheets that propagate in the [*ab*] plane. These sheets are linked together by iodate anions to create a three-dimensional structure.

The I–O bond lengths range from 1.794(5) to 1.827(5) Å, but due to the contortion required of the IO_3^{1-} anions to stabilize and maintain their bonding, all I(2)–O bond lengths are longer than those of I(1)–O. The $I(1)O_3^{1-}$ anion is more uniform and has O–I(1)–O bond angles ranging from 94.5(3) to 98.8(3)°. The $I(2)O_3^{1-}$ anion shows more deformity with O–I(2)–O bond angles of 92.8(2), 100.1(2), and 100.6(2)°. Cr–O bond lengths are also consistent with literature values,[17] ranging from 1.616(5) to 1.664(5) Å, with the terminal O(3) atom having the obvious and expected shortest bond length to Cr(1). There are no exceptional deviations from tetrahedral geometry with its O–Cr–O bond angles of 107.7(3) to 111.0(3)°. Selected bond distances and angles for **3** can be found in Table 6.4. Bond valence sums calculations were performed on all polyhedral central atoms. Th(1) resulted in a sum of 4.32, Cr(1) 5.97, I(1) 5.19, and I(2) 4.93; all results being within a reasonable error of the stated oxidation state.[23,24]

CONCLUSIONS

In this report we have demonstrated that the structural chemistry of thorium with heavy oxoanions is diverse and rich with previously unknown bonding motifs. The high coordination number of Th(IV), nine-coordinate in the compounds reported herein, provides a platform for crystallizing solids with both layered and chiral networks. It is noteworthy that one does not solely obtain routine centrosymmetric three-dimensional structures as one might have predicted to occur with Th(IV) and anions of this type. A future report will detail the structural chemistry of thorium selenites and iodates.

Table 6.4. Selected Bond Distances (Å) and Angles (°) for $Th(CrO_4)(IO_3)_2$.

Distances (Å)			
Th(1)–O(1)	2.382(5)	Cr(1)–O(2)	1.663(5)
Th(1)–O(2)'	2.670(5)	Cr(1)–O(3)	1.616(5)
Th(1)–O(4)'	2.547(5)	Cr(1)–O(4)	1.642(5)
Th(1)–O(5)	2.345(5)	I(1)–O(5)	1.794(5)
Th(1)–O(6)'	2.402(5)	I(1)–O(6)	1.803(5)
Th(1)–O(7)'	2.408(5)	I(1)–O(7)	1.795(5)
Th(1)–O(8)	2.526(5)	I(2)–O(8)	1.809(5)
Th(1)–O(9)'	2.361(5)	I(2)–O(9)	1.812(5)
Th(1)–O(10)'	2.418(5)	I(2)–O(10)	1.827(5)
Cr(1)–O(1)	1.664(5)		
Angles (°)			
O(5)–I(1)–O(6)	97.5(2)	O(1)–Cr(1)–O(2)	108.8(3)
O(5)–I(1)–O(7)	98.8(3)	O(1)–Cr(1)–O(3)	109.9(3)
O(6)–I(1)–O(7)	94.5(3)	O(1)–Cr(1)–O(4)	110.2(3)
O(8)–I(2)–O(9)	100.6(2)	O(2)–Cr(1)–O(3)	111.0(3)
O(8)–I(2)–O(10)	92.8(2)	O(2)–Cr(1)–O(4)	109.1(3)
O(9)–I(2)–O(10)	100.1(2)	O(3)–Cr(1)–O(4)	107.7(3)

Table 6.5. Atomic Coordinates and Equivalent Isotropic Displacement Parameters for $Th(SeO_3)(SeO_4)$ (**1**).

Atom	*x*	*y*	*z*	U_{eq} (Å^2)[a]
Th1	0.79089(3)	0.46012(2)	0.13414(3)	0.00888(8)
Se1	0.87862(9)	0.81878(7)	-0.01771(7)	0.01175(15)
Se2	0.67108(9)	0.40531(7)	-0.24986(7)	0.00934(14)
O1	0.7468(7)	0.6907(5)	0.0234(6)	0.0159(10)
O2	0.7331(7)	0.9140(5)	-0.1466(5)	0.0147(10)
O3	0.9562(7)	0.9122(5)	0.1347(5)	0.0175(10)
O4	1.0567(7)	0.7652(5)	-0.0933(6)	0.0169(10)
O5	0.5490(6)	0.4413(5)	-0.1088(5)	0.0108(9)
O6	0.8940(7)	0.4394(5)	-0.1268(5)	0.0117(9)
O7	0.6588(7)	0.2295(5)	-0.2555(5)	0.0143(10)

[a] U_{eq} is defined as one-third of the trace of the orthogonalized $\mathbf{U}_{ij}$ tensor.

Table 6.6. Atomic Coordinates and Equivalent Isotropic Displacement Parameters for $Th(IO_3)_2(SeO_4)(H_2O)_3 \cdot H_2O$ (**2**).

Atom	*x*	*y*	*z*	U_{eq} (Å^2)[a]
Th1	-0.04274(5)	0.41249(5)	0.129524(18)	0.01278(13)
I1	0.26156(9)	0.24072(9)	0.00315(4)	0.01602(17)
I2	0.25381(9)	0.73316(9)	0.05121(3)	0.01485(17)
Se1	0.35374(14)	0.29853(14)	0.26897(5)	0.0143(2)
O1	0.0800(12)	0.2338(10)	0.0513(4)	0.0238(18)
O2	0.1241(10)	0.3231(11)	-0.0733(4)	0.0229(18)
O3	0.2585(11)	0.0235(9)	-0.0197(4)	0.0186(16)
O4	0.2181(11)	0.5359(11)	0.0916(5)	0.0258(19)
O5	0.2663(11)	0.6429(12)	-0.0301(4)	0.0231(18)
O6	0.4946(10)	0.7506(10)	0.0803(4)	0.0176(16)
O7	0.2114(10)	0.2810(10)	0.1973(4)	0.0202(17)
O8	0.4407(11)	0.1166(10)	0.2861(4)	0.0222(18)
O9	0.5176(11)	0.4257(10)	0.2608(4)	0.0226(18)
O10	0.2444(10)	0.3603(11)	0.3271(4)	0.0209(17)
O11	-0.3429(10)	0.4990(11)	0.1511(4)	0.0219(17)
O12	-0.1101(11)	0.3238(11)	0.2473(4)	0.0205(17)
O13	0.8439(12)	0.1210(10)	0.1371(4)	0.0240(18)
O14	0.4447(13)	0.1284(13)	0.1156(5)	0.033(2)

[a] U_{eq} is defined as one-third of the trace of the orthogonalized $\mathbf{U}_{ij}$ tensor.

Table 6.7. Atomic Coordinates and Equivalent Isotropic Displacement Parameters for $Th(CrO_4)(IO_3)_2$ (**3**).

Atom	*x*	*y*	*z*	U_{eq} (Å^2)[a]
Th1	0.28484(4)	0.47827(3)	0.17429(2)	0.00862(7)
I1	0.27550(7)	0.76526(5)	0.41736(4)	0.01116(10)
I2	0.14710(6)	0.75896(5)	-0.04405(4)	0.00880(10)
Cr1	-0.19558(17)	0.55427(12)	0.30372(9)	0.0102(3)
O3	-0.2473(7)	0.4896(5)	0.4252(4)	0.0182(12)
O1	-0.0116(7)	0.4730(6)	0.2539(5)	0.0152(11)
O10	-0.0703(7)	0.8525(5)	-0.0499(5)	0.0116(11)
O5	0.2769(8)	0.6904(6)	0.2788(4)	0.0186(12)
O9	0.1180(7)	0.6344(5)	-0.1590(4)	0.0131(11)
O8	0.0763(7)	0.6493(5)	0.0730(4)	0.0125(12)
O7	0.5073(7)	0.8239(6)	0.4238(5)	0.0163(12)
O6	0.3165(8)	0.6019(6)	0.4934(4)	0.0183(13)
O2	-0.3649(8)	0.5321(6)	0.2131(4)	0.0187(12)
O4	-0.1566(7)	0.7257(5)	0.3195(5)	0.0206(12)

[a] U_{eq} is defined as one-third of the trace of the orthogonalized $\mathbf{U}_{ij}$ tensor.

REFERENCES

1. a) Gramer, C. J.; Raymond, K. N. *Inorg. Chem.* **2004**, *43*, 6397. b) Xu, J.; Whisenhunt, D. W., Jr.; Veeck, A. C.; Uhlir, L. C.; Raymond, K. N. *Inorg. Chem.* **2003**, *42*, 2665. c) Whisenhunt, D. W., Jr.; Neu, M. P.; Hou, Z.; Xu, J.; Hoffman, D. C.; Raymond, K. N. *Inorg. Chem.* **1996**, *35*, 4128.
2. Kim, J.-Y.; Norquist, A. J.; O'Hare, D. *Chem. Commun.* **2002**, *19*, 2198.
3. Kim, J.-Y.; Norquist, A. J.; O'Hare, D. *J. Am. Chem. Soc.* **2003**, *125*, 12688.
4. Sullens, T. A.; Albrecht-Schmitt, T. E. *Inorg. Chem.* **2005**, *44*, 2282.
5. a) Almond, P. M.; Albrecht-Schmitt, T. E. *Am. Mineral.* **2004**, *89*, 976. b) Almond, P. M.; Albrecht-Schmitt, T. E. *Inorg. Chem.* **2003**, *42*, 5693.
6. a) Jobiliong, E.; Oshima, Y.; Brooks, J. S.; Albrecht-Schmitt, T. E. *Solid State Commun.* **2004**, *132*, 337. b) Almond, P. M.; Sykora, R. E.; Skanthakumar, S.; Soderholm, L.; Albrecht-Schmitt, T. E. *Inorg. Chem.* **2004**, *43*, 958. c) Albrecht-Schmitt, T. E.; Almond, P. M.; Sykora, R. E. *Inorg. Chem.* **2003**, *42*, 3788.
7. a) Bean, A. C.; Scott, B. L.; Albrecht-Schmitt, T. E.; Runde, W. *J. Solid State Chem.* **2004**, *176*, 1346. b) Bean, A. C.; Scott, B. L.; Runde, W.; Albrecht-Schmitt, T. E. *Inorg. Chem.* **2003**, *42*, 5632. c) Runde, W.; Bean, A. C.; Albrecht-Schmitt, T. E.; Scott, B. L. *Chem. Commun.* 2003, *4*, 478.
8. Runde, W.; Bean, A. C.; Scott, B. L. *Chem. Commun.* **2003**, *15*, 1848.
9. Sykora, R. E.; Z. Assefa, Z.; Haire, R. G.; Albrecht-Schmitt, T. E. *J. Solid State Chem.* **2004**, *177*, 4413.

10. a) Tranter, T. J.; Todd, T. A.; Lewis, L. C.; Henscheid, J. P. *U.S. Pat. Appl. Publ.* **2004**, U.S. 2004052705. b) Collee, R. *Can. J. Chem.* **1968**, *46*, 1691. c) Chernikhov, Yu. A.; Uspenskaya, T. A. *Zavod. Lab.* **1940**, *9*, 276.

11. Nesterenko, V. P.; Glybin, V. P. *Czech. J. Phys.* **1999**, *49*, 903.

12. Mashirov, Yu. G.; Yadrintsev, V. B. *Radiokhim.* **1982**, *24*, 256.

13. Lopez, M. L.; Veiga, M. L.; Jerez, A.; Pico, C. *J. Less-Common Met.* **1991**, *175*, 235.

14. a) Effenberger, H. *Mineral. Petrol.* **1987**, *36*, 3. b) Giester, G. *Monatsh. Chem*. **1989**, *120*, 661. c) Morris, R. E.; Wilkinson, A. P.; Cheetham, A. K. *Inorg. Chem*. **1992**, *31*, 4774. d) Krügermann, I.; Wickleder, M. S. *Z. Anorg. Allg. Chem.* **2002**, *628*, 147. e) Weil, M.; Kolitsch, U. *Acta Crystallogr.* **2002**, *C58*, 47. f) Baran, J.; Lis, T.; Marchewka, M.; Ratajczak, H. *J. Mol. Struct.* **1991**, *250*, 13. g) Giester, G. *Monatsh. Chem*. **1992**, *123*, 957. h) Harrison, W. T. A.; Zhang, Z. *Eur. J. Solid State Inorg. Chem*. **1997**, *34*, 599.

15. Wickleder, M. S.; Buechner, O.; Wickleder, C.; el Sheik, S.; Brunklaus, G.; Eckert, H. *Inorg. Chem.* **2004**, *43*, 5860.

16. a) Halasyamani, P. S.; Poeppelmeier, K. R. *Chem. Mater.* **1998**, *10*, 2753. b) Kurtz, S. K.; Perry, T. T. *J. Appl. Phys.* **1968**, *39*, 3798.

17. a) Sykora, R. E.; Wells, D. M.; Albrecht-Schmitt, T. E. *Inorg. Chem.* **2002**, *41*, 2304. b) Sykora, R. E.; McDaniel, S. M.; Wells, D. M.; Albrecht-Schmitt, T. E. *Inorg. Chem.* **2002**, *41*, 5126.

18. Sheldrick, G. M. SHELXTL PC, Version 6.12, An Integrated System for Solving, Refining, and Displaying Crystal Structures from Diffraction Data; Siemens Analytical X-Ray Instruments, Inc.: Madison, WI 2001.

19. Sheldrick, G. M. *SADABS* 2001, Program for absorption correction using SMART CCD based on the method of Blessing: R. H. Blessing, *Acta Crystallogr.* **1995**, *A51,* 33.

20. Bean, A. C.; Peper, S. M.; Albrecht-Schmitt, T. E. *Chem. Mater.* **2001**, *13*, 1266.

21. Hector, A. L.; Henderson, S. J.; Levason, W.; Webster, M. *Z. Anorg. Allg. Chem.* **2002**, *628*, 198.

22. Douglas, P.; Hector, A. L.; Levason, W.; Light, M. E.; Matthews, M. L.; Webster, M. *Z. Anorg. Allg. Chem.* **2004**, *630*, 479.

23. Brown, I. D.; Altermatt, D. *Acta Crystallogr*. **1985**, *B41*, 244.

24. N. E. Brese, M. O'Keeffe, *Acta Crystallogr.* **1991**, *B47*, 192.

Chapter 7

SYNTHESIS AND CHARACTERIZATION OF THORIUM IN NOVEL THREE-DIMENSIONAL TOPOLOGIES: $Th_2(CrO_4)_4(H_2O)_2$ AND $Th(SeO_3)_2$.

ABSTRACT

A modified compositional diagram using the reaction of $Th(NO_3)_4 \cdot xH_2O$, $Cr(NO_3)_3 \cdot 9H_2O$, and H_2SeO_4 has been completed to yield two new thorium compounds, $Th_2(CrO_4)_4(H_2O)_2$ (**1**) and $Th(SeO_3)_2$ (**2**), which are synthesized under mild hydrothermal conditions. The structure of **1** is three-dimensional, consisting of thorium in both a ThO_8 dodecahedron and ThO_9 tri-capped trigonal prism, simultaneously. The individual types of thorium polyhedra are bridged by chromate to form a two-dimensional sheet. These two unique sheets are then further bridged by chromate to form the three-dimensional structure. In contrast the structure of **2** contains only ThO_8 dodecahedra which edge-share to form one-dimensional chains. These chains are stitched together through selenite to form a three-dimensional structure. Unfilled channels form in **2** between the selenite anions. Crystallographic data: **1**, orthorhombic, space group *Pbca*, a = 10.9824(6) Å, b = 11.6668(6) Å, c = 22.459(1) Å, Z = 8; **2**, monoclinic, space group $P2_1/n$, a = 7.150(1) Å, b = 10.752(2) Å, c = 7.407(1) Å, β = 107.526(3)º, Z = 4.

INTRODUCTION

One method of creating compounds, such as ion-exchange, piezo-electric, and non-linear optical materials, is to use the natural polarity of oxoanions, such as SeO_3^{2-},[1-5] IO_3^{2-},[6-10] IO_4^{3-},[11,12] TeO_3^{2-},[4,5,13,14] and distorted TeO_6^{6-} [15-17,21] and IO_6^{5-}, [11,18-21] incorporated within a structure to aid in the development of either non-centrosymmetric compounds or structures with channels or open frameworks, though inclusion of these anions is no guarantee of success. With the exception of the octahedral anions mentioned, these moieties contain a stereochemically active lone electron pair, garnering both polarity for the anion and an inherent lack of bonding to the electron site. The octahedral anions will exhibit this polarity only when a distortion exists. The desire to produce noncentrosymmetric compounds comes from their ability to exhibit a second-harmonic generation (SHG) response through frequency doubling of incident light.[8-10,22-24] With the incorporation of polar anions in a crystal structure, the likelihood of developing a compound with this SHG response is increased.

Open-framework, or simply channel-structure compounds, can also be made by using this same polar anion synthetic approach.[19,20] In the case of $K_2[(UO_2)_2(VO)_2(IO_6)_2O]\cdot H_2O$,[20] channels are developed through the use of distorted VO_6^{5-} and IO_6^{5-} octahedra, nonbonding oxoatoms of the uranyl unit, and coordinating water molecules, in conjunction with symmetry-imposed mirror planes to cause the formation of channels within the structure. It is reasonable to extend the logic of terminal ends leading to open-framework structures by manipulating the lack of bonding of the lone electron pair or to use the multiple coordinating ions to form channel structures. The entrapment of alkaline or alkaline earth cations within these channels can then yield

materials suitable for ion-selective exchange, as for the nuclear fission products ^{90}Sr and ^{137}Cs.

The combination of the desire to create these novel compounds with structure-property relationships corresponds well with our continued progress in the f-block. The sheer number of coordination modes that the actinides exhibit can only augment the possibility of creating either of the desired structure-specific results. The selection of the anions also plays a large role in this effect with C_{3v} oxoanions alone able to participate in nine distinct binding modes, with that number increasing rapidly as the number of oxygen atoms in the anion increase. To further increase the diversity of coordination capabilities in these reactions, tetrahedral anions, which have been previously shown to yield these desired effects,[25-27] are introduced in the systems. Also, with the substitution of one of the coordinating oxygen atom on ThO_9 by a water molecule, this unit then becomes polar, while leaving a terminal position within the structure, and can therefore be tailored to result in an extended number of novel structures with either of these structural properties.

This report is a result of recently acquired compounds stemming from experimentation with polar anions, though none of the reported compounds exhibit the SHG response desired. However, thorium selenite does contain a channel, as preferred, but this channel is too small to contain a cation, and is therefore unusable as an ion exchange material.

EXPERIMENTAL

Syntheses. Cs_2CO_3 (99.99%, Alfa Aesar), $Th(NO_3)_4 \cdot xH_2O$ (Alfa Aesar), and H_2SeO_4 (40% aqueous soln., Alfa Aesar), and $Cr(NO_3)_3 \cdot 9H_2O$ (Fisher) were used as received. Distilled and Millipore-filtered water with a resistance 18.2 MΩ·cm was used in all reactions. Reactions were run in Parr 4749 autoclaves with 23-mL PTFE liners. SEM/EDX analysis was performed using a JEOL 840/Link Isis instrument. The reported preparations are those that gave the highest purity of phases possible.

$Th_2(CrO_4)_4(H_2O)_2$ (1). $Th(NO_3)_4 \cdot xH_2O$ (0.2727g, 5.48×10^{-4} mol) and $Cr(NO_3)_3 \cdot 9H_2O$ (0.2273g, 5.68×10^{-4} mol) were loaded into a 23 mL PTFE-lined autoclave with 1.0 mL H_2O. The autoclave was sealed and placed in a box oven preheated at 200 °C to react under autogeneous pressure. The autoclave was heated for 3 d and then cooled at a rate of 9 °C per hour to room temperature. The brown mother liquor was decanted and the products were rinsed with distilled water and methanol and allowed to dry. Dark red, octahedral, $Th_2(CrO_4)_4(H_2O)_2$ crystals were interspersed throughout metallic chromium and an unidentifiable yellow powder. Yield of this reaction was extremely low with only a few crystals synthesized in each reaction. EDX analysis results in a Th:Cr ratio of approximately 1:2.

$Th(SeO_3)_4$ (2). Cs_2CO_3 (0.1713g, 5.26×10^{-4} mol) and $Th(NO_3)_4 \cdot xH_2O$ (0.2524g, 5.26×10^{-6} mol) were loaded into a 23 mL PTFE-lined autoclave with 0.33 mL H_2O. 0.33 mL 40% H_2SeO_4 (1.28×10^{-3} mol) was then added drop-wise to the reaction mixture. The autoclave was sealed and placed in a box oven preheated at 185 °C to react under autogenous pressure. The autoclave was heated for 5d and then cooled at a rate of 5 °C per hour to 130 °C. The reaction was held for 10 hours and then cooled 5 °C per hour to

room temperature. The mother liquor was decanted and the products were rinsed with distilled water and methanol and allowed to dry. The two resulting products, $Th(SeO_3)_2$ and $Th(SeO_3)(SeO_4)$, could not be readily isolated from each other due to intergrowth of the crystals. $Th(SeO_3)_2$ and $Th(SeO_3)(SeO_4)$ were visually distinguishable allowing for single crystal diffraction. EDX analysis confirmed that Th and Se were the only detectable elements present in the compound yielding in a 1:2 Th:Se ratio. Although single crystals could be isolated, the intergrowth lead to the inability to measure an accurate percent yield, though the majority of the product was $Th(SeO_3)_2$.

Crystallographic Studies. Single crystals of $Th_2(CrO_4)_4(H_2O)_2$ (**1**) and $Th(SeO_3)_2$ (**2**) were selected and mounted on glass fibers using epoxy. The mounted crystal were cooled to -80 ºC during data collection using an Oxford Cryostream and optically aligned on a Bruker SMART APEX CCD X-ray diffractometer. Intensity measurements were performed using graphite monochromated Mo-Kα radiation from a sealed tube with a monocapillary collimator. SMART was used for preliminary determination of the cell constants and data collection control. For all compounds, the intensities of reflections of a sphere were collected by a combination of 3 sets of exposures (frames). Each set had a different ϕ angle for the crystal and each exposure covered a range of 0.3° in ω. A total of 1800 frames were collected with an exposure time per frame of 30 s for **1** and 40 s for **2**.

For all compounds, determination of integral intensities and global cell refinement were performed with the Bruker SAINT (v 6.02) software package using a narrow-frame integration algorithm. A face-indexed analytical absorption correction was initially applied using XPREP.[28] Individual shells of unmerged data were corrected analytically

and exported in the same format. These files were subsequently treated with a semi-empirical absorption correction with SADABS.[29] The program suite SHELXTL (v 5.1) was used for space group determination (XPREP), direct methods structure solution (XS), and least-squares refinement (XL).[28] Hydrogen atom positions for **1** were not located from the difference maps and were not included in the final refinement. The final refinements included anisotropic displacement parameters for all non-hydrogen atoms and no secondary extinction was apparent (Table 7.1).

RESULTS AND DISCUSSION

Syntheses. The syntheses of both **1** and **2** that are reported are not the only methods to produce the products, but rather the most effective. Throughout the completion of the modified phase diagram with the reported reactants and H_5IO_6, many examples of **1** and **2** were discovered as secondary products. Chromium, with a reduction potential of 1.350V at STP[30] is readily oxidized from Cr(III) to Cr(VI) in the formation of **1**. Reduction of $Se(VI)O_4^{2-}$, from the starting material, to the $Se(IV)O_3^{2-}$ in **2** has a reduction potential of 1.151V[30] and can oxidize water under mild hydrothermal conditions. Though a slow cooling process can be used to form larger or higher quality crystalline products, it is not observed that any other process is necessary than that reported.

Table 7.1. Crystallographic data for $Th_2(CrO_4)_4(H_2O)_2$ (**1**) and $Th(SeO_3)_2$ (**2**).

Compound	$Th_2(CrO_4)_4(H_2O)_2$	$Th(SeO_3)_2$
Formula mass	960.08	485.96
Crystal system	Orthorhombic	Monoclinic
Space group	*Pbca* (No. 61)	$P2_1/n$ (No. 14)
a (Å)	10.9824(6)	7.150(1)
b (Å)	11.6668(6)	10.752(2)
c (Å)	22.459(1)	7.407(1)
α (deg.)	90	90
β (deg.)	90	107.526(3)
γ (deg.)	90	90
V (Å^3)	2877.6(3)	543.0(2)
Z	8	4
T (°C)	–80	–80
λ (Å)	0.71073	0.71073
ρ_{calcd} (g cm^{-3})	4.432	5.945
μ(Mo $K\alpha$, cm^{-1})	236.04	408.22
$R(F)$ for $F_o^2 > 2\sigma(F_o^2)$ [a]	0.0228	0.0412
$R_w(F_o^2)$ [b]	0.0539	0.0990

[a] $R(F) = \sum \left| |F_o| - |F_c| \right| / \sum |F_o|$. [b] $R_w\left(F_o^2\right) = \left[\sum \left[w\left(F_o^2 - F_c^2\right)^2 \right] / \sum wF_o^4 \right]^{1/2}$.

Structures. $Th_2(CrO_4)_4(H_2O)_2$ (1). The structure of $Th_2(CrO_4)_4(H_2O)_2$ (Figures 7.1 and 7.2) is far more complicated and interesting than the simple thorium chromate name or formula suggests. The two unique thorium oxide polyhedra have distinct differences in coordination, although both Th(1) and Th(2) retain the common Th(IV) valence. This valence has been confirmed through bond valence sum calculations.[31] Th(1) exists as a ThO_8 dodecahedron with one coordinating water molecule within this polyhedron. In this moiety thorium bonds to these oxygen atoms are from 2.294(4) Å to the distance to the coordinating water molecule of 2.548(4) Å, which is the expected longest bond distance. All other oxygen atoms are bridging to the four chromium atoms that exist within the structure. However, Th(2) exists as the more often observed ThO_9 tri-capped trigonal prism. The second coordinating water molecule forms one of the bases for the trigonal prism. Once again all remaining oxygen atoms are bridging to chromium atoms with no chelating involved. The Th(2)–O bond distances range from 2.385(4) Å to 2.530(4) Å. In this polyhedron the coordinating water does not lay claim to the longest bond distance, presumably due to the bonding nature of the chromate moieties. Neither of the thorium oxide polyhedra interacts with each other except through bridging chromate.

All chromate (CrO_4^{2-}) moieties exist as tetrahedra with no significant distortion. The chromium (VI) valence has also been confirmed by bond valence sum calculations.[31] Bond angles for O–Cr–O range from 107.6(2)º to 111.8(2)º. All of these moieties are similar to each other in shape, charge, and ability to coordination to both thorium atoms; however, no two have the same coordination environment. $Cr(1)O_4$ is the

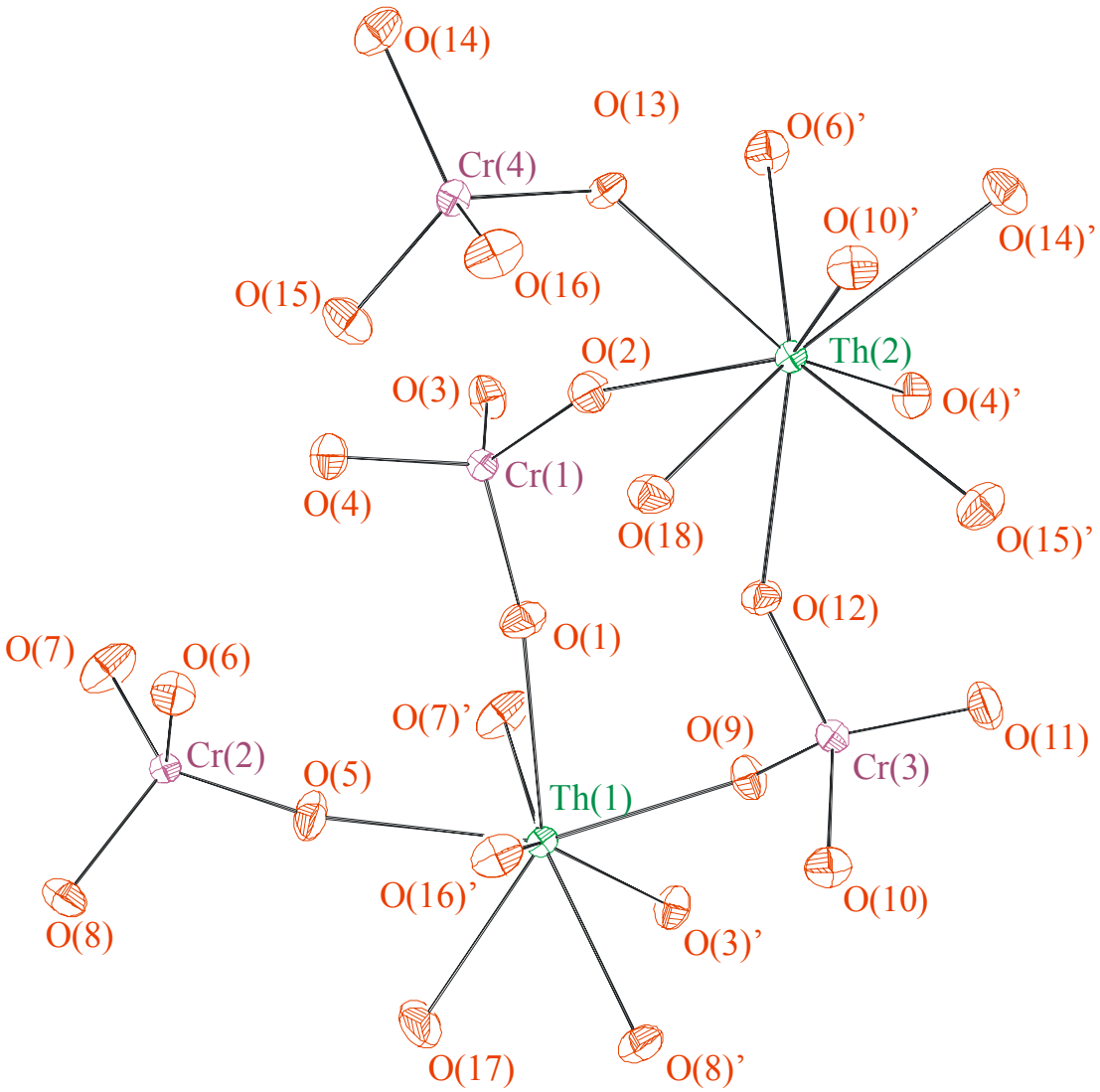

Figure 7.1. Thermal ellipsoid plot of the asymmetric unit of $Th_2(CrO_4)_2(H_2O)_2$ at 50% probability. All oxygen atoms depicted are part of either a chromate unit except O(17) and O(18) which are water molecules.

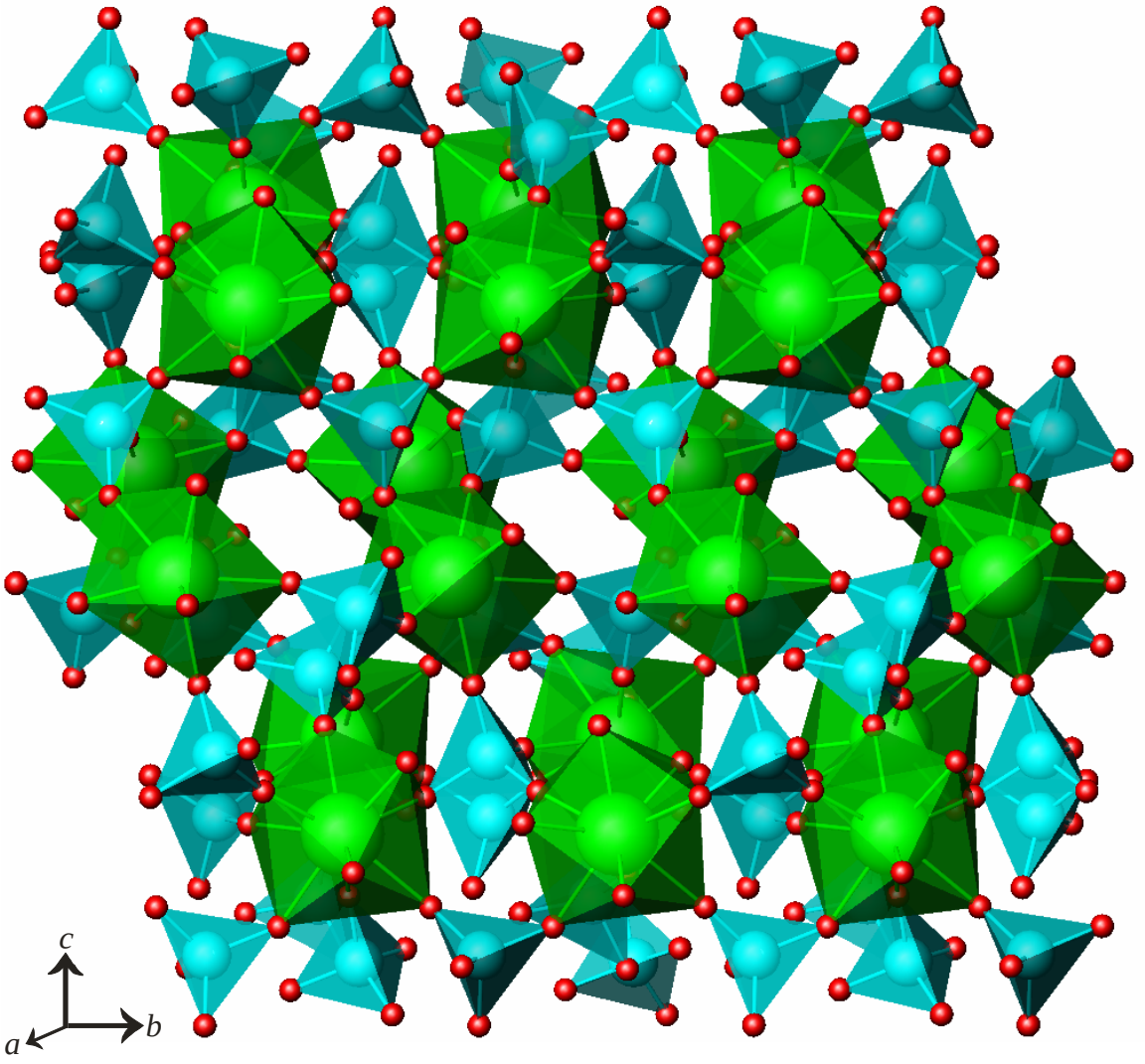

Figure 7.2. A view of $Th_2(CrO_4)_4(H_2O)_2$ down the *a*-axis showing the bridging individual layers that are formed. These layers are joined by the chromate anion.

only unit that bridges equally to Th(1) and Th(2) with O(1) and O(3) bonding to separate Th(1) atoms, and the remaining two bridging to separate Th(2) atoms. This unit's center is shifted toward Th(2) with O(2) and O(4) having the shortest bond distances to chromium of 1.638(4) and 1.646(4) Å, respectively.

Cr(2) and Cr(4) chromate anions are the most similar to each other with three of their respective oxygen atoms coordinating to one type of thorium, and the remaining oxygen atom bridging to the other. $Cr(2)O_4$ is the most interactive of the chromate anions with Th(1), as O(5), O(7), and O(8) bond to three separate Th(1) atoms, and O(6) to Th(2). $Cr(4)O_4$ is essentially the opposite with O(13), O(14), and O(15) bonding to Th(2), and O(16) to Th(1). In both cases the oxygen atom that coordinates to the opposite type of thorium atom than the others has the shortest bond distances to its respective chromium atoms. The Cr(2)–O(6) bond distance is 1.632(4) Å, while that of Cr(4)–O(14) is similar with 1.631(4) Å.

$Cr(3)O_4$ is the only chromate unit that contains a terminal oxygen atom (O(11)). This atom has the distinctively shortest bond distance to Cr(3) with a distance of 1.588(4)Å while all other Cr(3)–O bond distances are significantly longer. O(10) and O(12) bond to Th(2) and have identical Cr(3)–O bond distances, 1.655(4) Å. Cr(3)–O(9) is the longest chromium oxygen bond distance in this structure at 1.720(4) Å. Selected bond distances for **1** are shown in Table 7.2.

Owing to the propensity of bonding in chromate chemistry, each of the unique thorium atoms is awarded the opportunity to form layers with the other thorium atoms of its type. Each $Th(1)O_8$ is bound to five adjacent $Th(1)O_8$ polyhedra through five CrO_4 units with one unit ($Cr(3)O_4$) being terminal in this regard. Of these units three ($Cr(2)O_4$)

Table 7.2. Selected Bond Distances (Å) for $Th_2(CrO_4)_4(H_2O)_2$.

Distances (Å)			
Th(1)–O(1)	2.400(4)	Cr(1)–O(1)	1.647(4)
Th(1)–O(3)’	2.390(4)	Cr(1)–O(2)	1.638(4)
Th(1)–O(5)	2.427(4)	Cr(1)–O(3)	1.664(4)
Th(1)–O(7)’	2.354(4)	Cr(1)–O(4)	1.646(4)
Th(1)–O(8)	2.416(4)	Cr(2)–O(5)	1.644(4)
Th(1)–O(9)	2.294(4)	Cr(2)–O(6)	1.632(4)
Th(1)–O(16)	2.332(4)	Cr(2)–O(7)	1.645(4)
Th(1)–O(17)	2.548(5)	Cr(2)–O(8)	1.652(4)
Th(2)–O(2)	2.442(4)	Cr(3)–O(9)	1.720(4)
Th(2)–O(4)’	2.398(4)	Cr(3)–O(10)	1.655(4)
Th(2)–O(6)’	2.462(4)	Cr(3)–O(11)	1.588(4)
Th(2)–O(10)’	2.413(4)	Cr(3)–O(12)	1.655(4)
Th(2)–O(12)	2.432(4)	Cr(4)–O(13)	1.661(4)
Th(2)–O(13)	2.438(4)	Cr(4)–O(14)	1.631(4)
Th(2)–O(14)	2.530(4)	Cr(4)–O(15)	1.632(4)
Th(2)–O(15)	2.385(4)	Cr(4)–O(16)	1.668(4)
Th(2)–O(18)	2.450(4)		

bridge to two other $Th(1)O_8$ units, while the remaining two $Cr(1)O_4$ only bridge to one, forming a $^{2}_{\infty}[Th(CrO)(CrO_2)_3(H_2O)]$ sheet along the *a/b* plain (Figure 7.3). The coordinating O(17) water molecule then fills a small channel that extends down the *a*-axis within the layer.

A second sheet, also along the *a/b* plain, is comprised of the $Th(2)O_9$ polyhedra (Figure 4). Seven CrO_4 units bind one $Th(2)O_9$ moiety to six others: four bridging to one unit and three bridging two units, as well as one seemingly terminal chromate. This $^{2}_{\infty}[Th(CrO_2)_3(CrO_3)(H_2O)]$ is not exclusive from the previously described sheet including Th(1). These two sheets are joined through utilizing all CrO_4 units and alternate to form the $^{3}_{\infty}[Th(CrO_4)_4(H_2O)_2]$ structure. These two layers are jointed through O(6), O(9), O(16), and the entirety of $Cr(1)O_4$ (Figure 5).

To maintain the structural stability of $Th_2(CrO_4)_4(H_2O)_2$ the chromate units must maintain a close interaction with the thorium atoms forming the individual layers. Due to chromate bridging the layers, some of the Th–O bond lengths differ from the expected value. The prime examples in this structure are the bond lengths within $Th(2)O_9$. Because $Cr(2)O_4$ and $Cr(4)O_4$ are bound to three thorium atoms in one sheet and one opposing thorium atom, the Th(2)–O bond lengths to O(6) and O(14) are extended beyond expectation. This phenomenon is essential to the stability of the structure because of the complicated structural pattern.

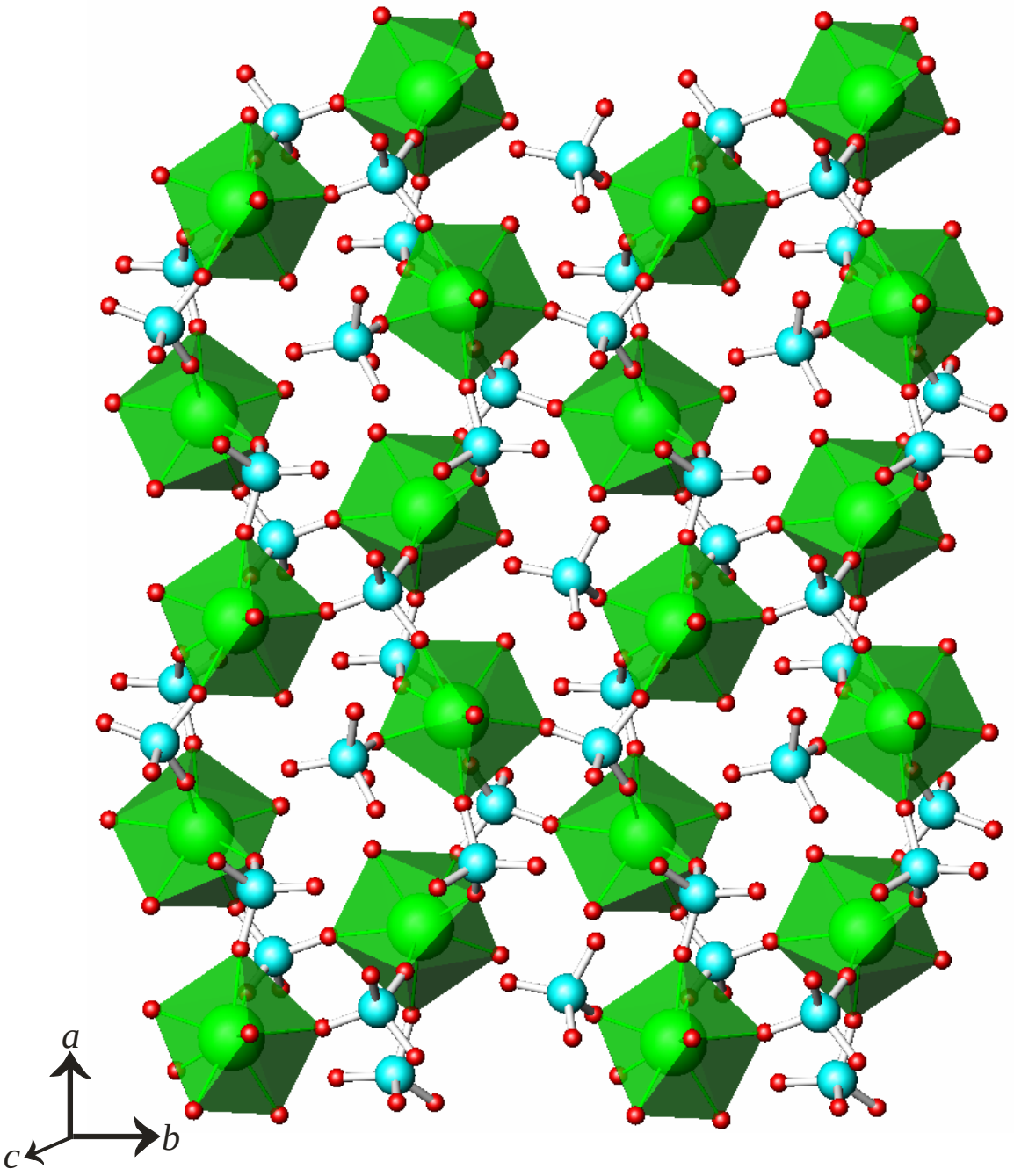

Figure 7.3. The *a/b* plane shows the $^{2}_{\infty}$[$Th(CrO)(CrO_2)_3(H_2O)$] sheet formed with the eight coordinate $Th(1)O_8$ polyhedron.

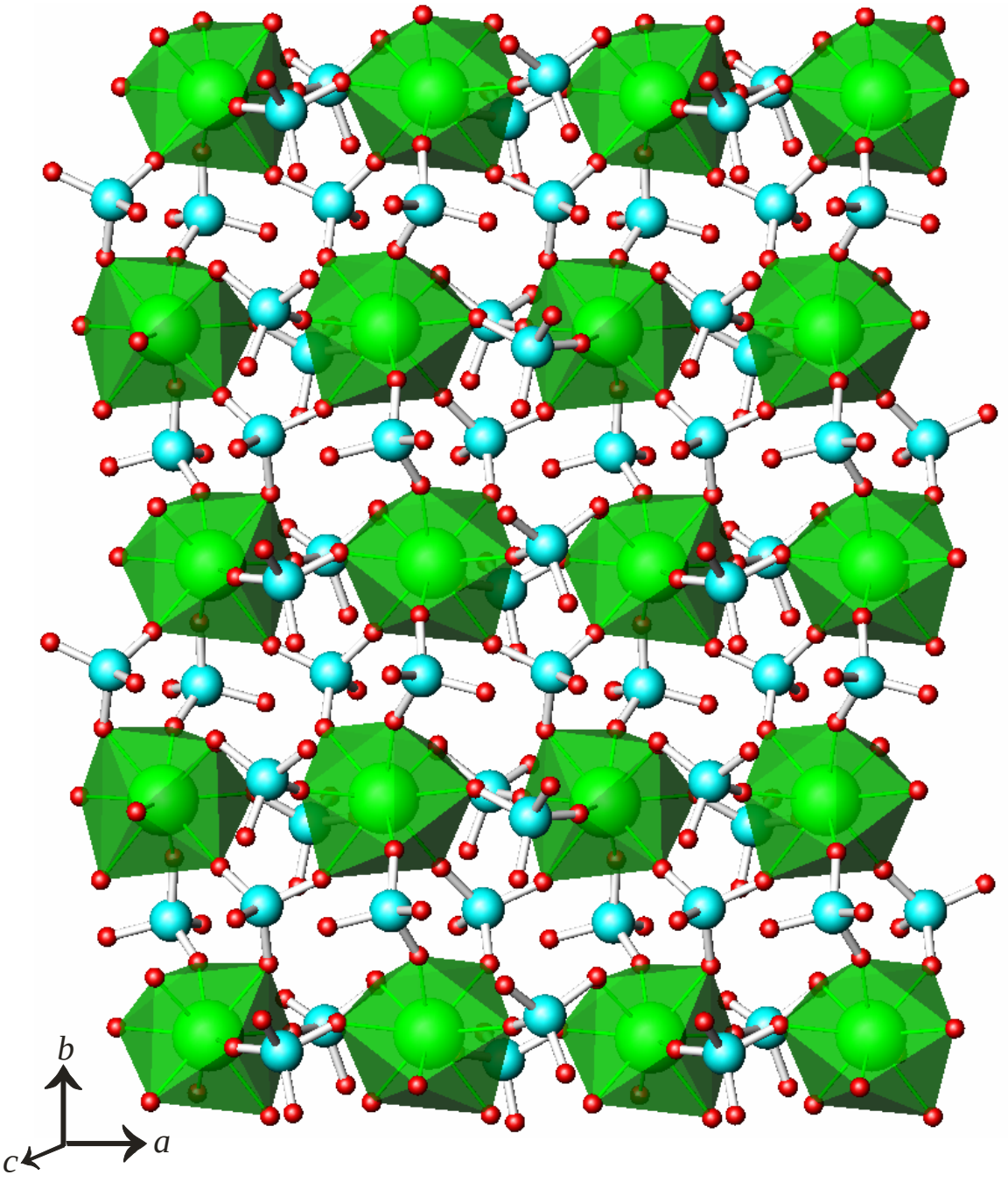

Figure 7.4. Another view of the *a/b* plain showing the second thorium chromate sheet, $^{2}_{\infty}$[$Th(CrO_2)_3(CrO_3)(H_2O)$], composed of the $Th(2)O_9$ polyhedron.

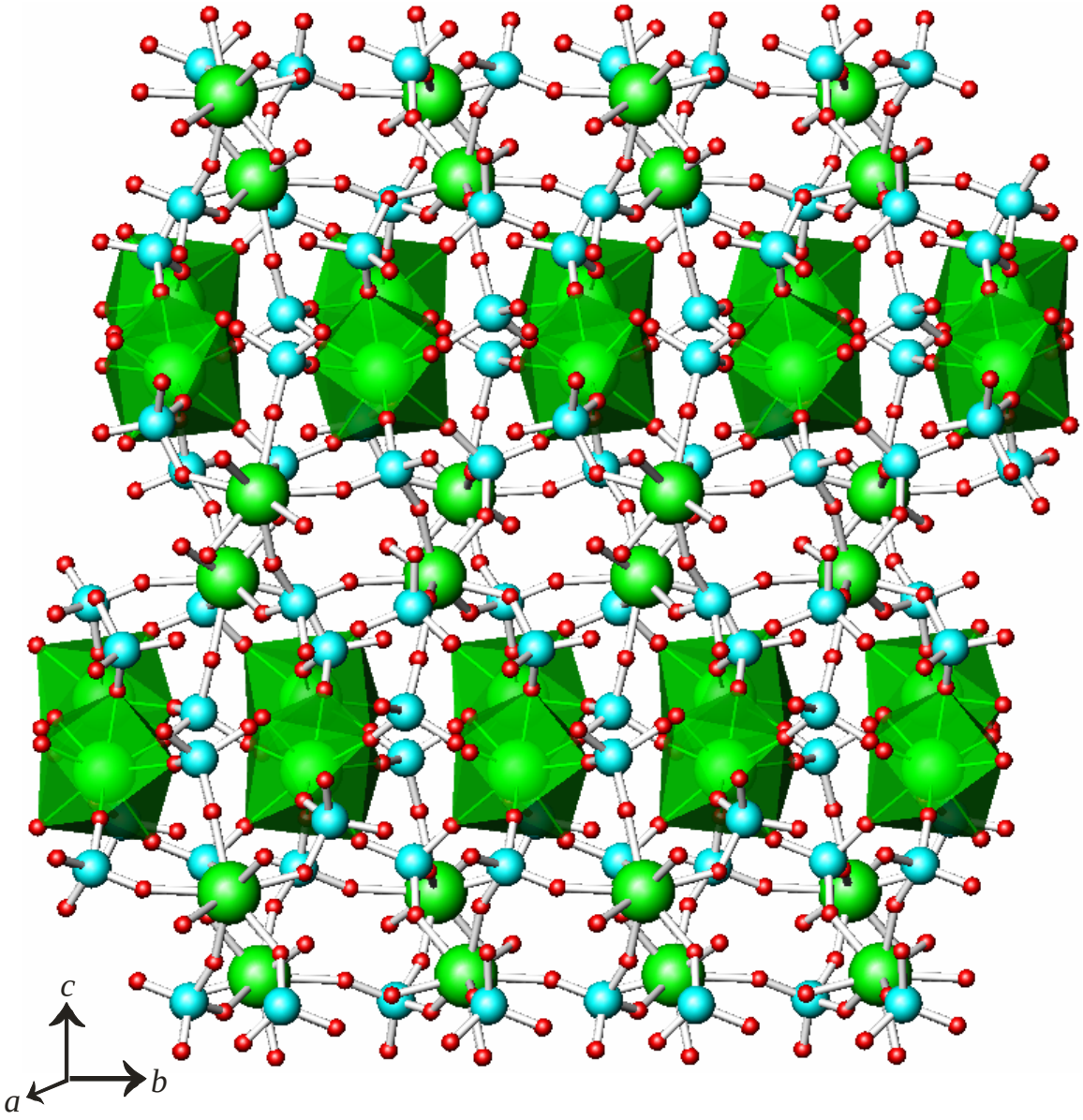

Figure 7.5. Figure 1 shown with $Th(2)O_9$ as a polyhedron and $Th(1)O_8$ as the bare moiety. This exemplifies the alternation of the two sheet typologies, which are ultimately joined by chromate.

$Th(SeO_3)_2$ (2). The structure of $Th(SeO_3)_2$ consists of one unique thorium(IV) atom bound by eight oxygen atoms forming a distorted dodecahedron (Figure 7.6). Each ThO_8 polyhedron is connected to two adjacent polyhedra through edge-sharing interactions to form the one-dimensional thorium oxide chains that extend infinitely down the *a*-axis. All oxygen atoms in this structure are either bridging or μ_3.

Every oxygen coordinates a singular Se(IV) atom giving the SeO_3^{2-} anions. $Se(1)O_3$ chelates to thorium at the point of the thorium polyhedral edge sharing, causing these two oxygen atoms to be μ_3. The remaining oxygen atom bound to Se(1) bridges to a thorium atom of a second chain.

Se(2) is coordinated only by bridging oxygen, of which two are bound to one chain and one to another. The packing of this structure reveals a pseudo-channel extending down the *a*-axis (Figure 7.7). The lone pair of electrons of Se(2) is directed into the channel in an opposing and alternating fashion, resulting in an alternation of open space throughout its length. These selenite anions stitch each chain to four adjacent chains forming the overall three-dimensional structure (Figure 7.8). The net effect of the selenite coordination pattern is an alignment of the stereochemically active lone electron pairs of all selenite anions on each chain (Figure 7.9). Unfortunately the symmetry within this structure causes an effective cancellation of this polarity negating any potential second-harmonic generation response.

Th–O bond lengths range from 2.319(9) to 2.576(7) Å, which are within the normal range. The Th–μ_3O bond lengths of 2.471(7) Å (O2') and 2.576(7) Å (O3') are the two longest bond lengths, as expected. Se(1) bond lengths to these same μ_3-O atoms are again the longest with 1.711(7) and 1.726(7) Å (O3' and O2' respectively). Se–O

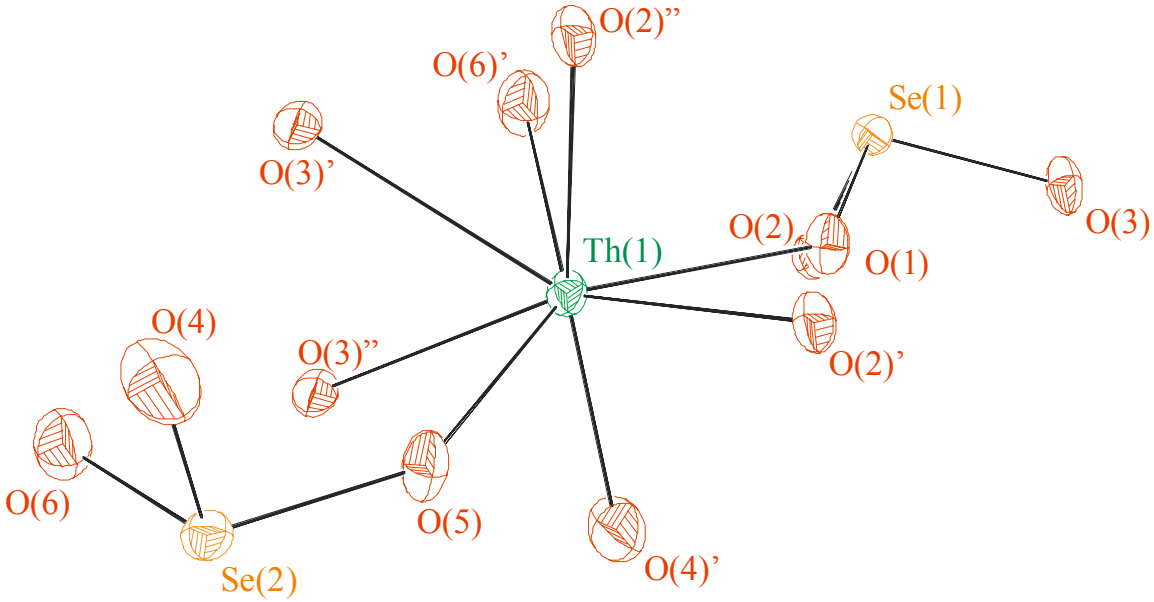

Figure 7.6. Thermal ellipsoid plot of the asymmetric unit of $Th(SeO_3)_2$ at 50% probability. All oxygen atoms depicted are part of a selenite unit.

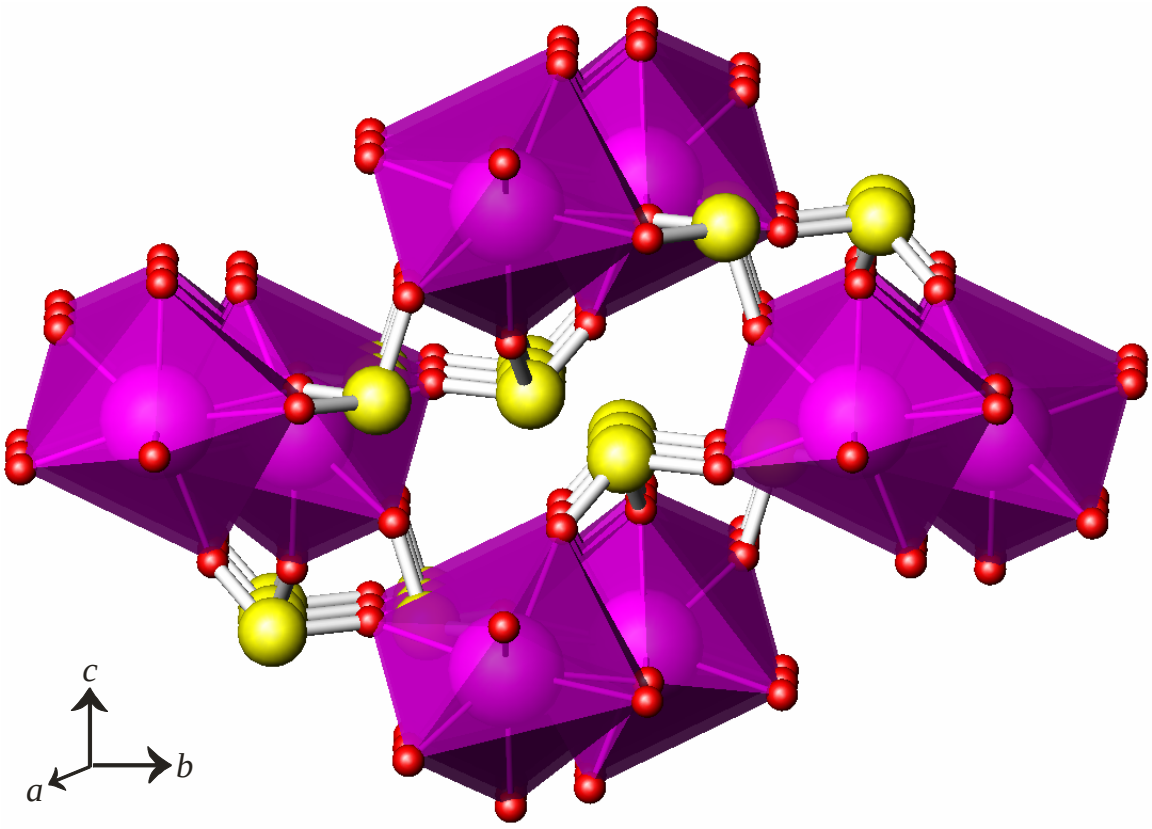

Figure 7.7. A view down the *a*-axis of $Th(SeO_3)_2$ showing an area between four thorium oxide chains formed by the opposing polarities of two selenite anions in which the electron pairs reside.

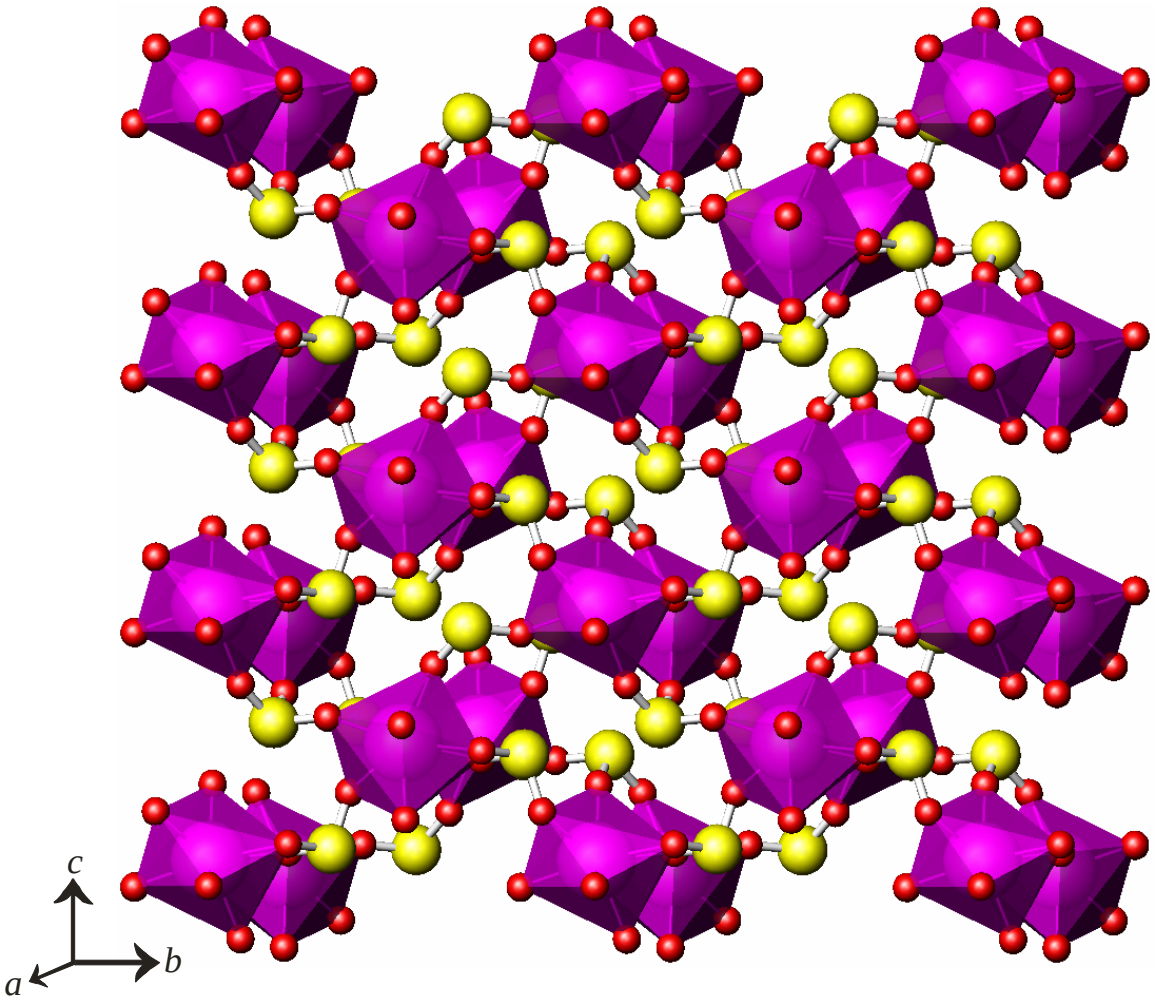

Figure 7.8. An expanded view down the *a*-axis showing the entirety of the $Th(SeO_3)_2$ structure.

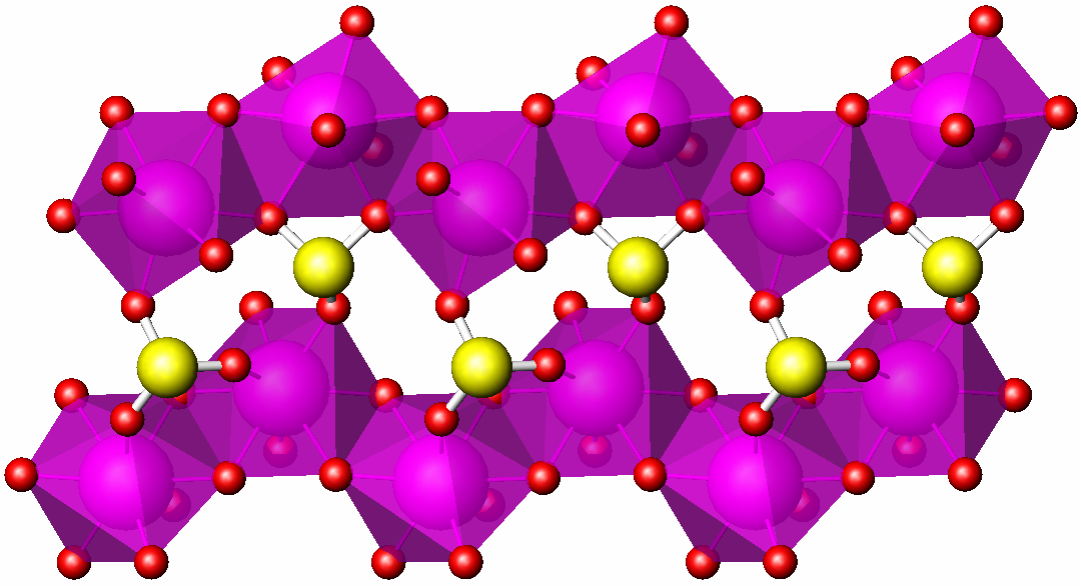

Figure 7.9. This view down the *c*-axis demonstrates the edge sharing that occurs within the $Th(SeO_3)_2$ structure. Both the $Se(1)O_3$ and $Se(2)O_3$ coordination patterns are also shown stitching two chains together, as well as the alignment of the stereochemically active lone electron pairs on each anion.

bond lengths are from 1.663(9) to 1.726(7) Å. O–Se–O bond angles range between 91.7(4)° to 106.3(4)° with the shortest angle belonging to the chelating O(2)–Se(1)–O(3) angle. Selected bond distances and bond angles are shown in Table 7.3.

CONCLUSION

Though these specific results have not yielded the desired structure types, other as yet unpublished works have revealed the fruitfulness of this endeavor. Great potential has been exhibited in the compounds that were formed with thorium adopting two coordination geometries in the formation of two distinctly different sheet typologies in $Th_2(CrO_4)_4(H_2O)_2$ and the formation of a gap between the selenite anions in $Th(SeO_3)_2$ where the electron pairs reside. The exploitation of these and similar oxoanions has lead to great strides in the advance of actinide crystal-phase synthesis as the field begins a shift toward structure specificity.

Table 7.3. Selected Bond Distances (Å) and Angles (°) for $Th(SeO_3)_2$.

Distances (Å)			
Th(1)–O(1)	2.384(7)	Th(1)–O(6)	2.331(9)
Th(1)–O(2)	2.444(7)	Se(1)–O(1)	1.665(7)
Th(1)–O(2)'	2.576(7)	Se(1)–O(2)	1.727(7)
Th(1)–O(3)	2.410(7)	Se(1)–O(3)	1.711(7)
Th(1)–O(3)'	2.471(7)	Se(2)–O(4)	1.663(9)
Th(1)–O(4)	2.319(9)	Se(2)–O(5)	1.696(7)
Th(1)–O(5)	2.332(8)	Se(2)–O(6)	1.699(8)
Angles (°)			
O(1)–Se(1)–O(2)	101.0(4)	O(4)– Se(2)–O(5)	101.3(4)
O(1)–Se(1)–O(3)	101.6(4)	O(4)– Se(2)–O(5)	99.4(5)
O(2)–Se(1)–O(3)	91.7(3)	O(5)–Se(2)–O(6)	106.3(4)

Table 7.4. Atomic Coordinates and Equivalent Isotropic Displacement Parameters for $Th_2(CrO_4)_4(H_2O)_2$.

Atom	*x*	*y*	*z*	U_{eq} (Å^2)[a]
Th1	0.138294(17)	0.713478(16)	0.052600(8)	0.00956(6)
Th2	-0.302282(17)	0.913318(16)	0.204540(8)	0.00900(6)
Cr1	-0.21600(8)	0.66059(7)	0.09005(4)	0.00960(16)
Cr2	0.06510(8)	0.38313(7)	0.08362(4)	0.00973(16)
Cr3	0.02982(8)	0.95739(7)	0.14273(4)	0.01053(16)
Cr4	-0.42307(8)	0.64236(7)	0.27894(4)	0.00987(16)
O1	-0.0724(4)	0.6959(4)	0.07938(19)	0.0190(9)
O2	-0.2786(4)	0.7526(4)	0.13583(18)	0.0177(8)
O3	-0.2852(4)	0.6642(4)	0.02415(18)	0.0178(8)
O4	-0.2223(4)	0.5298(3)	0.11736(18)	0.0172(8)
O5	0.1130(4)	0.5071(4)	0.0578(2)	0.0226(10)
O6	-0.0086(4)	0.4016(4)	0.14601(18)	0.0171(8)
O7	-0.0251(4)	0.3222(4)	0.03445(19)	0.0262(10)
O8	0.1825(4)	0.2983(4)	0.09675(19)	0.0191(9)
O9	0.0746(4)	0.8948(3)	0.07693(18)	0.0160(8)
O10	0.1386(4)	0.9455(4)	0.19332(18)	0.0169(8)
O11	0.0035(4)	1.0890(3)	0.1301(2)	0.0209(9)
O12	-0.0949(4)	0.8942(3)	0.16795(18)	0.0146(8)
O13	-0.4378(3)	0.7625(3)	0.23987(17)	0.0132(8)
O14	-0.5576(4)	0.5844(3)	0.28525(18)	0.0179(9)
O15	-0.3275(4)	0.5575(4)	0.24503(19)	0.0190(8)
O16	-0.3651(4)	0.6743(4)	0.34557(18)	0.0180(8)
O17	0.3206(5)	0.6025(4)	0.0126(3)	0.0365(13)
O18	-0.1813(4)	0.7951(3)	0.27252(18)	0.0155(8)

[a] U_{eq} is defined as one-third of the trace of the orthogonalized $\mathbf{U}_{ij}$ tensor.

Table 7.5. Atomic Coordinates and Equivalent Isotropic Displacement Parameters for $Th(SeO_3)_2$.

Atom	*x*	*y*	*z*	U_{eq} (Å^2)[a]
Th1	0.23899(5)	0.90076(3)	0.48106(5)	0.01213(17)
Se1	0.26376(13)	0.71440(9)	0.06371(14)	0.0121(2)
Se2	0.22765(15)	1.06544(10)	0.93677(15)	0.0143(2)
O1	0.3529(10)	0.7605(7)	0.2880(11)	0.0164(15)
O2	0.5974(10)	0.8974(6)	0.5829(12)	0.0159(16)
O3	-0.0694(11)	0.8965(6)	0.5503(13)	0.0176(16)
O4	0.1805(14)	0.7050(8)	0.5839(15)	0.035(2)
O5	0.3156(11)	0.9799(7)	0.7879(12)	0.0206(17)
O6	0.0124(12)	0.9070(8)	0.1797(13)	0.0263(19)

[a] U_{eq} is defined as one-third of the trace of the orthogonalized $\mathbf{U}_{ij}$ tensor.

REFERENCES

1. Almond, P. M.; Albrecht-Schmitt, T. E. *Inorg. Chem.* **2003**, *42*, 5693.
2. Jones, P. G.; Sheldrick, G. M.; Schwarzmann, E.; Vielmaeder, A. *Zeitschrift fuer Naturforschung, Teil B: Anorganische Chemie, Organische Chemie* **1983**, *38B*, 10.
3. Magataev, V. K.; Gladkii, V. V. *Fizika Tverdogo Tela* **1977**, *19*, 583.
4. Andersen, L.; Lindqvist, O.; Moret, J. *Acta Cryst.* **1984**, *C40*, 586.
5. Kohn, K.; Inoue, K.; Horie, O.; Akimoto, S. *J. Solid State Chem.* **1976**, *18*, 27.
6. Shvareva, T. Y.; Almond, P. M.; Albrecht-Schmitt, T. E. *J. Solid State Chem.* **2005**, *178*, 499.
7. Li, G.; Shi, Z.; Liu, X.; Dai, Z.; Gao, L.; Feng, S. *Inorg. Chem.* **2004**, *43*, 8224.
8. Galez, C.; Mugnier, Y.; Bouillot, J.; Rosso, C. *Optical Mat.* **2002**, *19*, 33.
9. Tsvetkov, E. G.; Tyurikov, V. I. *J. Crystal Growth.* **2000**, *217*, 138.
10. Shehee, T. C.; Sykora, R. E.; Ok, K. M.; Halasyamani, P. S.; Albrecht-Schmitt, T. E.. *Inorg. Chem.* **2003**, *42*, 457.
11. Sykora, R. E.; Wells, D. M.; Albrecht-Schmitt, T. E. *Inorg. Chem.* **2002**, *41*, 2697.
12. Bean, A. C.; Campana, C. F.; Kwon, O.; Albrecht-Schmitt, T. E. *J. Am. Chem. Soc.* **2001**, *123*, 8806.
13. Almond, P. M.; McKee, M. L.; Albrecht-Schmitt, T. E. *Ange. Chem., Int. Ed.* **2002**, *41*, 3426.
14. Kohn, K.; Inoue, K.; Horie, O.; Akimoto, S.. *J. Solid State Chem.* **1976**, *18*, 27.
15. Sullens, T. A.; Albrecht-Schmitt, T. E. *Inorg. Chem.* **2005**, *44*, 2282.

16. Becker, R.; Johnsson, M. *Solid State Sci*. **2004**, *6*, 519.

17. Meier, S. F.; Schleid, T. *J. Solid State Chem.* **2003**, *171*, 408.

18. Alexandrova, M.; Haeuseler, H. *J. Mol. Struct.* **2004**, *706*, 7.

19. Sullens, T. A.; Jensen, R. A.; Shvareva, T. Y.; Albrecht-Schmitt, T. E. *J. Am. Chem. Soc.* **2004**, *126*, 2676.

20. Sykora, R. E.; Albrecht-Schmitt, T. E. *Inorg. Chem.* **2003**, *42*, 2179.

21. Hector, A. L.; Levason, W.; Webster, M. *Inorg. Chim. Acta* **2003**, *343*, 90.

22. Rentzepis, P. M.; Pao, Y. *Applied Physics Letters* **1964**, *5*, 156.

23. Kleinman, D. A. *Physical Review* **1962**, *128*, 1761.

24. Damazyan, G. S.; Esayan, S. K.; Manukyan, A. L. *Kristallografiya* **1986**, *31*, 408.

25. Brandao, P.; Almeida P., Filipe A.; Rocha, J. *Chem. Com.* **2005**, *2*, 171.

26. Locock, A. J.; Burns, P. C. *J. Solid State Chem.* **2003**, *175*, 372.

27. Duan, L.; Liu, F.; Wang, X.; Wang, E.; Qin, C.; Li, Yangguang; Wang, X.; Hu, C. *J. Mole. Struct.* **2004**, *705*, 15.

28. Sheldrick, G. M. SHELXTL PC, Version 5.0, An Integrated System for Solving, Refining, and Displaying Crystal Structures from Diffraction Data; Siemens Analytical X-Ray Instruments, Inc.: Madison, WI 1994.

29. *SADABS*. Program for absorption correction using SMART CCD based on the method of Blessing: Blessing, R. H. *Acta Crystallogr.* **1995**, *A51*, 33.

30. *CRC Handbook of Physics and Chemistry*, David R. Lide, Ed., Boca Raton, 75th Ed., **1995**.

31. Brese, N. E.; O'Keeffe, M. *Acta Cryst.* **1991**, *B47*, 192.